MODELING AND EXPERIMENTAL INVESTIGATION ON ULTRASONIC-VIBRATION-ASSISTED GRINDING

by

NA QIN

B.S., Jilin University, 2003

AN ABSTRACT OF A DISSERTATION

submitted in partial fulfillment of the requirements for the degree

DOCTOR OF PHILOSOPHY

Department of Industrial and Manufacturing Systems Engineering
College of Engineering

KANSAS STATE UNIVERSITY
Manhattan, Kansas

2011

Abstract

Poor machinability of hard-to-machine materials (such as advanced ceramics and titanium) limits their applications in industries. Ultrasonic-vibration-assisted grinding (UVAG), a hybrid machining process combining material-removal mechanisms of diamond grinding and ultrasonic machining, is one cost-effective machining method for these materials. Compared to ultrasonic machining, UVAG has much higher material removal rate while maintaining lower cutting pressure and torque, reduced edge chipping and surface damage, improved accuracy, and lower tool wear rate. However, physics-based models to predict cutting force in UVAG have not been reported to date. Furthermore, edge chipping is one of the technical challenges in UVAG of brittle materials. There is no report related to effects of cutting tool design on edge chipping in UVAG of brittle materials.

The goal of this research is to provide new knowledge of machining these hard-to-machine materials with UVAG for further improvements in machining cost and surface quality. First, a thorough literature review is given to show what has been done in this field. Then, a physics-based predictive cutting force model and a mechanistic cutting force model are developed for UVAG of ductile and brittle materials, respectively. Effects of input variables (diamond grain number, diamond grain diameter, vibration amplitude, vibration frequency, spindle speed, and federate) on cutting force are studied based on the developed models. Interaction effects of input variables on cutting force are also studied. In addition, an FEA model is developed to study effects of cutting tool design and input variables on edge chipping. Furthermore, some trends predicted from the developed models are verified through experiments.

The results in this dissertation could provide guidance for choosing reasonable process variables and designing diamond tools for UVAG.

THEORETICAL AND EXPERIMENTAL STUDY ON ULTRASONIC-VIBRRATION-ASSISTED GRINDING

by

NA QIN

B.S., Jilin University, 2003

A DISSERTATION

submitted in partial fulfillment of the requirements for the degree

DOCTOR OF PHILOSOPHY

Department of Industrial and Manufacturing Systems Engineering
College of Engineering

KANSAS STATE UNIVERSITY
Manhattan, Kansas

2011

Approved by:

Major Professor
Dr. Zhijian Pei

Copyright

Abstract

Poor machinability of hard-to-machine materials (such as advanced ceramics and titanium) limits their applications in industries. Ultrasonic-vibration-assisted grinding (UVAG), a hybrid machining process combining material-removal mechanisms of diamond grinding and ultrasonic machining, is one cost-effective machining method for these materials. Compared to ultrasonic machining, UVAG has much higher material removal rate while maintaining lower cutting pressure and torque, reduced edge chipping and surface damage, improved accuracy, and lower tool wear rate. However, physics-based models to predict cutting force in UVAG have not been reported to date. Furthermore, edge chipping is one of the technical challenges in UVAG of brittle materials. There is no report related to effects of cutting tool design on edge chipping in UVAG of brittle materials.

The goal of this research is to provide new knowledge of machining these hard-to-machine materials with UVAG for further improvements in machining cost and surface quality. First, a thorough literature review is given to show what has been done in this field. Then, a physics-based predictive cutting force model and a mechanistic cutting force model are developed for UVAG of ductile and brittle materials, respectively. Effects of input variables (diamond grain number, diamond grain diameter, vibration amplitude, vibration frequency, spindle speed, and federate) on cutting force are studied based on the developed models. Interaction effects of input variables on cutting force are also studied. In addition, an FEA model is developed to study effects of cutting tool design and input variables on edge chipping. Furthermore, some trends predicted from the developed models are verified through experiments.

The results in this dissertation could provide guidance for choosing reasonable process variables and designing diamond tools for UVAG.

Table of Contents

List of Figures

List of Tables

Acknowledgements

I would like to take this opportunity to express my appreciation to many people who have been helping me during my PhD study.

First and foremost, I must thank my major advisor, Dr. Zhijian Pei, for his constant support, guidance, sage advice, and infinite patience. He has been patient all the way during my PhD study. He has been supportive of my ideas when the future was uncertain. His open-minded research approaches inspired me all the time in my research. His detailed comments on the earlier drafts of the dissertation have been helpful to me. He helped me in countless ways, from early stage of finding the research topic to the completion of this dissertation. I thank him for encouraging me to pursue the current topic, and for challenging me in the design of the research methodology. He is not only knowledgeable himself, but also knows how to bring out the potentials of a student. I have learned a great deal as his student. I am grateful.

I also want to thank Dr. Dongming Guo, my advisor in China. His support and encouragements have been giving me strength to complete the dissertation. I cannot thank him enough for trusting me even when I began to doubt myself in the middle of my PhD study.

My sincere thanks also go to Dr. Xiaojiang Xin from Mechanical and Nuclear Engineering Department, whose broad knowledge in numerical modeling impressed me very much. His valuable advice helped me to refine the numerical model in this study. Meanwhile, I would like to thank other members of my supervisory committee for their advice, feedback and consent to serve in my dissertation committee: Dr. Shuting Lei from Industrial & Manufacturing Systems Engineering Department and Dr. Haiyan Wang from Statistics Department. I also thank

Dr. Vikas Berry from Chemical Engineering Department to serve as the chairperson of my examining committee.

In addition, I would like to thank our department head, Dr. Bradley A. Kramer for all his help and support to my research work and all the other department staff for their assistance and the research facilities provided.

Thanks are also due to the support from my family. Family members' support encourages me to walk in this long journey. I must thank my husband, Chunlin Ye, whose unconditional love and support have been a bright light that shines on me even in the darkest hours, who motivated me and kept my spirit high whenever I wanted to give up. I love you and wouldn't change anything. To my mother and father, mother-in-law, and father-in-law, I am sorry for the long distance that separates us and sorrow the long distance has caused, and thank you for your undivided love and wishing me always the best.

I would like to acknowledge my colleagues and friends: Peifeng Zhang, Qi Zhang, Weilong Cong, Meng Zhang, Xiaoxu Song, Zhenzhen Shi, Nikhil Churi, S.H. Chou, Yanhui Lu, Xin Xie, Bellerive Adam, Stephanie Perry, and everyone else that has an impact on me.

It is impossible to personally thank everyone who has facilitated successful completion of a project. To those of you who I did not specifically name, I also give my thanks for moving me towards my goal.

Dedication

I would like to dedicate this work to my family. It would not have been possible without their love and support.

Chapter 1 - Introduction

1.1 Background of UVAG process

Ultrasonic-vibration-assisted grinding (UVAG), developed from ultrasonic machining (USM) [1], is a hybrid machining process for hard-to-machine materials. It combines material removal mechanisms of diamond grinding and ultrasonic machining. As shown in Figure 1.1, a rotating diamond core drill is ultrasonically vibrated while being fed into the workpiece at a constant pressure or a constant feedrate. Coolant pumped through the core of the drill washes away the swarf, prevents jamming of the drill and keeps it cool.

Figure 1.1 Illustration of ultrasonic-vibration-assisted grinding (after [2])

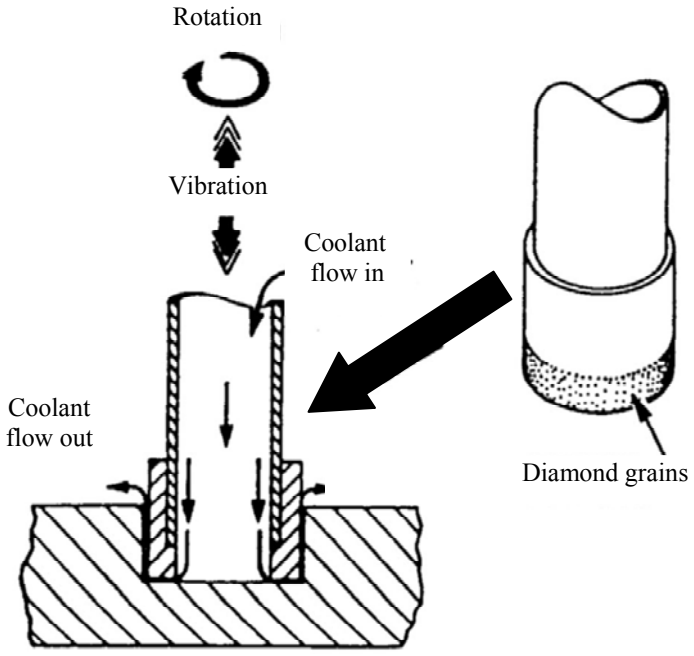

In USM, the slurry has to be fed to and removed from the gap between tool and workpiece, resulting in low material removal rate (MRR) especially with increase of penetrating depth, wear of the machined hole wall when the slurry passes back towards the surface, low accuracy, and severe tool wear by the abrasives in slurry [1].

In order to overcome the shortcoming of USM, UVAG was invented in 1964 by Percy Legge, a technical officer at United Kingdom Atomic Energy Authority (UKAEA) [3]. In UVAG, the slurry in USM is replaced with abrasives bonded to a tool. UVAG gets much higher material removal rate than USM, clean cuts [1,3], low energy input [4] while maintaining low cutting pressures and torque [5], reduced chipping and breakout [4], little surface damage and consequently strength reduction, improved accuracy, and low tool wear [6].

1.2 Motivations, objective, and significance of this research

A lot of research work on UVAG has been carried out since it was invented [7-21]. Most of published papers focus on effects of input variables in UVAG of ductile and brittle materials on its performances by conducting experiments. Reported modeling work on UVAG is concentrated on predicting MRR. However, these existing models were developed for one type of UVAG machines that use constant pressure (or force) to feed the tool into the workpiece. These models do not apply to another type of machines that employ constant feedrate (instead of constant pressure). For this type of UVAG machines, there is no need to predict MRR since MRR is determined by feedrate. A thorough literature survey did not produce any report on mechanism of UVAG with constant feedrate. In addition, edge chipping is one of the technical challenges associated with UVAG of brittle materials, and cutting tool is one important factor,

but there is no report related to effects of cutting tool design on edge chipping in UVAG of brittle materials either.

The objective of the research is to provide new knowledge of machining hard-to-machine materials with UVAG. Specific research tasks are as follows:

1. Developing a physics-based predictive model for cutting force in drilling ductile materials (Ti) with UVAG and verifying the developed model through experiments.
2. Developing a mechanistic model for cutting force in UVAG of brittle materials (silicon and ceramics) and verifying the developed model through experiments.
3. Studying interaction effects of input variables on cutting force in UVAG of ductile materials.
4. Studying interaction effects of input variables on cutting force in UVAG of brittle materials.
5. Developing an FEA model to investigate edge chipping with three different cutting tools, and effects of tool angle, wall thickness of tool, and process variables on edge chipping, and verifying the simulation results by experiments.

Knowledge generated from this research will fill gaps in the literature on UVAG of hard-to-machine materials under the condition of constant feedrate. Results from this research can also help in understanding other vibration-assisted machining processes. In addition, The results in this dissertation also can provide theoretical guidance for choosing reasonable process variables and designing diamond drilling tools and UVAG equipment, and will benefit industries where hard-to-machine materials is widely used and its machining (especially drilling) is required.

1.3 Research approaches

This research investigates the fundamental mechanisms in UVAG of hard-to-machine materials theoretically, numerically, and experimentally. As for the theoretical research work, two predictive models for cutting force in UVAG of hard-to-machine materials are developed based on physics and experiments. These models can be used to investigate effects of six input variables on cutting force. As for the numerical research work, a finite element analysis is conducted to investigate effects of cutting tool design on edge chipping. When it comes to the experimental research work, experiments are conducted to investigate effects of process variables on edge chipping in UVAG of brittle materials, and also to verify the results obtained from models and finite element analysis.

1.4 Outline of this dissertation

This dissertation is divided into eight chapters. Chapter 1 is an introduction presenting the background, motivations, objective, significance, and outline of this dissertation. Chapter 2 reviews the literature on experimental investigations of UVAG. Experimental results are summarized and compared. The inconsistent results and their reasons are discussed. Furthermore, directions of future research on UVAG are also presented.

The physics-based predictive model and mechanistic model for cutting force in UVAG of ductile and brittle materials are developed in Chapter 3 and 4 respectively. In both chapters, the model development is first described step by step. Afterwards, using the developed model, influences of input variables (diamond grain number, diamond grain size, vibration amplitude, vibration frequency, spindle speed, and feedrate) on cutting force (and on intermediate variables

used in some steps of the model development) are predicted. Finally, these predicted influences are compared with experimental results.

Based on the developed models, full-factorial design of experiments is utilized to study the main effects and interaction effects of input variables on cutting force systematically for UVAG of ductile and brittle materials in Chapters 5 and 6, respectively. In Chapter 7, finite element analysis is utilized to study three cutting tool designs and six process variables on edge chipping in UVAG of brittle materials and the simulation results are verified by experiments. Chapter 8 summarizes the achievements and conclusions of this research.

References

[1] Prabhakar, D., Ferreira, P.M., and Haselkorn, M., 1992, "An Experimental Investigation of Material Removal Rates in Rotary Ultrasonic Machining," Transactions of the North American Manufacturing Research Institute of SME, **10**, pp. 211-218.

[2] Stinton, D., 1988, "Assessment of the State of the Art Machining and Surface Preparation of Ceramics," ORNL/TM Report No. 10791, Oak Ridge National Laboratory, Oak Ridge, TN.

[3] Legge, P., 1966, "Machining without Abrasive Slurry," Ultrasonics, **2**, pp. 157-162.

[4] Cleave, D. V., 1976, "Ultrasonics Gets Bigger Jobs in Machining and Welding," *Iron Age,* September 13, pp. 69-72.

[5] J. Cusumano, J. Huber, and K.T. Marshall, Ultrasonic drilling of boron fiber composite, Modern plastics, 52 (6), 1974 pp. 88-90.

[6] A.I. Markov et al., Ultrasonic drilling and milling of hard non-metallic materials with diamond tools, Machine and Tooling 48 (9) (1977) 45-47.

[7] Churi, N.J., Li, Z.C., Pei, Z.J., and Treadwell, C., 2005, "Rotary Ultrasonic Machining of Titanium Alloy: A Feasibility Study," *Proc. 2005 ASME International Mechanical Engineering Congress and Exposition (IMECE),* November 5-11, 2005, Orlando, FL, Vol. 16-2, pp. 885-892.

[8] Churi, N.J., Li, Z.C., Pei, Z.J., and Treadwell, C., 2006, "Rotary Ultrasonic Machining of Titanium Alloy: Effects of Machining Variables," Mach. Sci. Tech., **10**(3), pp. 301-321.

[9] Churi, N.J., Li, Z.C., Pei, Z.J., and Treadwell, C., 2007, "Rotary Ultrasonic Machining of Titanium Alloy (Ti-6Al-4V): Effects of Tool Variables," Int. J. of Precision Technology, **1**(1), pp. 85-96.

[10] Churi, N.J., Li, Z.C., Pei, Z.J., and Treadwell, C., 2007, "Wheel Wear Mechanisms in Rotary Ultrasonic Machining of Titanium," *Proc. 2007 ASME International Mechanical Engineering Congress and Exposition (IMECE),* November 11-15, 2007, Seattle, WA, Vol. 3, pp. 399-407.

[11] Kubota, M., Tamura, Y., and Shimamura, N., 1977, "Ultrasonic Machining with a Diamond Impregnated Tool," Bull. Jpn. Soc. Precis. Eng., **11**(3), pp. 127-132.

[12] Markov, A., 1977, "Ultrasonic Drilling and Milling of Hard Non-Metallic Materials with Diamond Tools," Machine and Tooling, **48**(9), pp. 45-47.

[13] Pei, Z.J., Prabhakar, D., Ferreira, P.M., and Haselkorn, M., 1995, "Rotary Ultrasonic Drilling and Milling of Ceramics," Ceram Trans, **48**, pp. 185-196.

[14] Petrukha, P., 1970, "Ultrasonic Diamond Drilling of Deep Holes in Brittle Materials," Russ. Eng. J., **50**(10), pp. 70-74.

[15] Prabhakar, D., 1992, "Machining Advanced Ceramic Materials Using Rotary Ultrasonic Machining Process," MS Thesis, University of Illinois at Urbana-Champaign, Illinois, USA.

[16] Wang, H., and Lin, L., 1993, "Improvement of Rotary Ultrasonic Deep Hole Drilling of Glass Ceramics-Zerodur," *Proc. 7th International Precision Engineering Seminar,* The Japan Society of Applied Physics, Kobe, Japan, pp. 719-730.

[17] Pei, Z.J., and Ferreira, P.M., 1998, "Modeling of Ductile-Mode Material Removal in Rotary Ultrasonic Machining," Int. J. Mach. Tool. Manufact., **38**(10-11), pp. 1399-1418.

[18] Pei, Z.J., Prabhakar, D., Ferreira, P.M., and Haselkorn, M., 1995, "A Mechanistic Approach to the Prediction of Material Removal Rates in Rotary Ultrasonic Machining," J. Eng. for Industry, **177**(2), pp. 142-151.

[19] Zhang, Q.H., Wu, C.L., Sun, J.L., and Jia, Z.X., 2000, "Mechanism of Material Removal in Ultrasonic Drilling of Engineering Ceramics," *Proc. Institution of Mechanical Engineers, Part B: Journal of Engineering Manufacture,* **214**(9), pp. 805-810.

[20] Chao, C.L., Chou, W.C., Chao, C.W., and Chen, C.C., 2007, "Material Removal Mechanisms Involved in Rotary Ultrasonic Machining of Brittle Materials," Key Engineering Materials, **329**, pp. 391-396.

[21] Prabhakar, D., Pei, Z.J., Ferreira, P.M., and Haselkorn, M., 1993, "A Theoretical Model for Predicting Material Removal Rates in Rotary Ultrasonic Machining of Ceramics," Transactions of the North American Manufacturing Research Institute of SME, **21**, pp. 167-172.

Chapter 2 - Literature review

Paper Title:

Experimental investigations on Ultrasonic-Vibration-Assisted Grinding- A review

Authors' Names:

Na Qin[a,b], Z. J. Pei[a],. D. M. Guo[b]

Authors' Affiliation:

[a]Department of Industrial and Manufacturing Systems Engineering, Kansas State University, Manhattan, KS 66506, USA

[b]School of Mechanical Engineering, Dalian University of Technology, Dalian, Liaoning 116024, China

Abstract

Ultrasonic-vibration-assisted grinding (UVAG), a hybrid machining process combining material removal mechanisms of diamond grinding and ultrasonic machining, has been used to machine various hard-to-machine materials. Large amount of research work on UVAG has been carried out since it is invented. However, there are no review papers to cover the current literature on UVAG. This paper reviews the literature on experimental investigations of UVAG. Experimental results are summarized and compared. The inconsistent results and their reasons are discussed. Furthermore, directions of future research on UVAG are also presented.

2.1 Introduction

Ultrasonic-vibration-assisted grinding (UVAG), also known as rotary ultrasonic machining (RUM), is a hybrid process which combines material removal mechanisms of ultrasonic machining and diamond grinding. UVAG has the potential for high material removal rate (MRR) and clean cuts [1]. It is reported that UVAG has 6-10 times higher MRR than traditional grinding [2], and it is about 10 times faster than USM (ultrasonic machining) [3]. Tool pressure and torque in UVAG are low [3-4]. Lower pressure is especially helpful when drilling small holes, deep holes, or adjacent holes with thin dividing walls [3]. UVAG also brings in reduced edge chipping, breakout, and damage [3]. In addition, UVAG can easily fit in with traditional machines with some modifications [1]. Furthermore, UVAG can increase hole accuracy and reduce tool wear rate [5].

Large amount of research work on UVAG has been carried out since it is invented in 1964 [1-44]. In 1995, Pei et al. summarized the literature on UVAG of structural ceramics. They reviewed the development history of UVAG process and equipment, as well as experimental and theoretical studies [45]. In 2004 and 2006, Zeng et al. reviewed the literature on UVAG of ceramics, including MRR modeling, effects of five input variables on MRR and tool wear [33, 36]. In 2007, Churi et al. summarized the literature on UVAG of hard-to-machine materials, including alumina, silicon carbide, ceramic matrix composites, and titanium alloys. They reviewed effects of three input variables (rotational speed, feedrate, and ultrasonic power) on UVAG performances (cutting force, surface roughness, and edge chipping) [10]. More UVAG research results have been reported after these review papers were published, especially results from experimental investigations on UVAG. However, there are no systematical reviews to

include these new results.

This paper reviews experimental investigations on UVAG (while theoretical investigations and modeling work will be reviewed in a separate paper). It summarizes what has been done and what has not yet, as well as some inconsistent results in the literature. Directions of future research on UVAG are also discussed.

This paper is organized into nine sections. Following this introduction section, section 2.2 provides definitions and significance of UVAG input variables. Sections 2.3 to 2.7 present experimental investigations on five UVAG output variables (MRR, surface roughness, cutting force and torque, tool wear, and edge chipping), respectively. Section 2.8 contains concluding remark.

2.2 Definitions and significance of UVAG input variables

Figure 2.1 is a schematic illustration of UVAG. A rotating diamond core drill is ultrasonically vibrated while being fed into the workpiece at a constant pressure or a constant feed rate. Coolant pumped through the core of the drill washes away the swarf, prevents jamming of the drill and keeps it cool [1].

In this paper, experimental investigations using two types of machines (constant feedrate and constant pressure) are included. For the type of machines with constant feedrate, constant feedrate is applied on the tool (or workpiece) to feed the tool (or workpiece) towards the workpiece (or tool), and cutting force is variable. For the other type of machines, constant pressure is applied on the tool (or workpiece) to feed the tool (or workpiece) towards the workpiece (or tool), and feedrate is variable.

Figure 2.1 Illustration of ultrasonic-vibration-assisted grinding (after [46])

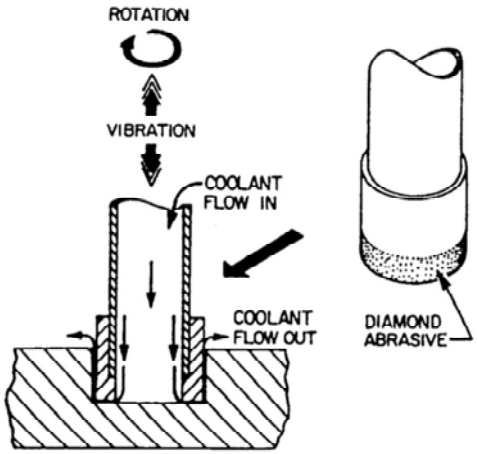

Important input variables in UVAG can be classified into three categories:

- Variables related to cutting tool: diamond type, diamond grain size, diamond concentration, bond type, tool geometry (number of slots, outer diameter, chamfer direction and angle, and wall thickness);
- Variables related to process: ultrasonic vibration amplitude, ultrasonic vibration frequency, tool rotational speed, and feedrate or pressure;
- Other variables: workpiece material type, coolant delivery mode, and support length of workpiece (which is the radial length of the contact area between workpiece and fixture).

2.2.1 Diamond type

The cutting tool used in UVAG is a core drill. The end portion of the drill contains bonded abrasives, as shown in Figure 2.1. Diamond grains are commonly used in UVAG [47]. Two types of diamond are reported for UVAG: natural and synthetic diamond [43].

One grade of nature diamond (A16) and three grades of synthetic diamond (SAM, ASP 16, ASV 16) are reported [28]. One grade of nature diamond (A16) and three grades of synthetic diamond (SAM, ASP 16, ASV 16) are reported [28].

2.2.2 Diamond grain size

The grain size of diamond abrasives in UVAG is usually expressed as mesh size. It corresponds to the number of openings per linear inch in the wire gauze used to "size" abrasive grains. But this wire gauze is employed primarily for sizes ranging from mesh #4 to mesh #240 [47]. For smaller grain sizes, the diameter of the abrasive grains is used to express the abrasive grain size [48].

Different diamond grain sizes are reported in UVAG. For example, mesh 40/50, mesh 40/170, mesh 60/80, mesh 80/100 [7], mesh 270/325 [13], mesh 315/400 [5], mesh 60-800 [15], mesh 100-240 [49], mesh 80 [31], mesh 325, mesh 500, mesh 600, mesh 800 [30], 50-220 μm [1], 50-250 μm [28], and 181μm [50].

2.2.3 Diamond concentration

Diamond concentration is defined as the weight of the diamond in each cubic inch of the bond material. "When 72 carats of diamonds are added in 1 cubic inch of bond material, then the diamond concentration is called as 100 concentration" [51]; when 54 carats of diamond grains

are added in 1 cubic inch of bond material, then the diamond concentration is called as 75 concentration. Each increase or decrease of 18 carats will cause the concentration to change by 25% [51].

Diamond concentration is a crucial characteristic of diamond tools [28, 51]. It is related to the grinding or cutting efficiency and the machining costs. “If the concentration is too high, many diamonds will fall off the tool prematurely, resulting in waste of the diamonds. If it is too low, the grinding efficiency will be reduced” [51]. In reported investigations on UVAG of brittle materials, the concentration used ranged from 50 to 200 [4-5, 15, 28, 30].

2.2.4 Bond type

Bond material in the cutting tool holds diamond grains in place and plays an important role in determining the cutting tool’s performance [52-53]. The physical and mechanical properties of the bond substantially influence the cutting properties of a cutting tool[28]. There are three common types of bond: resin, ceramic, and metal [51]. Electroplate and sinter are two methods for fabricating diamond cutting tool [17, 54]. Most electroplated tools have only one layer of diamond coated on a steel body. Diamonds sit only on the surface of the tool. The cutting tool will slow down when the diamond portion is worn out or peeled off. Sintered tools have diamond sintered in a matrix made of various metal combinations. Multiple layers of diamonds are impregnated inside the metal matrix. This means that sintered tools have diamond content throughout the tip of the drill. The metal bond must wear away to continuously keep re-exposing for the diamond tool to continue cutting [54].

Different bond-types change workpiece/tool hardness ratio. This ratio is inversely proportional to penetration depth of a diamond grain into workpiece, and consequently different

bond-types result in different penetration depth of diamond grains into workpiece in each ultrasonic cycle [1].

Diamond tools with metal bonds are used in UVAG [1, 5, 15, 17, 30, 49]. Bronze-bonded, steel-bonded, brass-copper alloy bonded, and iron-nickel alloy bonded were reported.

2.2.5 Tool geometry (number of slots, outer diameter, chamfer direction and angle, and wall thickness)

Slots are designed on the end surface of cutting tool as shown in Figure 2.2. The number of slots can be 0, 2, or 4. They will influence the coolant flow rate during cutting process, and then influence MRR, surface roughness of workpiece, cutting force, and tool wear [6, 35].

Figure 2.2 Illustration of UVAG cutting tool with slots (after [6])

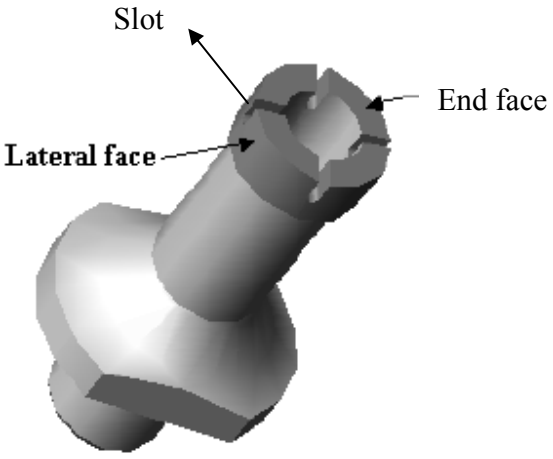

Since the cutting tool is hollow, it has outer and inner diameters. Wall thickness is 1/2 of the difference between outer diameter and inner diameter. Wall thickness has a significant effect

on MRR and cutting force [14, 24]. In addition, according to the chamfer direction, three types of tool are defined: normal, inner, and outer tools, as shown in Figure 2.3. Also, chamfer direction and angle, and wall thickness have significant effects on edge chipping [55].

Figure 2.3 Schematic illustration of angle for three cutting tools

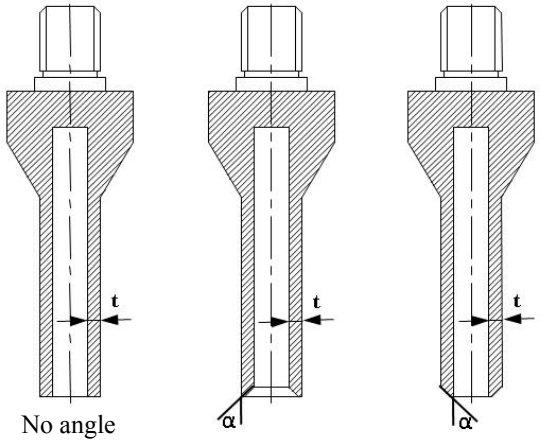

(a) Normal tool (b) Inner tool (c) Outer tool

2.2.6 Ultrasonic vibration amplitude

Ultrasonic power supply converts electrical supply to high-frequency electrical impulses. These impulses are fed to a piezoelectric transducer and transformed into mechanical vibrations of ultrasonic frequency, and the vibration amplitude is then amplified by a horn and transmitted to the tool. Ultrasonic vibration amplitude of the cutting tool is an important input variable since it is a measure of the amount of energy input per cycle [2, 5].

The vibration amplitude of tool for different power settings can be measured by an optical vibration sensing system. Power settings ranging from 0 to 100% are related to different vibration amplitudes [2]. Both power percentage and vibration amplitude are used to express the vibration amplitude of cutting tool.

These vibration amplitudes are reported in the literature: 2-5 μm [31], 2-16 μm [28], 3-15 μm [5], 10-23 um [50] , 10-50 μm [15], 23-33 μm [2], and 20-50% [8, 11].

2.2.7 Ultrasonic vibration frequency

Testing has shown that 20 kHz systems appear to be the most efficient of the three frequency (16, 20, 40 kHz) [4]. The gripping of the drill bit becomes more difficult at higher frequencies [4].

The following ultrasonic vibration frequencies are reported in the literature: 16-24 kHz [17], 17.4 -40 kHz [15], 19.5 - 20.5 kHz [50], 24.5-43.5 kHz [28], 16, 20, 40 kHz [2, 4, 31], and 42.5 kHz [5].

2.2.8 Rotational speed

Rotational speed refers to the rotational speed (rpm, or revolution per minute) of workpiece or cutting tool (Figure 2.1 shows an example for rotational cutting tool). Either of them rotates around the axis of symmetry at a certain speed during UVAG.

The following rotational speeds are reported in the literature: 0-5000 rpm [50], 50-5000 rpm [56], 450-540 rpm [31], 500-1600 rpm [49], 900 rpm [15, 57], 1000-3000 rpm [2], 2000-5000 rpm [8, 11], 4000-6100 rpm [4], 2000 rpm [5], and 2420 rpm [28].

2.2.9 Feedrate

Feedrate refers to the rate at which cutting tool (or workpiece) is fed towards workpiece (or tool). These feedrates are reported in the literature: 0.008-0.015 mm/s [7], 0.02-0.05 mm/s [21], 0.06-0.25 mm/s, 0.07-1.67 mm/s [31], and 0.09-0.16 mm/s [13, 22], 0.55-1.16 mm/s [28].

2.2.10 Constant pressure

Constant pressure has a great effect on MRR [45]. In the literature, these values of constant pressure are used: 3-4 psi [49], 22-32 psi [2], 427 psi [28], 100-1137 psi [15], and 284-1137 psi [5].

2.2.11 Workpiece material type

There are many types of workpiece materials reported in the literature, and they can be classified into two types: brittle materials and ductile materials. Several brittle materials (Al2O3, CMC, Dental ceramics, SiC, Poly-crystallin, Mg/ZirO2, Quartz glass) have been studied, and two ductile materials (titanium and stainless steel) were reported.

2.2.12 Coolant delivery mode

Two coolant delivery modes have been investigated: continuous mode and intermittent mode. With continuous mode, coolant is delivered at a constant pressure, as shown in Figure 2.4 (a). Intermittent model delivers coolant at alternative pressures between on and off states, as shown in Figure 2.4 (b). In practice, the intermittent mode was utilized approximately as shown in Figure 2.4 (c).

Figure 2.4 Different coolant delivery modes in UVAG [23]

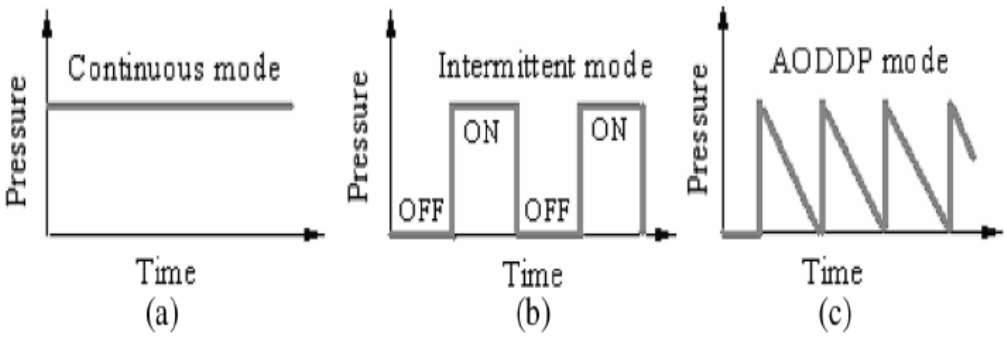

2.2.13 Support length of workpiece

Support length of workpiece is the radial length of the contact area between workpiece and fixture, as shown in Figure 2.5. It is determined by the diameter of the hole in the fixture. This hole is used to receive the rod drilled from workpiece.

Figure 2.5 Schematic illustration of support length of workpiece in UVAG

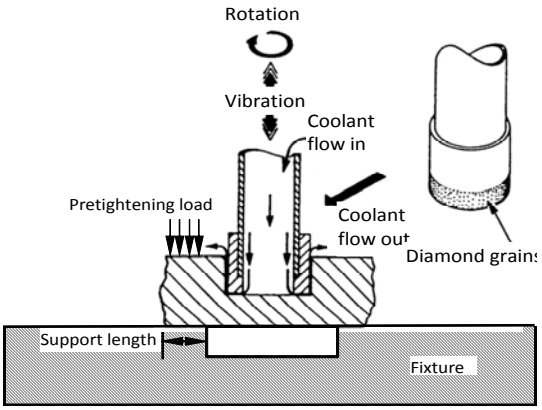

2.3 Experimental investigations on material removal rate

Material removal rate in UVAG was calculated by the following equation [1, 5-6, 8, 12, 15, 22-23, 28, 31, 51] :

$$MRR = \frac{\text{Volume of material removal}}{\text{Time}} = \frac{\pi L\left[\frac{D_o^2}{4} - \frac{D_i^2}{4}\right]}{T} \quad (1)$$

Where, Do is outer diameter of cutting tool, Di inner diameter of cutting tool, L length of drilled hole, and T the time it takes to drill the hole.

Table 2.1 summarizes experimental investigations on MRR reported in the literature. Five workpiece materials (Ti, Al2O3, CMC, Mg/ZrO2, glass) were tested, and ten of the 13 variables described in section 2.2 were studied for brittle materials and only four of them were studied for ductile materials.

Table 2.1 Experimental investigations on MRR in UVAG

Input variable	Ductile workpiece material	Brittle workpiece material	Reference
Diamond grain size	*	Al2O3, Mg/ZrO2, Glass	[2, 12, 15, 28]
Diamond	*	Glass	[28]
Diamond type	*	Glass	[28]
Bond type	*	Mg/ZrO2, Glass	[2, 28]
Vibration amplitude	Ti	Al2O3, CMC, Mg/ZrO2, Glass	[2, 8, 12, 15, 22, 28,
Vibration frequency	*	Glass	[28]
Rotational speed	Ti	Al2O3, CMC, Mg/ZrO2,Glass	[2, 8, 12, 15, 22, 31]
Feedrate	Ti	Al2O3, CMC	[8, 12, 22]
Workpiece material	*	*	
Support length	*	*	
Tool design	Ti	*	[22]
Static force	*	Mg/ZrO2, Glass	[2, 15, 31]
Diameter of tool	*	Glass	[44]

* Means that no reports are available

Using a constant feedrate system, MRR was only affected by feedrate, and proportional to feedrate in UVAG of Ti and Al2O3 [6, 8]. While in UVAG of CMC (ceramic matrix composites), MRR was not only affected by feedrate, but also by rotational speed and vibration amplitude, and increased with increase of all of these three input variables, but no interaction effects were found [22]. However, in UVAG of Al2O3, feedrate, rotational speed, and vibration amplitude have significant interaction effects on MRR [12].

For experimental investigations using a constant pressure system, two types of workpiece materials (magnesia stabilized zirconia and glass) were tested. In UVAG of magnesia stabilized zirconia (Mg/ZrO2), four input variables (constant pressure, vibration amplitude, rotational speed, and grain size) has significant effects on MRR and constant pressure had the most significant effects. MRR increased with increase of all the four input variables. There existed some two-factor interaction effects on MRR [2]. In UVAG of glass, with increase of vibration amplitude, constant pressure, and diamond concentration, MRR increased first, and then decreased. In addition, high strength synthetic cutting (synthetic cutting single-crystals) gives higher MRR than natural cutting, but natural cutting has a lower wear rate and surface roughness than synthetic cutting [28]. As rotational speed and feedrate increased, MRR increased [5, 15, 28, 31].

It can be seen that, in constant pressure system, experimental results are inconsistent. Most of the input variables have significant effects on MRR, and there exist two interaction effects. However, in constant feedrate system, different experimental results are obtained when drilling different workpiece materials. In addition, the mechanical properties of workpiece may act as an important factor in UVAG. But no effects of workpiece mechanical properties on MRR have been reported.

2.4 Experimental investigations on surface roughness

Surface roughness (Ra) of both machined rod surface and hole surface is measured along the feed direction by a surface profilometer (contact mode) [6, 8-9, 11, 33, 58-59]. It is also measured by microscope ZKM01-250C (non-contact mode) [30]. Although the contact method can more accurately measure the surface roughness of the drilled hole along the axial direction, the traveling length is limited, and is not easy to adjust the instrument vs. specimen. Ra, Pt and Rq are used to measure the surface roughness of the hole [30], where Pt is the vertical distance between the highest peak and the lowest valley of the unfiltered profile [60].

Table 2.2 Experimental investigations on surface roughness in UVAG

Input variable	Ductile workpiece material	Brittle workpiece material	Reference
Diamond grain size	Ti	Al_2O_3, SiC, Glass, Zerodur	[7, 9, 12, 28]
Diamond concentration	Ti	Glass	[9, 28]
Bond type	Ti	Glass	[9, 28]
Diamond type	*	Glass	[28]
Ultrasonic vibration amplitude	Ti and stainless steel	Al_2O_3, Dental ceramics, SiC, Glass	[7-8, 11-12, 28, 32]
Ultrasonic vibration frequency	*	Glass	[28]
Rotational speed	Ti and stainless steel	Al_2O_3, Dental ceramics, SiC	[7-8, 11-12, 32]
Feedrate	Ti and stainless steel	Al_2O_3, Dental ceramics, SiC	[7-8, 11-12, 32]
Workpiece material	*	Poly-crystalline	[21]
Support length	*	*	
Tool design	Ti	*	[6]
Static force	*	Glass	[2]
Diameter of tool	*	*	

* Means that no reports are available

Experimental investigations on surface roughness reported in the literature are summarized in Table 2.2. According to this table, five brittle materials (Al2O3, dental ceramics, SiC, poly-crystalline, and glass) and two ductile materials (Ti and stainless steel) were studied. Ten of the 13 parameters described in section 2.2 were studied for brittle materials and seven of them were studied for ductile materials.

Compared with cutting grinding, UVAG produces lower Ra. Ra could also be improved by applying different coolant delivery modes [23]. According to the experimental results provided in the literature, with different workpiece materials, tool slots have different influences on Ra. In UVAG of Ti, higher Ra was observed with slots than without. But in UVAG of hot-press alumina, lower Ra was obtained with slots [6, 35]. In addition, Ra was proportional to diamond grain size, and inversely proportional to rotational speed except for UVAG of dental ceramics. In UVAG of dental ceramics, Ra increased first and then decreased as rotational speed increased. In UVAG of Al2O3, the rotational speed ranged from 1000 rpm to 4000 rpm [35], while in UVAG of dental ceramics, it ranged from 2000 rpm to 5000 rpm [11].

When it comes to feedrate and vibration amplitude, inconsistent results were obtained. In UVAG of SiC, Ra is proportional to federate [7], in UVAG of Al2O3, feedrate had no obvious effects on Ra [35] or Ra was proportional to feedrate [12], and in UVAG of dental ceramics, there existed an optimum feedrate that produced the lowest Ra [11]. In addition, there were no interaction effects on Ra in UVAG of SiC [7], while in UVAG of Al2O3 and stainless steel, significant interaction effects existed [12, 59].

The most obvious inconsistence has been observed regarding the effects of vibration amplitude. In UVAG of dental ceramics, Ra increased first and then decreased as vibration amplitude increased [11, 28]. In contrast, in UVAG of Al2O3, Ra decreased first and then

increased [35] or did not change much as vibration amplitude changed [12]. In UVAG of SiC, Ra was inversely proportional to vibration amplitude [7].

2.5 Experimental investigations on cutting force

Cutting force was investigated in constant feedrate systems. It is directly related to cutting temperature, surface roughness, workpiece accuracy, and surface residual stress, etc. The average or maximum cutting force along the feedrate direction was measured by a KISTLER 9257 or 9272 dynamometer [6-9, 11-13, 20, 22, 58-59].

Table 2.3 Experimental investigations on cutting force in UVAG

Input variable	Ductile workpiece material	Brittle workpiece material	Reference
Diamond grain size	Ti	Al_2O_3, SiC	[7, 9, 12]
Diamond concentration	Ti	*	[9]
Bond type	Ti	*	[9]
Diamond type	*	*	
Ultrasonic vibration amplitude	Ti and stainless steel	Al_2O_3, Dental ceramics, SiC, CMC	[7-8, 11-12, 22, 32, 58]
Ultrasonic vibration frequency	*	*	
Rotational speed	Ti and stainless steel	Al_2O_3, Dental ceramics, SiC, CMC	[7-8, 11-12, 22, 32, 58]
Feedrate	Ti and stainless steel	Al_2O_3, Dental ceramics, SiC, CMC	[7-8, 11-12, 22, 32, 58]
Workpiece material	*	Poly-crystalline, ZrO_2/ Al_2O_3	[21, 24]
Support length	*	Al_2O_3	[39]
Tool design	Ti	*	[6]
Diameter of tool	*	*	

* Means that no reports are available

Table 2.3 summarizes experimental investigations on cutting force reported in the literature. According to this table, six brittle materials (Al2O3, ZrO2/ Al2O3, dental ceramics,

SiC, poly-crystalline, CMC) and two ductile materials (Ti and stainless steel) were studied. Seven of the 12 input variables were studied for ductile materials and six of them were studied for brittle materials [7-8, 11-12, 21-22, 32].

Cutting force in UVAG was lower than that in diamond grinding. It was also lower with slots than that without slots in UVAG of Ti [6, 35], but there was no obvious difference when drilling alumina [35]. For all the experimental results given in the literature, cutting force increased with increase of feedrate and diamond grain size. But it decreased as rotational speed increased except for CMC. In UVAG of CMC, no obvious effects of rotational speed on cutting force were observed.

Inconsistence also existed regarding the effects of vibration amplitude. Six experiments have been conducted for UVAG of brittle and ductile materials, five of them were for brittle materials and one for ductile materials. Four of the six were DOE experiments (design of experiment) for four workpiece materials (SiC, CMC, Al2O3, stainless steel). No obvious effects of vibration amplitude have shown in the DOE experiments of brittle materials but obvious effects of vibration amplitude existed in UVAG of stainless steel. In the other two experiments, cutting force decreased first and then increased in one experiment, while decreased all the time in the other one as vibration amplitude increased. In addition, interaction effects existed in UVAG of SiC, alumina, and stainless steel, but not in UVAG of CMC. Cutting force was affected by mechanical properties (fracture toughness and hardness) and microstructure of workpiece materials [24].

2.6 Experimental investigations on tool wear

Diamond grains on the tool may have attritious wear, grain fracture, grain pullout and

catastrophic failure during machining process [38, 61-66]. “Attritious wear refers to a type of wear where sharp edges of an abrasive grain become dull due to attrition by workpiece material, developing flat areas” [38, 61] as shown in Figure 2.6. “Attritious wear increases the area of wear flats and determines the magnitude of the grinding force and quality of the ground surface” [38]. Grain fracture causes the abrasive fragment to be removed within the grain and the fractured area exposes new cutting edges [38]. Grain pullout refers to a type of wear where the diamond grains on the wheels were dislodged prematurely, before completing their effective working lives, as shown in Figure 2.7. Catastrophic failure refers to cracking of metal bond and diamond grains. This type of failure will cause sudden failure (breakage) of the cutting tool as the number of drilled holes increase. Since cracking of metal bond has more significant effects on cutting tool life, it is more undesirable than cracking of diamond grain [38].

Figure 2.6 Attritious wear [38]

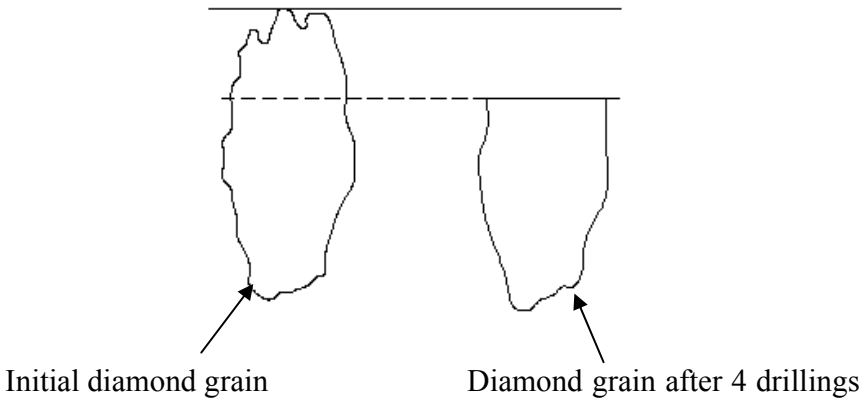

Bond fracture may happen during diamond grinding [38, 61, 66]. It refers to a type of wear where “the bond material is eroded. The bond strength is reduced and diamond grain

dislodgement is promoted due to bond fracture. Bond fracture is responsible for the self-sharpening of grinding wheels and loss of form and size of the grinding wheels".

Figure 2.7 Diamond pull out [38]

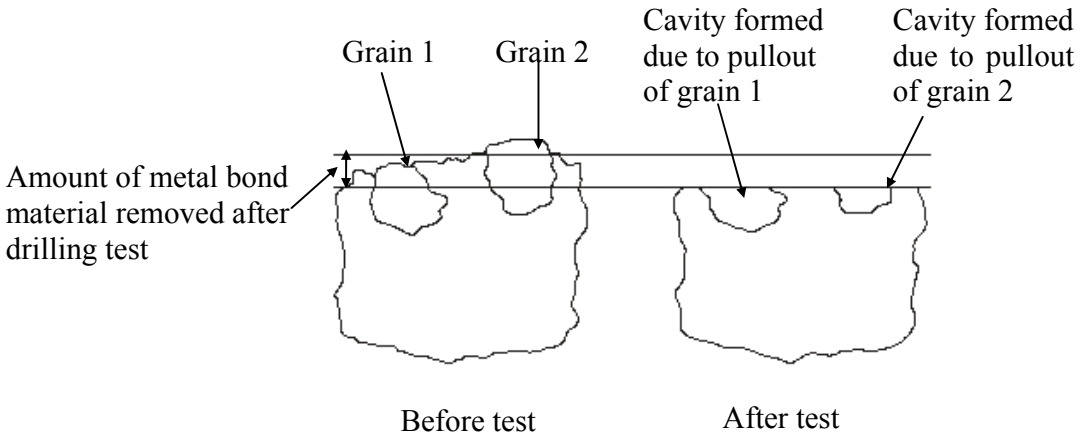

In UVAG, tool wear could be measured by the difference between two length measurements along the axial direction before and after each test. The tool length of the core drill was measured by a vernier caliper [6, 9]. Tool wear could also be measured by wear ratio, the ratio of the volume of material removed by tool to the volume of tool wear [28]. The tool wear was also observed by digital microscope [33-34, 37-38].

Table 2.4 summarizes experimental investigations on tool wear reported in the literature. Only one brittle material (glass) and one ductile material (Ti) were tested by two researchers, respectively. Six of the 13 input variables were studied for glass and four of them were studied for Ti.

Little research has been done for tool wear in UVAG. Two of these investigations were conducted to study influences of input variables on tool wear [9, 28]. Others were done to find the phenomena related to tool wear [21, 34, 37-38]. Due to poor machinability of ductile material Ti, more tool wear was observed in Ti UVAG than in UVAG of brittle materials. Tool wear in UVAG is lower than that in diamond grinding. Tool with slots has higher wear rate than without slots [6].

Table 2.4 Experimental investigations on tool wear in UVAG

Input variable	Ductile workpiece material	Brittle workpiece material	Reference
Diamond grain size	Ti	Glass	[9, 28]
Diamond concentration	Ti	Glass	[9, 28]
Bond type	Ti	Glass	[9, 28]
Diamond type	*	Glass	[28]
Ultrasonic vibration amplitude	*	Glass	[28]
Ultrasonic vibration frequency	*	Glass	[28]
Rotational speed	*	*	
Feedrate	*	*	
Workpiece Material	*	*	
Support length	*	*	
Tool design	Ti	*	[6]
Static force	*	*	
Diameter of tool	*	*	

* Means that no reports are available

2.7 Experimental investigations on edge chipping

During UVAG of brittle materials, "there is a tendency for machined rod to break-off before the tool has cut through the workpiece. This phenomenon gives rise to edge chipping at the exit of hole" [11]. Edge chipping includes two parameters: chipping thickness and size. They were measured on the rod or on the hole, as shown in Figure 2.8, and by a vernier caliper or a

microscope [11, 20].

Edge chipping is not acceptable on finished workpieces, since it “not only compromises geometric accuracy, but also causes possible failure of the component during service” [67], so it has to be machined off by extra processes after UVAG. The larger the edge-chipping thickness, the higher the total machining cost. Furthermore, it was stated that Ra is not enough to estimate hole quality in CMC drilling, and “chippings are the key barrier of drilling high-quality holes on CMC panels”, so chipping size and thickness were utilized to estimate the hole quality in UVAG of CMC [22].

Figure 2.8 Illustration of edge chipping [20]

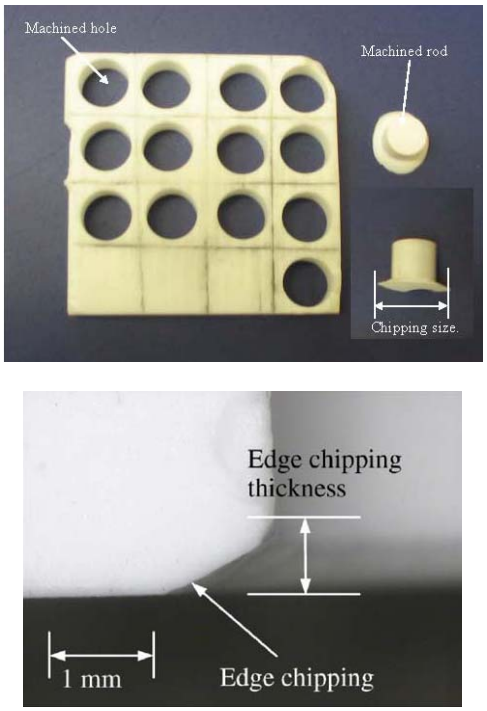

Experimental investigations on edge chipping of brittle materials are summarized in Table 2.5. Four materials and five input variables were studied. It was found that chipping thickness and size were inversely proportional to rotational speed and diamond grain size and proportional to feedrate and vibration amplitude [7, 11, 13, 20, 22, 67]. In UVAG of SiC, no significant interactions has been found [7], while in UVAG of CMC and alumina, there existed interaction effects among input variables [13, 22]. In addition, it was reported that edge-chipping thickness could be reduced by increasing the support length [20, 39]. However, no research has been reported on effects of tool design up to date.

Table 2.5 Experimental investigations on edge chipping in UVAG

Input variable	Brittle workpiece material	Reference
Diamond grain size	Al2O3, SiC	[7, 12-13]
Diamond concentration	*	
Bond type	*	
Diamond type	*	
Ultrasonic vibration amplitude	Al2O3, Dental ceramics, SiC, CMC	[7, 11-13, 22]
Ultrasonic vibration frequency	*	
Spindle speed	Al2O3, Dental ceramics, SiC, CMC	[7, 11-13, 22]
Feedrate	Al2O3, Dental ceramics, SiC, CMC	[7, 11-13, 22]
Material mechanical property	*	
Support length	Al2O3	[20]
Tool design	*	
Static force	*	
Diameter of tool	*	

* Means that no reports are available

2.8 Concluding remarks

Large amount of research work on UVAG has been carried out. The research work focused on theoretical and experimental investigations. This paper reviewed the literature on

experimental investigations of UVAG. Tables 2.1-2.5 summarize experimental investigations reported on five output variables.

According to these tables, among all reported experimental investigations, only two types of ductile materials (Ti and stainless steel) have been investigated and all the experiments were conducted by the same research group. Also, totally only seven input variables are studied in their experiments. Thus, in order to comprehensively understand the mechanisms of UVAG of ductile materials, one future research direction could be to investigate more input variables and with more types of ductile materials.

From section 2.3 to section 2.7, mechanical properties of workpiece material may play an important role for the inconsistences among reported experimental results. However, no reports have been focused on this topic. In order to understand and explain these inconsistences, mechanical properties of workpiece material could be the third research direction.

Several DOE experiments have been conducted to study interaction effects of input variables on output variables. It has been showed that even for same workpiece material, different researchers got different experiment results. This may be due to their different experimental conditions, but also may be due to large number of input variables and data range of variables. Ultrasonic vibration amplitude, rotational speed and feedrate are the most frequently studied input variables. Higher cost and longer duration of time will be required to study other input variables, such as diamond grain size and concentration, bond type and diamond type, and diameter of tool. Especially, vibration frequency cannot be changed on most UVAG machines since it was usually fixed when the machines were built.

The last direction could be about tool wear. Only little research was done on this topic. Many input variables can affect tool wear, such as tool design, machining variables, coolant,

workpiece, etc. Effects of most of these input variables on tool wear have not been systematically studied.

Acknowledgements

This study was supported by the National Science Foundation through the Award CMMI-0900462**.**

References

[1] Prabhakar, D., 1992, "Machining Advanced Ceramic Materials Using Rotary Ultrasonic Machining Process," MS Thesis, University of Illinois at Urbana-Champaign, Illinois, USA.

[2] Prabhakar, D., Ferreira, P.M., and Haselkorn, M., 1992, "An Experimental Investigation of Material Removal Rates in Rotary Ultrasonic Machining," Transactions of the North American Manufacturing Research Institute of SME, **10**, pp. 211-218.

[3] Cleave, D.V., 1976, "Ultrasonic Gets Bigger Jobs in Machining and Welding," Iron Age, **218** (11), pp. 69-72.

[4] Cusumano, J., Huber, J., and Marshall, K.T., 1974, "Ultrasonic Drilling of Boron Fiber Composite". Modern plastics, **52** (6), pp. 88-90.

[5] Markov, A., 1977, "Ultrasonic Drilling and Milling of Hard Non-Metallic Materials with Diamond Tools," Machine and Tooling, **48** (9), pp. 45-47.

[6] Churi, N.J., Li, Z.C., Pei, Z.J., and Treadwell, C., 2005, "Rotary Ultrasonic Machining of Titanium Alloy: A Feasibility Study," Proceedings of International Mechanical Engineering Congress and Exposition (IMECE), Orlando, FL, pp. 885-892.

[7] Churi, N.J., Pei, Z.J., Treadwell, C., and Shorter, D., 2007, "Rotary Ultrasonic Machining of Silicon Carbide: Designed Experiments," International Journal of Manufacturing Technology and Management, **12** (1-3), pp. 284-298.

[8] Churi, N.J., Li, Z.C., Pei, Z.J., and Treadwell, C., 2006, "Rotary Ultrasonic Machining of Titanium Alloy: Effects of Machining Variables," Mach. Sci. Tech., **10** (3), pp. 301-321.

[9] Churi, N.J., Li, Z.C., Pei, Z.J., and Treadwell, C., 2007, "Rotary Ultrasonic Machining of Titanium Alloy (Ti-6Al-4V): Effects of Tool Variables," International Journal of Precision Technology, **1** (1), pp. 85-96.

[10] Churi, N. J., Pei, Z. J., and Treadwell, C., 2007, "Experimental Investigations on Rotary Ultrasonic Machining of Hard-to-Machine Materials". Materials Processing under the Influence of External Fields, Proceedings of the 2007 TMS Annual Meeting & Exhibition, Orlando, FL, pp. 139-144.

[11] Churi, N.J., Pei, Z.J., Treadwell, C., and Shorter, D.C., 2009, "Rotary Ultrasonic Machining of Dental Ceramics," International Journal of Machining and Machinability of Materials, **6** (3-4), pp. 270-284.

[12] Jiao, Y., Hu, P., Pei, Z.J., and Treadwell, C., 2005, "Rotary Ultrasonic Machining of Ceramics: design of experiments," International Journal of Manufacturing Technology and Management, **7** (2-4), pp. 192-206.

[13] Jiao, Y., Liu, W. J., and Pei, Z. J., 2005,"Study on Edge Chipping in Rotary Ultrasonic Machining on Ceramics: An Integration of Designed Experiment and FEM Analysis," Journal of Manufacturing Science and Engineering, **127** (4), pp. 752-758.

[14] Komaraiah, M., and Reddy, P N., 1991, "Rotary Ultrasonic Machining -- A New Cutting Process and Its Performance," International Journal of Production Research, **29** (11), pp. 2177-2187.

[15] Kubota, M., Tamura, Y., and Shimamura, N., 1977, "Ultrasonic Machining with a Diamond Impregnated Tool," Bulletin of Japanese Society of Process Engineer, **11** (3), pp. 127-132.

[16] Kuo, L. K., 2008, "A Study of Glass Milling Using Rotary Ultrasonic Machining," Key Engineering Materials, **364-366**, pp. 624-628.

[17] Legge, P., 1964, "Ultrasonic Drilling of Ceramics. Industrial Diamond Review," **24** (278), pp. 20-24.

[18] Legge, P., 1966, "Machining without Abrasive Slurry," Ultrasonics, pp. 157-162.

[19] Li, R., 2007, "Experimental and Numerical Analysis of High-Throughput Drilling of Titanium Alloys," Ph.D. thesis, University of Michigan, MI, USA.

[20] Li, Z.C., Cai, L.W., Pei, Z.J., and Treadwell, C., 2006, “Edge-Chipping Reduction in Rotary Ultrasonic Machining of Ceramics: Finite Element Analysis and Experimental Verification,” International Journal of Machine Tools and Manufacture, **46**, pp. 1469-1477.

[21] Li, Z.C., Jiao, Y., and Deines, T.W., 2004, "Experimental Study on Rotary Ultrasonic Machining of Poly-Crystalline Diamond Compact," Proceedings of 2004 IIE annual conference and exhibition, Houston, Texas, pp. 769-774.

[22] Li, Z.C., Jiao, Y., Deines, T.W., Pei, Z.J., and Treadwell, C., 2005, "Rotary Ultrasonic Machining of Ceramic Matrix Composites: Feasibility Study and Designed Experiments," International Journal of Machine Tools and Manufacture, **45**, pp. 1402-1411.

[23] Li, Z.C., Jiao, Y., Deines, T.W., and Pei, Z.J., 2005, "Development of Innovative Coolant System for Rotary Ultrasonic Machining," International Journal of Manufacturing Technology and Management, 7 (4), pp. 318-328.

[24] Li, Z.C., Pei, Z.J., Kwon, P., Zeng, W.M., and Treadwell, C., 2005, "Experimental Study on Cutting Force in Rotary Ultrasonic Machining Of Zicronia/Alumina Composites," Transactions of the North American Manufacturing Research Institute of SME, **33**, pp. 89-96.

[25] Markov, A.I., 1966, Ultrasonic Machining of Intractable Materials (translated from Russian), Illife Books, London.

[26] Markov, A.I., and Ustinov, I.D., 1972, "A Study of the Ultrasonic Diamond Drilling of Nonmetallic Materials," Industrial Diamond Review, pp. 97-99.

[27] Markov, A.I., 1970, "Ultrasonic Drilling of Deep Holes in Quartz, with A Bonded Abrasive-Diamond Tool," Electrophysical and Electrochemical Methods of Machining, NIIMASh, No. 5-6 (Quoted in Petrukha et al.).

[28] Petrukha, P.G., 1970, “Ultrasonic Diamond Drilling of Deep Holes in Brittle Materials,” Journal of Russian engineering, **50** (10), pp. 70-74.

[29] Tyrrell, W.R., 1970, “Rotary Ultrasonic Machining,” SME Technical Paper, MR70-516.

[30] Wang, H., and Lin, L., 1993, “Improvement of Rotary Ultrasonic Deep Hole Drilling of Glass Ceramics-Zerodur,” Proceedings of the 7th International Precision Engineering Seminar, The Japan Society of Applied Physics, Kobe, Japan, pp. 719-730.

[31] Ya, G., Qin, H.W., and Xu, Y.W., 2001, "An Experimental Investigation on Rotary Ultrasonic Machining," Key Engineering Materials**, 202-203**, pp. 277-280.

[32] Zeng, W.M., Li, Z.C., Churi, N. J., and Pei, Z. J., 2004, "Experimental Investigation into Rotary Ultrasonic Machining of Alumina," Proceedings of 2004 ASME International Mechanical Engineering Congress and Exposition, Anaheim, California, USA.

[33] Zeng, W.M., Li, Z.C., Pei, Z. J., and Churi, N. J., 2004, "Tool Wear in Rotary Ultrasonic Machining of Advanced Ceramics," 7th International Conference on Progress of Machining Technology, Shuzhou, China.

[34] Zeng, W.M., Li, Z.C., Pei, Z.J., and Treadwell, C., 2005, “Experimental Observation of Tool Wear in Rotary Ultrasonic Machining of Advanced Ceramics,” International Journal of Machine Tools and Manufacture, **45** (12–13), pp.1468–1473.

[35] Zeng, W.M., Li, Z.C., Xu, X.P., Pei, Z.J., Liu, J.D., and Pi, J., 2008, “Experimental Investigation of Intermittent Rotary Ultrasonic Machining,” Key Engineering Materials, **359-360**, pp.425-430.

[36] Zeng, W.M., Xu, X.P., and Pei, Z.J., 2006, “Rotary Ultrasonic Machining of Advanced Ceramics,” Materials Science Forum, **532-533**, pp. 361-364.

[37] Zeng, W.M., Xu, X.P., and Pei, Z.J., 2009, "Experimental Investigation of Tool Wear in Rotary Ultrasonic Machining of Alumina," Key engineering materials, **416**, pp. 182-186.

[38] Churi, N. J., Pei, Z.J., and Treadwell, C., 2007, "Wheel Wear Mechanisms in Rotary Ultrasonic Machining of Titanium," Proceedings of 2007 ASME International Mechanical Engineering Congress and Exposition, Seattle, Washington, USA.

[39] Li, Z.C., Cai, L.W., Pei, Z. J., and Treadwell, C., 2004, "Finite Element Simulation of Rotary Ultrasonic Machining of Advanced Ceramics," Proceeding of ASME International Mechanical Engineering Congress and Exposition, Anaheim, CA, USA.

[40] Pei, Z. J., and Ferreira, P.M., 1998, "Modeling of Ductile-Mode Material Removal in Rotary Ultrasonic Machining," International Journal of Machine Tools and Manufacture, **38** (10-11), pp. 1399-1418.

[41] Pei, Z. J., Ferreira, P.M., and Haseikorn, M., 1995, "Plastic Flow in Rotary Ultrasonic Machining of Ceramics," Journal of Material Processing Technology, **48**, pp. 771-777.

[42] Pei, Z. J., Prabhakar, D., Ferreira, P.M., and Haselkorn, M., 1995, "A Mechanistic Approach to the Prediction of Material Removal Rates in Rotary Ultrasonic Machining," Journal of Engineering for Industry, **117** (2), pp. 142-151.

[43] Prabhakar, D., Pei, Z. J., Ferreira, P.M., 1993, "A Theoretical Model for Predicting Material Removal Rates in Rotary Ultrasonic Machining of Ceramics," Transactions of the North American Manufacturing Research Institution of SME, XXI, pp. 167-172.

[44] Komaraiah, M., Mananm, A., and Narasimbam, P., 1988, "Investigation of Surface Roughness and Accuracy in Ultrasonic Machining," Precision Engineering, 10 (2), pp. 59-65.

[45] Pei, Z. J., Khann, N., and Ferrira, P.M., 1995, "Rotary Ultrasonic Machining of Structure Ceramics-A Review," Ceramic Engineering and Science Proceedings, 16 (1), pp. 259-278.

[46] Stinton, D.P., 1988, "Assessment of the State of the Art in Machining and Surface Preparation of Ceramics," ORNL/ TM-10791 [R], Oak Ridge:Oak Ridge National Laboratory.

[47] Salmon, S.C., 1992, "Modern Grinding Process Technology," New York, McGraw-Hill,

[48] Qin, N., Pei, Z. J., and Fisher, G. R., 2009, "Simultaneous Double-Side Grinding of Silicon Wafers: A Review and Analysis of Experimental Investigations," Machining Science and Technology, **13** (3), pp. 285-316.

[49] Hards, K.W. 1966, "Ultrasonic Speed Diamond Machining," Ceramics Age, **82** (12), pp. 34-36.

[50] Dam, H., Jensen, J., and Quist, P., 1993, "Surface Characterization of Ultrasonic Machined Ceramics With Diamond Impregnated Sonotrode," Machining of Advanced Materials, NIST Special Publication, **847**, pp. 125-133.

[51] Http://www.diamondbladeselect.com/tips/diamond-tools-how-to-choose-diamond-concentration.

[52] Jackson, M. J., 2002, "Wear of Perfectly Sharp Abrasive Grinding Wheels," Transactions of North American Manufacturing Research Institution of SME 30, pp. 287-294.

[53] Stoica, G. F., Capitanescu, C., and Biolan A.I., 2003, "Wear Behavior of Thin Coatings Based on Diamond". Proceedings of National Tribology Conference, pp. 133-135.

[54] http://www.ukam.com/diamond_drill_guide.htm.

[55] Qin, N., Pei, Z.J., Cong, W.L., and Guo, D.M., 2010, "Effects of Tool Design on Edge Chipping in Ultrasonic-Vibration-Assisted Grinding," Proceedings of the 2010 International Manufacturing Science & Engineering Conference (MSEC), Erie, Pennsylvania, USA.

[56] Kremer, D., Lhiaubet, C., and Moisan, A., 1991, "A Study of the Effect Of Synchronizing Ultrasonic Vibrations with Pulse in EDM," Annals of CIRP, **40** (1), pp. 211-214.

[57] Graff, K.F., 1975, "Ultrasonic Machining," Ultrasonics, 1**3** (3), pp. 103-109.

[58] Cong, W.L, Pei, Z.J., Churi, N.J., and Wang, Q.G., "Rotary Ultrasonic Machining of Stainless Steel: Design of Experiments," Transactions of the North American Manufacturing Research Institution of SME, **37**, pp. 261-268.

[59] Cong, W.L, Pei, Z.J., Wang, Q.G., 2009, "Surface Roughness in Rotary Ultrasonic Machining of Stainless Steels," Proceedings of the IIE Annual Conference and Expo 2009 – Innovations Revealed, Miami, FL.

[60] Thomas, T.R., 1999, "Rough Surfaces," London, Imperial College Press.

[61] Malkin, S., 1989, "Theory and Applications of Machining with Abrasives," Chichester, West Sussex, United Kingdom.

[62] Sathyanarayanan, G., and Pandit, S., 1985, "Fracture and Attritious Wear in Grinding by Data Dependent System," 13th North American Manufacturing Research Conference Proceedings, Manufacturing Engineering Transactions, University of California, Los Angeles, pp. 314-320.

[63] Xie, Z., Moon, R., and Hoffman, M., 2003, "Role of Microstructure in the Grinding and Polishing of A-Sialon Ceramics," Journal of European Ceramic Society, **23** (13), PP. 2351-2360.

[64] Cho, S., Huh, Y., and Yoon, K., 1994, "Aspects in Grinding of Ceramics," Journal of American Ceramic Society, **77** (9), pp. 2443-2444.

[65] Hagiwara, S., Obikawa, T., and Iwata, S., 1994, "Edge Fracture Characteristics of Diamond Grains in Stone Grinding Process," Nippon Kikai Gakkai Ronbunshu, **60** (577), pp. 2917-2923.

[66] Shi, Z., Malkin, S,. 2003, "An Investigation of Grinding with Electroplated CBN Wheels," CIRP Annals– Manufacturing technology, **52** (1), pp. 267-270.

[67] Ng, S., Le, D., and Tucker, S., 1996, "Control of Machining Induced Edge Chipping on Glass Ceramics," Proceedings of the 1996 ASME International Mechanical Engineering Congress and Exposition, Manufacturing Engineering Division, Atlanta, GA, pp. 229-236.

Chapter 3 - Cutting force model for ductile materials

The content of this chapter has been published in a journal paper.

Paper Title:

Physics-based predictive cutting force model in ultrasonic-vibration-assisted grinding for titanium drilling

Published in:

Journal of Manufacturing Science and Engineering, 2009, 131 (4): 041011-1-041011-9

Authors' Names:

Na Qin[a,c], Z. J. Pei[a],. Treadwell[b], D. M. Guo[c]

Authors' Affiliation:

[a]Department of Industrial and Manufacturing Systems Engineering, Kansas State University, Manhattan, KS 66506, USA

[b]Sonic-Mill, 7500 Bluewater Road N.W., Albuquerque, NM 87102, USA

[c]School of Mechanical Engineering, Dalian University of Technology, Dalian, Liaoning 116024, China

Abstract

Ultrasonic-vibration-assisted grinding (UVAG), or rotary ultrasonic machining (RUM), has been investigated both experimentally and theoretically. Effects of input variables on output variables in UVAG of brittle materials and titanium (Ti) have been studied experimentally. Models to predict material removal rate in UVAG of brittle materials have been developed. However, there is no report on models of cutting force in UVAG. This paper presents a physics-based predictive model of cutting force in UVAG of Ti. Using the model developed, influences of input variables on cutting force are predicted. These predicted influences are compared with those determined experimentally. This model can serve as a useful template and foundation for development of cutting force models in UVAG of other materials (such as ceramics and stainless steels) and models to predict torque, cutting temperature, tool wear, and surface roughness in UVAG.

Keywords: Cutting force; Drilling; Grinding; Machining; Titanium; Ultrasonic vibration.

3.1 Introduction

Titanium and its alloys (Ti) are attractive for many applications due to their superior properties [1]. These properties include high strength-to-weight ratio [2,3], creep strength, fatigue strength, fracture toughness, fabricability [1], heat and corrosion resistance at elevated temperature, and shock resistance [2,3]. Besides the aerospace industry that uses 60% of the titanium [4,5], Ti is also used in such industries as military [6,7], automotive [8], chemical [9,10], medical [11,12], and sporting goods [13].

Many Ti components require drilling operations. However, Ti is notorious for its poor machinability [14], resulting in high cost and low efficiency with current drilling methods.

Increasing use of Ti/composite stacks in the aerospace industry presents even greater challenges. Therefore, there is a critical need to develop more cost-effective Ti drilling processes.

Ultrasonic-vibration-assisted grinding (UVAG), also called rotary ultrasonic machining (RUM), has been used to drill Ti recently [15-18]. Figure 3.1 is the schematic illustration of UVAG. A rotary core drill with metal-bonded diamond grains is ultrasonically vibrated and fed towards the workpiece. Coolant pumped through the core of the drill washes away the swarf, prevents jamming of the drill and keeps it cool.

Figure 3.1 Illustration of ultrasonic-vibration-assisted grinding (after [19])

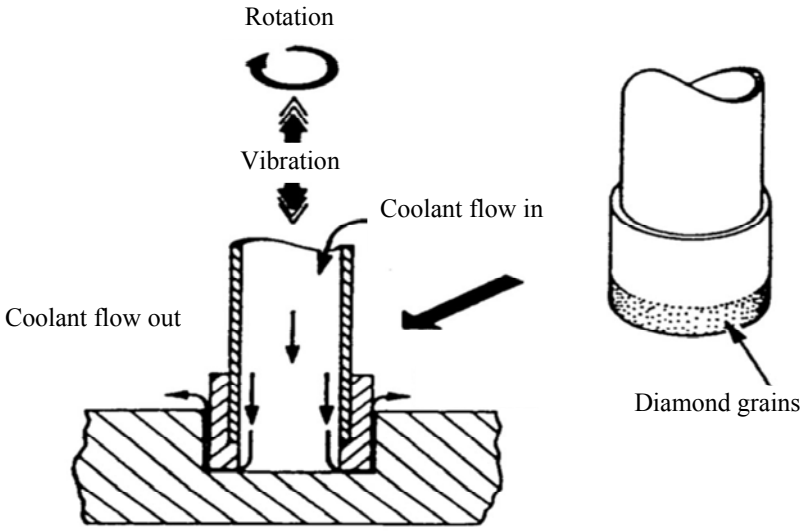

Since it was invented in 1960's [20], UVAG has been used primarily to drill brittle materials. Effects of input variables (diamond concentration, grain size, and type; bond type; vibration amplitude and frequency; spindle speed; and coolant type and pressure) on output variables (cutting force, material removal rate, and surface roughness) in UVAG of brittle materials have been investigated experimentally [21-27].

Churi et al. [15-18] were the first to perform feasibility experiments on UVAG of Ti. They also investigated effects of input variables (diamond concentration, diamond grain size, vibration power, spindle speed, and feedrate) on four output variables (cutting force, material removal rate, tool wear, and surface roughness) in UVAG of Ti.

In the literature, there are no physics-based models for UVAG of metals. For UVAG of ceramics, there exist several models [28-32] to predict material removal rate (MRR) but no physics-based models to predict cutting force. Furthermore, these existing models were developed for one type of UVAG machines that use constant pressure (or force) to feed the tool into the workpiece. These models do not apply to another type of machines that employ constant feedrate (instead of constant pressure). For this type of UVAG machines, there is no need to predict MRR since MRR is determined by feedrate. Physics-based models that can predict cutting force, cutting temperature, tool wear, and surface roughness will shed light on experimentally observed phenomena and provide fundamental understanding in UVAG of Ti.

This paper presents a physics-based predictive model for cutting force in UVAG of Ti. It first describes the model development step by step. Afterwards, using this developed model, it predicts influences of input variables (diamond grain number, diamond grain size, vibration amplitude, vibration frequency, spindle speed, and feedrate) on cutting force (and on

intermediate variables used in some steps of the model development). Finally, these predicted influences are compared with experimental results.

3.2 Model development

3.2.1 Approach to model development

Many grinding force models [33-38] began with an analysis of single abrasive grain. The total grinding force was then derived by summing up the forces on all abrasive grains taking part in cutting. A similar approach is used in this paper to develop the cutting force model in UVAG of Ti. Several assumptions and simplifications are listed below:

1) Diamond grains are rigid spheres of the same size;
2) Diamond grains located on the tool end surface have the same height, and all of them take part in cutting during each ultrasonic vibration cycle;
3) Workpiece material is rigid-plastic;

The volume of material removed by a diamond grain in one vibration cycle is approximately equal to the intersection volume between the diamond grain and the workpiece.

3.2.2 Relation between F_c and δ

In UVAG, the tool is fed into workpiece by a constant feedrate V. The tool is not in continuous contact with the workpiece due to its oscillatory motion. When a diamond grain penetrates into the workpiece to the maximum depth δ, the force acting on this diamond grain will be F_c / n, where F_c is the maximum contact force between the tool and workpiece and n the number of diamond grains taking part in cutting.

The interaction between a diamond grain and the workpiece may be considered as a penetration process. Since the workpiece material is assumed to be rigid-plastic, the penetration depth δ can be obtained by [39]:

$$\frac{F_c}{n} = \sigma_y B \tag{1}$$

Where,

F_c = maximum contact force between tool and workpiece

n = Number of diamond grains taking part in cutting

σ_y = Compressive strength of workpiece material

B = Projected area of the intersection between diamond grain and workpiece onto the plane of the workpiece surface

Figure 3.2 Relation between project area *B* and penetration depth *δ*

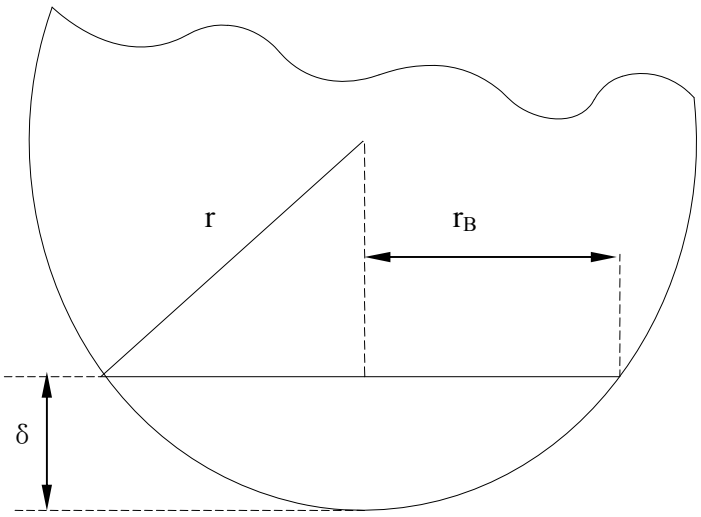

Since the diamond grains are assumed to be rigid spheres, penetration depth δ and B are related by the following equation (see Figure 3.2):

$$B = \pi\delta(2r - \delta) \tag{2}$$

where r is the radius of spherical diamond grains.

Combining Eqs. (1) and (2), the following relation between F_c and δ can be obtained:

$$\frac{F_c}{n} = \sigma_y \pi\delta(2r - \delta) \tag{3}$$

3.2.3 Relation between F and F_c

F_c is the maximum contact force between tool and workpiece. It is not the same as F, the cutting force observed during Ti UVAG experiments. The relation between F and F_c can be derived by equaling the impulse in terms of F_c to the impulse in terms of F during each vibration cycle.

Since it is assumed that the diamond grains are incompressible, the impulse in terms of the maximum contact force F_c during one cycle of ultrasonic vibration is:

$$\text{Impulse} = \int_{cycle} F_c dt \approx F_c \Delta t \tag{4}$$

where Δt is effective contact time (i.e. the period of time during which the diamond grains have penetrated into the workpiece). Δt can be obtained as follows.

Diamond grains on the tool end surface oscillate with an amplitude A and a frequency f. Their motions are sinusoidal. The position of each diamond grain relative to its mean position can be described by the following equation:

$$z = A \cdot \sin(2\pi f t) \tag{5}$$

Figure 3.3 Calculation of effective contact time Δt

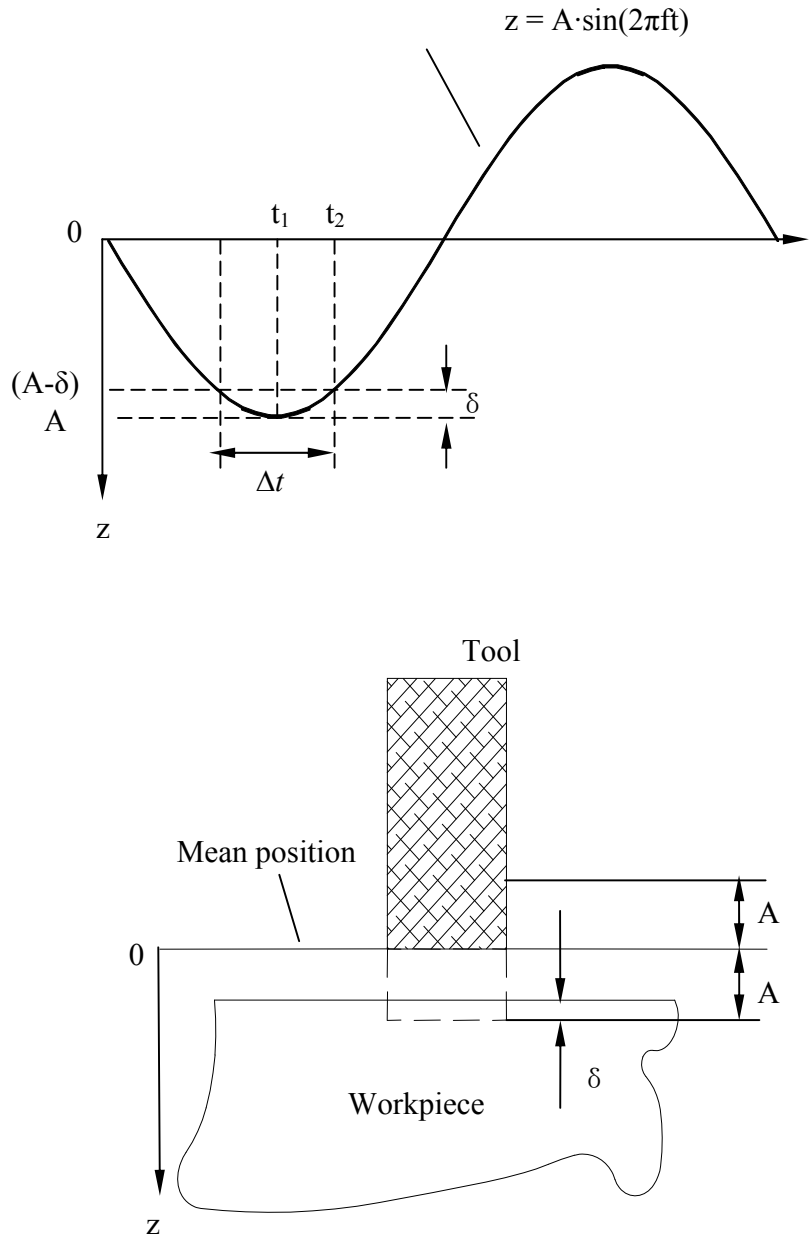

As illustrated in Figure 3.3, it will take a diamond grain $\frac{\Delta t}{2}$ to move from $z = (A - \delta)$ to $z = A$. So, Δt can be calculated using the following equation

$$\Delta t = 2(t_2 - t_1) = \frac{1}{\pi f} \times \left\{ \frac{\pi}{2} - \arcsin\left(1 - \frac{\delta}{A}\right) \right\} \tag{6}$$

The impulse in terms of the cutting force F during one cycle of ultrasonic vibration is:

$$\text{Impulse} = F\frac{1}{f} = \frac{F}{f} \tag{7}$$

By equating the two impulses in Eqs. (4) and (7),

$$\frac{F}{f} = F_c \Delta t \tag{8}$$

i.e.,

$$F = F_c \Delta t f \tag{9}$$

3.2.4 Relation between F and δ

Submitting Eqs. (3) and (6) to Eq. (9), cutting force F can be expressed as:

$$F = n\sigma_y \delta(2r - \delta)\left\{ \frac{\pi}{2} - \arcsin\left(1 - \frac{\delta}{A}\right) \right\} \tag{10}$$

On the right side of the above equation are σ_y (compressive strength of workpiece material), n (the number of diamond grains taking part in cutting), δ (the penetration depth of diamond grains into workpiece), r (diamond grain radius), and A (vibration amplitude). All of them except δ are known. So, if δ is determined, cutting force F can be predicted.

3.2.5 Relation between W and δ

W is the volume of material removed by a diamond grain during one vibration cycle. It is also the intersection volume between the diamond grain and workpiece. It was calculated using commercial software SolidWorks (SolidWorks Corp, Concord, Massachusetts, USA).

In ultrasonic-vibration-assisted grinding (UVAG), the tool oscillates up and down and rotates simultaneously. Therefore, each diamond grain on the tool end surface can be considered as moving along a sine curve. Figure 3.4 illustrates the volume each diamond grain sweeps during one vibration cycle. The envelope of this volume (diamond grain swept envelope or DGSE) is obtained in Solidworks by sweeping a circle ($w^2 + v^2 = r^2$) along the Sine curve:

$$X = \frac{\pi D_0 St}{60}$$

$$Y = 0 \tag{11}$$

$$Z = A\sin(2\pi ft)$$

where t is machining time (sec).

Figure 3.4 Diamond grain swept envelope (DGSE)

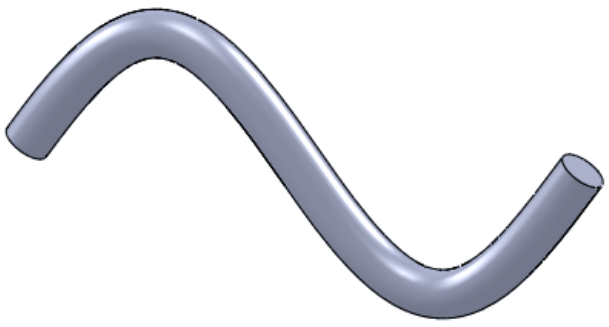

The two coordinate systems used to represent the circle and since curve are illustrated in Figure 3.5. The sine curve is in the x-z plane. The origin of the u-v-w coordinate system is always on the sine curve. The u axis is tangent to the sine wave. The u-w plane is in the x-z plane and the v axis is always parallel to the y axis.

In Solidworks, Eq. (11) was used to form the DGSE, as illustrated in Figure 3.6. Once the DGSE is obtained in Solidworks, for each value of W, a unique value of δ can be calculated.

Figure 3.5 Two coordinate systems for deriving DGSE

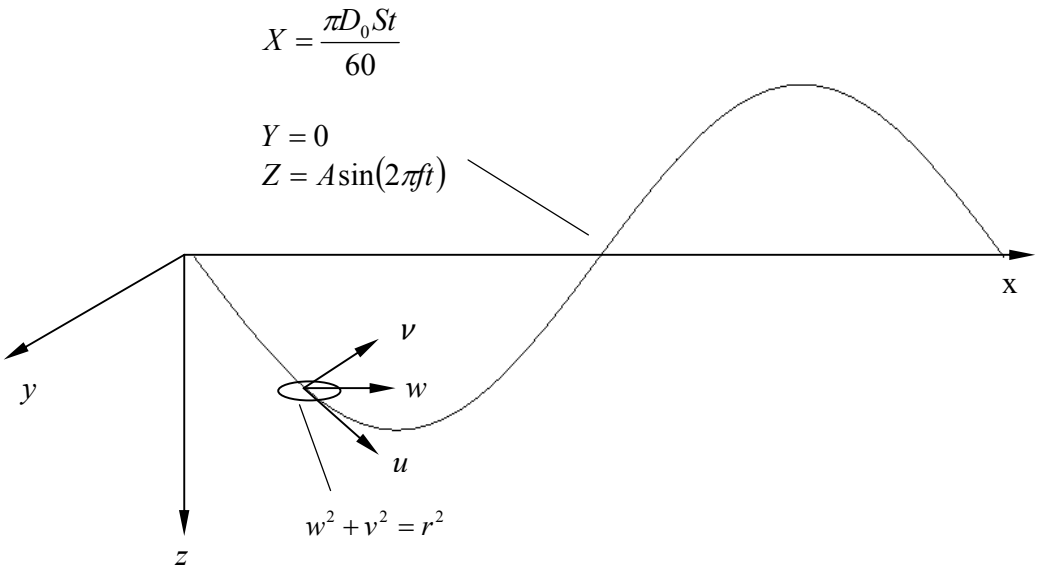

Figure 3.6 between intersection volume *W* and penetration depth *δ*

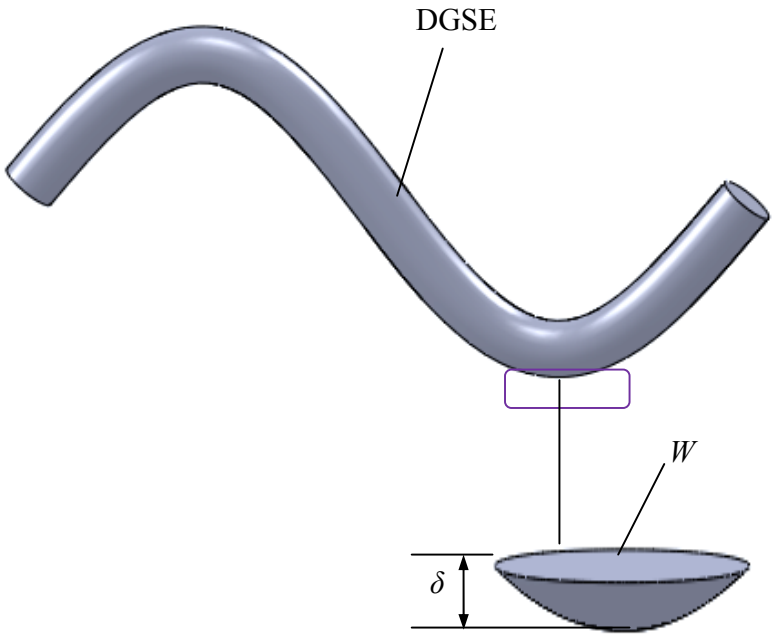

3.2.6 Relation between W and input variables

Material removal rate (MRR, mm^3/sec) can be obtained by:

$$MRR = nfw \tag{12}$$

It can also be expressed in terms of feedrate V ($mm \cdot s^{-1}$):

$$MRR = \frac{v\left(\pi D_0^2 - \pi D_i^2\right)}{4} \tag{13}$$

where D_0 and D_i are the outer and inner diameters of the cutting tool, (mm), respectively. From Eqs. (12) and (13), the relation between W and input variables can be expressed as:

$$w = \frac{\pi v\left(D_0^2 - D_i^2\right)}{4nf} \tag{14}$$

3.2.7 Relation between F and input variables

As shown in Eq. (10), cutting force F can be determined from indentation depth δ and four input variables (compressive strength of workpiece material σ_y, diamond grain number n, diamond grain radius r, and vibration amplitude A). δ can be obtained for every value of W using Solidworks once DGSE is determined by these input variables: outer diameter of cutting tool D_0, spindle speed S, vibration amplitude A, vibration frequency f, and diamond grain radius r. As shown in Eq. (13), W can be calculated from these input variables: feedrate V, outer diameter of cutting tool D_0, inner diameter of cutting tool D_i, diamond grain number n, and vibration frequency f. Therefore, cutting force F can be predicted from input variables.

3.3 Influences of input variables on cutting force

In the previous section, a physics-based predictive model was developed for the cutting force in UVAG of Ti. In this section, the developed model is used to predict how individual input variables influence the cutting force. Throughout the calculation, the compressive strength of Ti was taken as 370 N/mm^2, and the outer and inner diameters of cutting tool were 9.6 mm and 7.8 mm, respectively.

Predicted relations between cutting force F and diamond grain number n are plotted in Figure 3.7. Figure 3.8 shows changes of intermediate variables with diamond grain number n. As diamond grain number n increases, intersection volume W will decrease according to Eq. (14). When intersection volume W decreases, the penetration depth δ (calculated with

Solidworks) also decreases (note that DGSE will not be affected by a change in diamond grain number). A decrease in penetration depth δ will result in decrease in both contact force of single diamond grain $\frac{F_c}{n}$ (according to Eq. (3)) and effective contact time Δt (according to Eq. (6)). However, Contact force ($F_c = n\sigma_y \pi\delta(2r-\delta)$) will increase because diamond grain number n increases at a much faster rate than the rate at which penetration depth δ decreases. In Eq. (9), $F = F_c \Delta t f$, as diamond grain number n increases, vibration frequency f will remain unchanged, contact force F_c will increase at a much faster rate than the decreasing rate of effective contact time Δt, and therefore, cutting force F will increase.

Figure 3.7 Relation between diamond grain number and cutting force

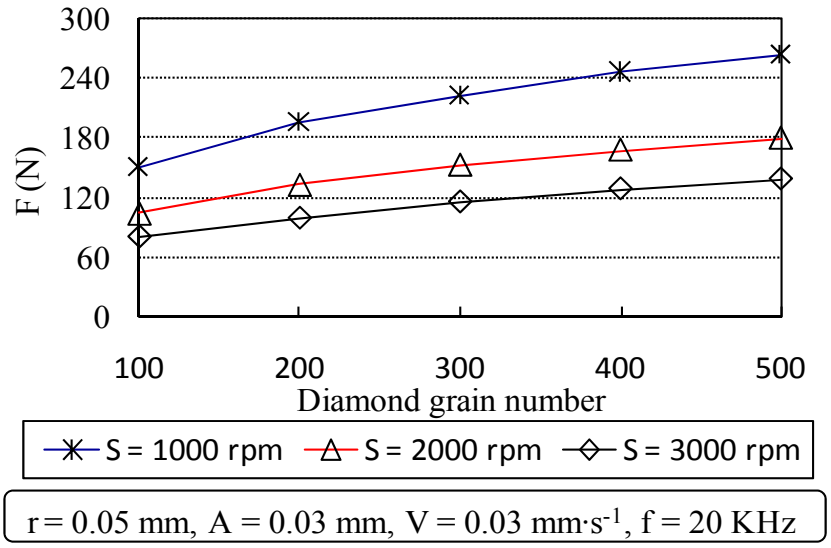

Figure 3.8 Influence of diamond grain number

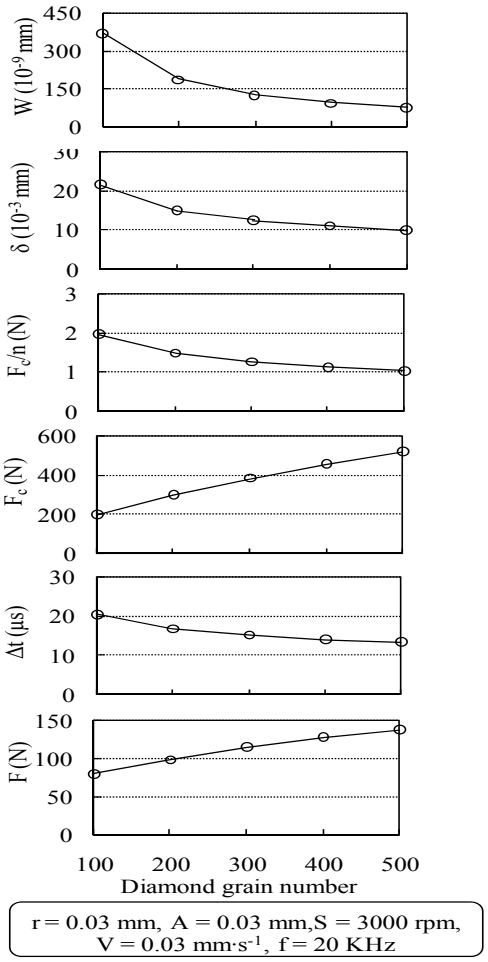

Predicted relations between cutting force F and diamond grain radius r are plotted in Figure 3.9. Changes of intermediate variables with diamond grain radius r are shown in Figure 3.10. As diamond grain radius r increases, the shape of DGSE will change as illustrated in Figure 3.11, while intersection volume W remains unchanged according to Eq. (14). Therefore, as diamond grain radius r increases, penetration depth δ will decrease to keep the intersection volume W unchanged, resulting in a decrease of effective contact time Δt according to Eq. (6).

Also, contact force F_c will increase according to Eq. (3). Furthermore, as diamond grain radius r increases, vibration frequency f will remain unchanged, contact force F_c will increase at a much faster rate than the decreasing rate of effective contact time Δt, and therefore, according to Eq. (9), cutting force F will increase.

Figure 3.9 Relation between diamond grain radius and cutting force

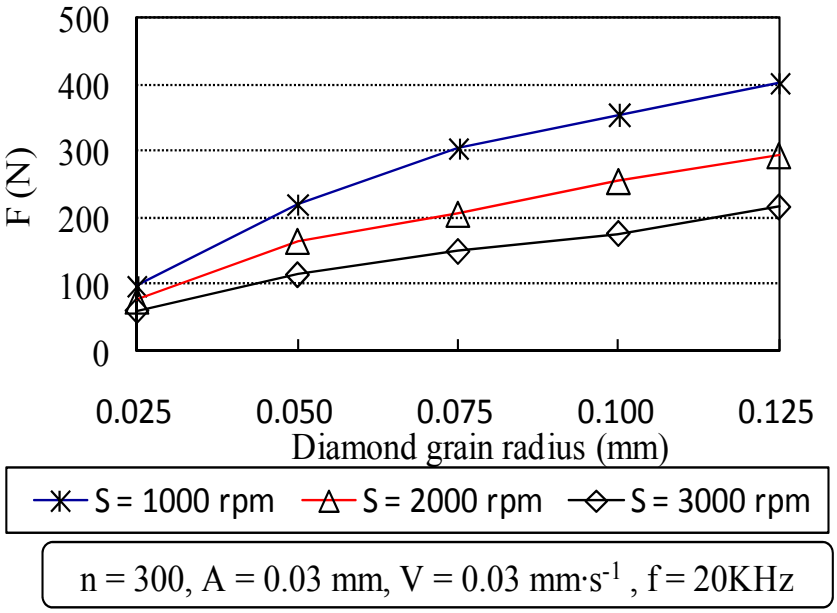

Figure 3.10 Influence of diamond grain radius

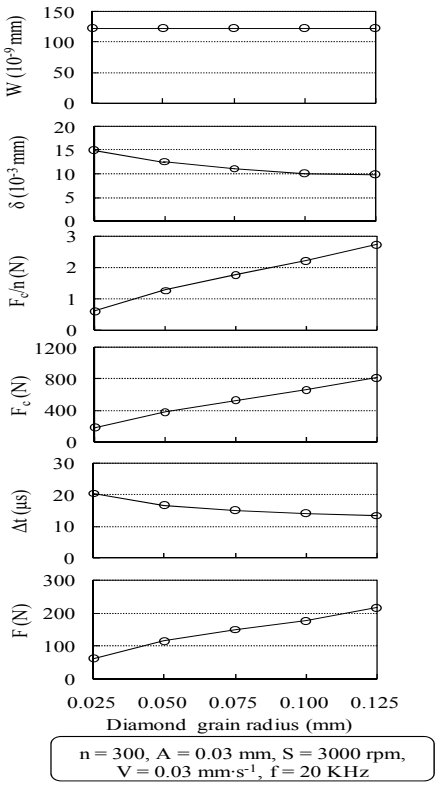

Predicted relations between cutting force F and vibration amplitude A are plotted in Figure 3.12. Figure 3.13 shows changes of intermediate variables with vibration amplitude A. As vibration amplitude A increases, the shape of DGSE will change as illustrated in Figure 3.14. As vibration amplitude A increases, intersection volume W remains unchanged according to Eq. (14), so penetration depth δ will have to increase. According to Eq. (3), contact force F_c will increase as penetration depth δ increases. Therefore, according to Eq. (6), effective contact time Δt will decrease. Finally, the decrease of effective contact time Δt overweighs the increase of contact force F_c, resulting in a decrease in cutting force F, according to Eq. (9).

Figure 3.11 Change in DGSE shape as diamond grain radius changes

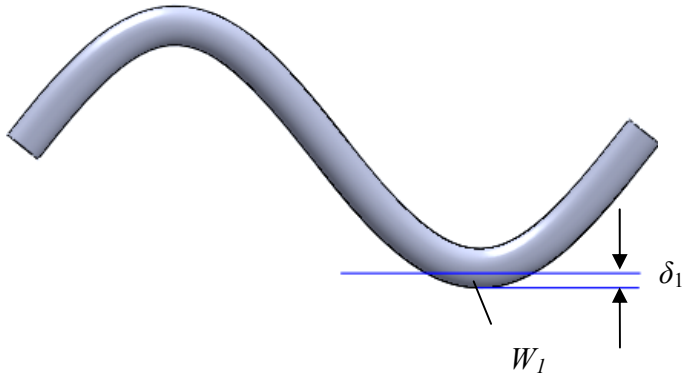

(a) $r = 0.025$ mm

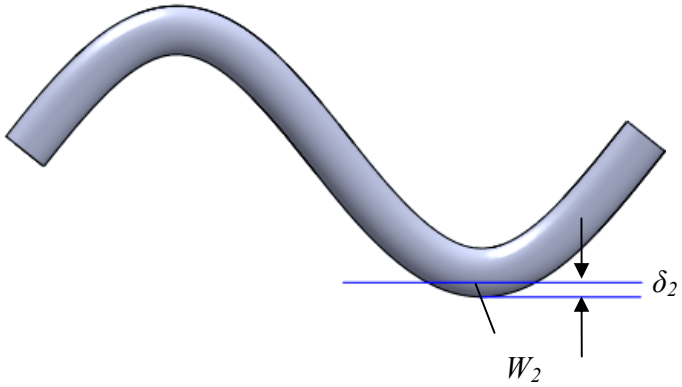

(b) $r = 0.03$ mm

$\delta_1 = \delta_2$, $W_1 < W_2$

Figure 3.12 Relation between vibration amplitude and cutting force

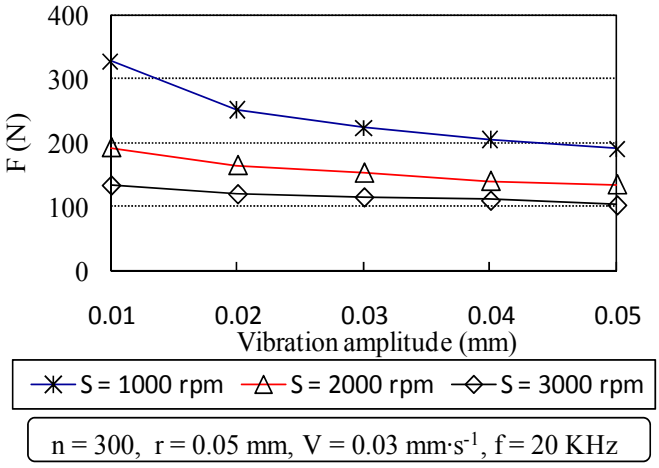

Figure 3.13 Influence of vibration amplitude

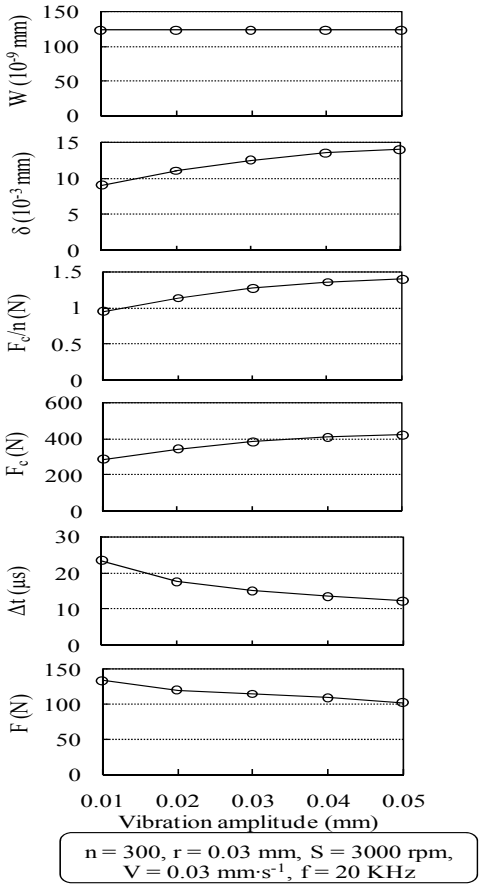

Figure 3.14 Change in DGSE shape as vibration amplitude changes

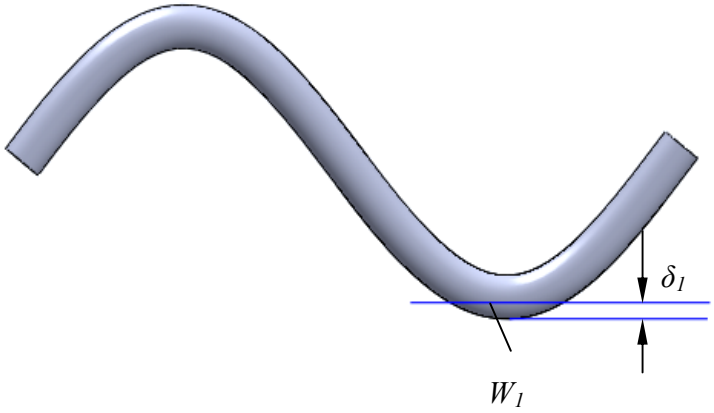

(a) A = 0.01 mm

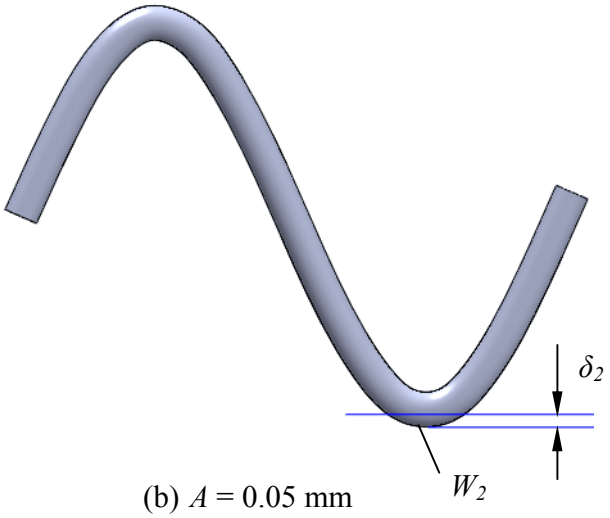

(b) A = 0.05 mm

$\delta_1 = \delta_2$, $W_1 > W_2$

Predicted relations between cutting force F and vibration frequency f are plotted in Figure 3.15. Figure 3.16 shows changes of intermediate variables with vibration frequency f. As

frequency f increases, the shape of DGSE will change as illustrated in Figure 3.17. As frequency f increases, intersection volume W will decrease according to Eq. (14), so penetration depth δ will decrease. And as penetration depth δ decreases, both contact force F_c and effective contact time Δt will decrease according to Eqs. (3) and (6), and their decreasing rate is faster than the increasing rate of vibration frequency f. From Eq. (9), cutting force F will decrease.

Figure 3.15 Relation between vibration frequency and cutting force

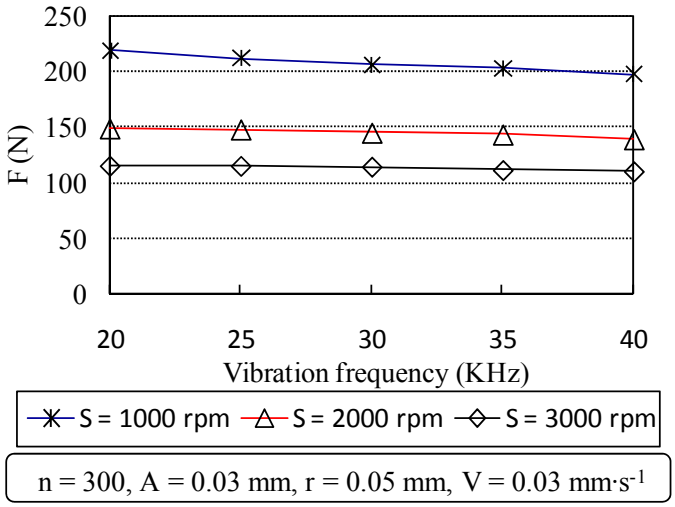

Figure 3.16 Influence of vibration frequency

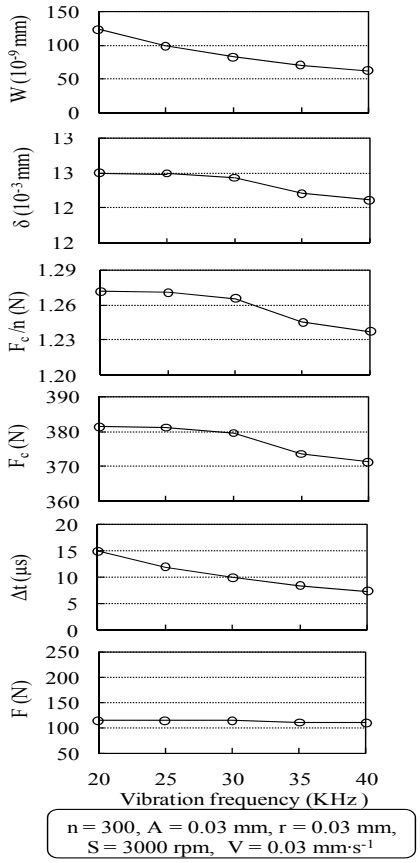

Predicted relations between cutting force F and spindle speed S are plotted in Figure 3.18. Figure 3.19 shows changes of intermediate variables with spindle speed S. As spindle speed S increases, intersection volume W remains unchanged, according to Eq. (14). As spindle speed S increases, since DGSE will change its shape as illustrated in Figure 3.20, penetration depth δ will decrease. As penetration depth δ decreases, both contact force F_c and effective contact time Δt will decrease according to Eqs. (3) and (6). From Eq. (9), with vibration frequency f remains unchanged as spindle speed S increases, cutting force F will decrease.

Figure 3.17 Change in DGSE shape as vibration frequency changes

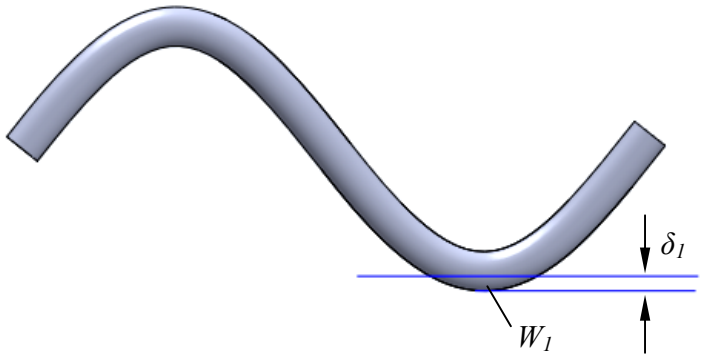

(a) f = 20 kHz

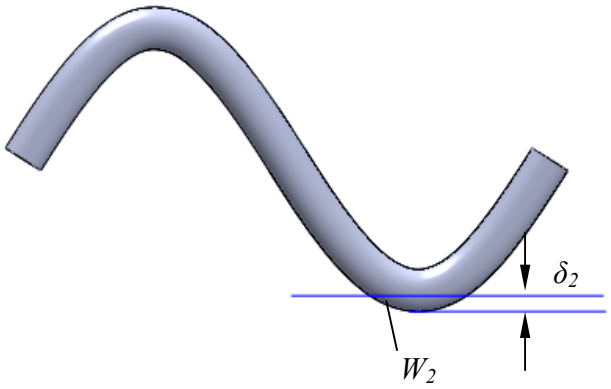

(b) f = 30 kHz

$\delta_1 = \delta_2$, $W_1 > W_2$

Figure 3.18 Relation between spindle speed and cutting force

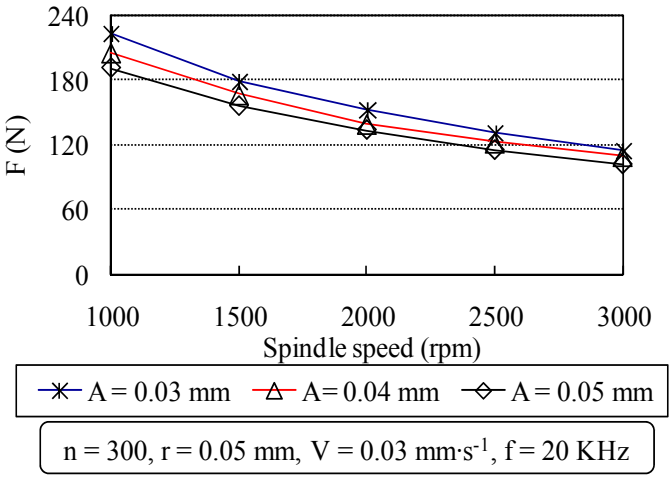

Figure 3.19 Influence of spindle speed

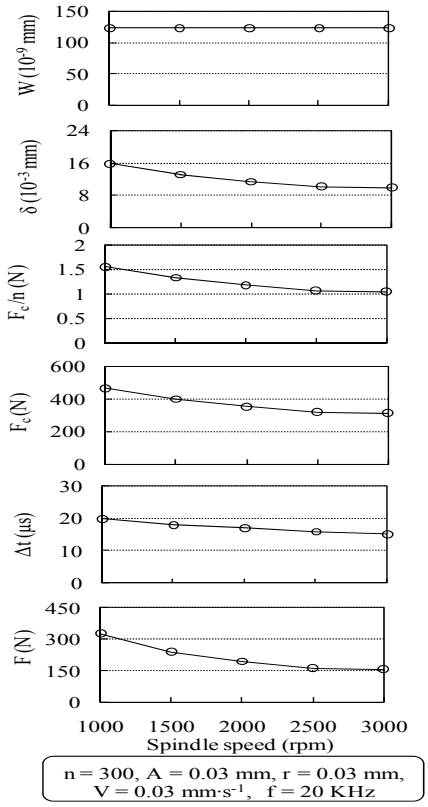

Figure 3.20 Change in DGSE shape as spindle speed changes

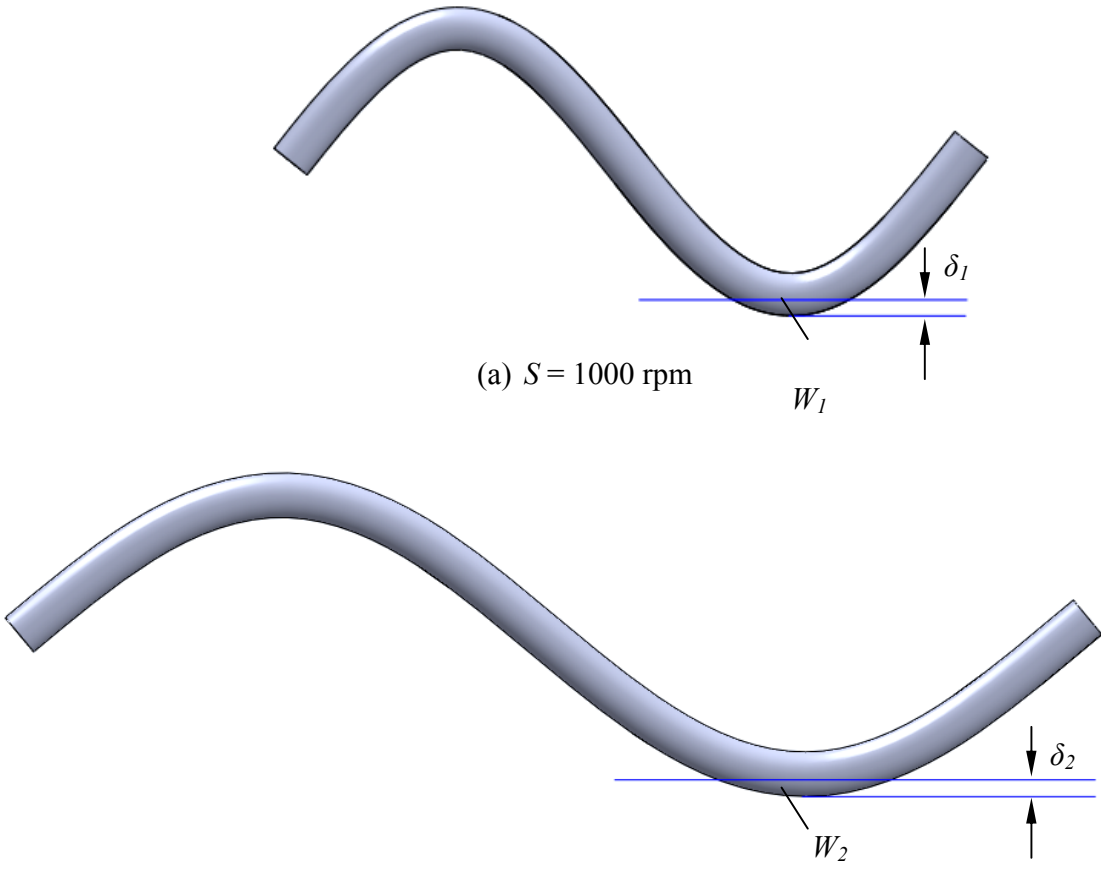

(a) $S = 1000$ rpm

(b) $S = 2000$ rpm

$\delta_1 = \delta_2$, $W_1 < W_2$

Predicted relations between cutting force F and feedrate V are plotted in Figure 3.21. Changes of intermediate variables with feedrate V are shown in Figure 3.22. As feedrate V increases, intersection volume W will increase according to Eq. (14). Since the DGSE shape remains unchanged as feedrate V increases, penetration depth δ will increase as intersection

volume W increases, and therefore, contact force F_c and effective contact time Δt will increase according to Eqs. (3) and (6). From Eq. (9), cutting force F will increase.

Figure 3.21 Relation between feedrate and cutting force

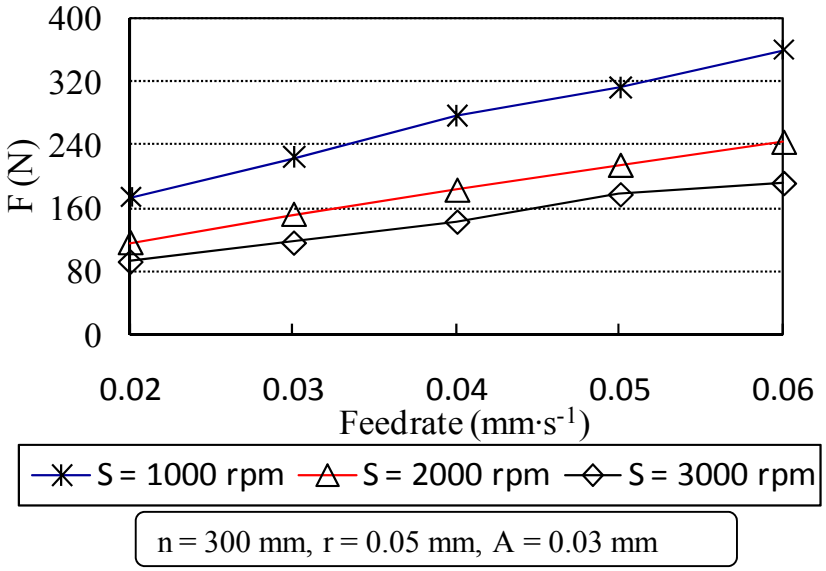

Figure 3.22 Influence of federate

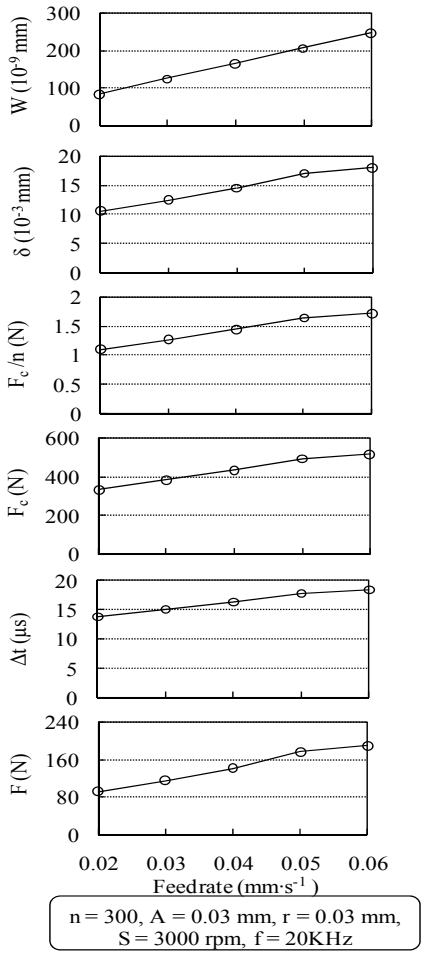

3.4 Comparison with experimental results

Experiments were conducted to study the influences of input variables on cutting force [16, 17]. A machine of Sonic Mill Series 10 (Sonic-Mill^{R}, Albuquerque, NM, USA) was used to perform the experiments. The workpiece material was titanium alloy (Ti-6Al-4V). Diamond cutting tools were provided by N.B.R. Diamond Tool Corp. (LaGrangeville, NY, USA).

Mobilemet® S122 water-soluble cutting oil (MSC Industrial Supply Co., Melville, NY, USA) was used as the coolant (diluted with water at 1 to 20 ratio). The experimental conditions are shown in Table 3.1 and the experimental results are shown in Figures 3.23-3.27.

Table 3.1 Experimental condition [16,17]

Parameter	Unit	Value
Vibration frequency	KHz	20
Ultrasonic power *	%	30, 40, 50, 60
Feedrate	mm·s-1	0.06, 0.14, 0.19, 0.25
Spindle speed	rpm	2000, 3000, 4000, 6000
Outer diameter of tool	mm	9.6
Inner diameter of tool	mm	7.8
Diamond grain size	mesh	60/80, 80/100
Diamond concentration		80, 100

* Ultrasonic power controls the amplitude of ultrasonic vibration.

Figure 3.23 Experimental relation between diamond concentration and cutting force (after [17]).

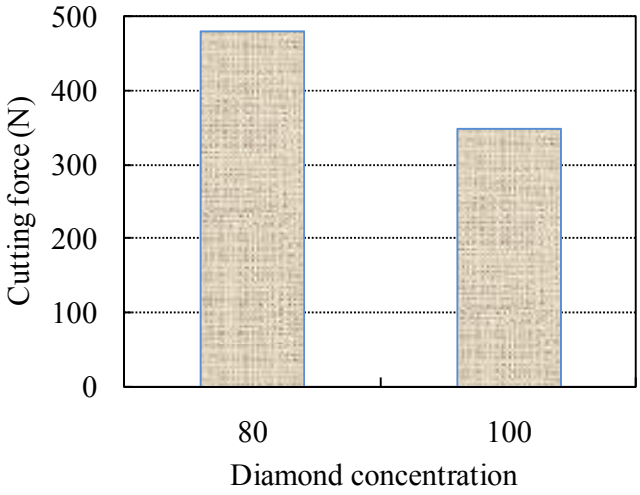

Figure 3.24 Experimental relation between diamond grain size and cutting force (after [17]).

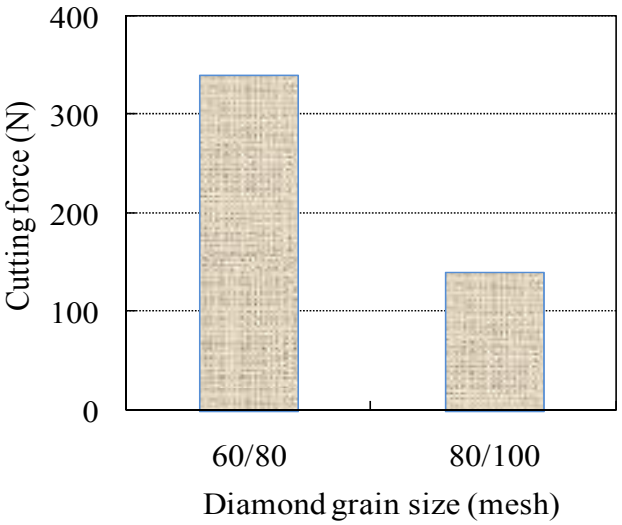

Figure 3.25 Experimental relation between ultrasonic power and cutting force (after [16])

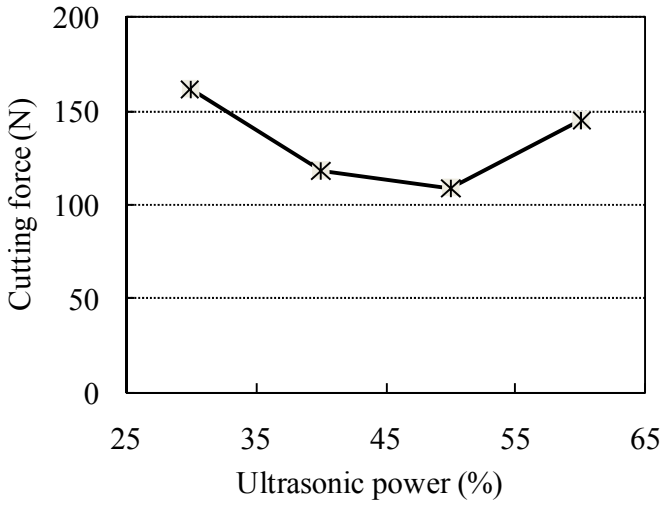

Figure 3.26 Experimental relation between spindle speed and cutting force (after [16])

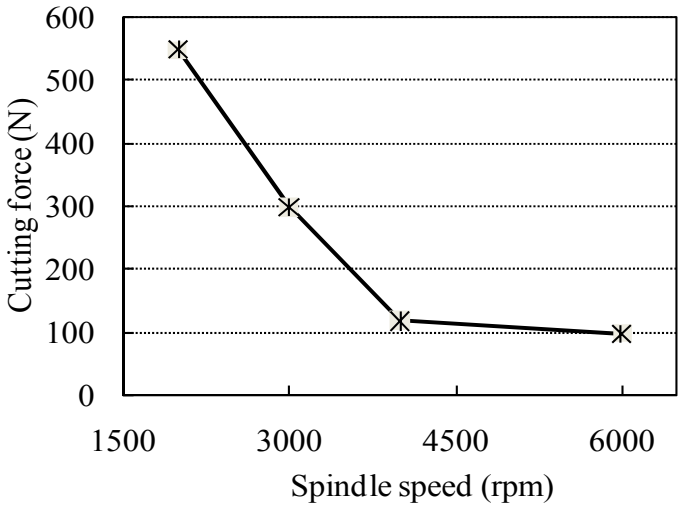

.

Figure 3.27 relation between feedrate and cutting force (after [16])

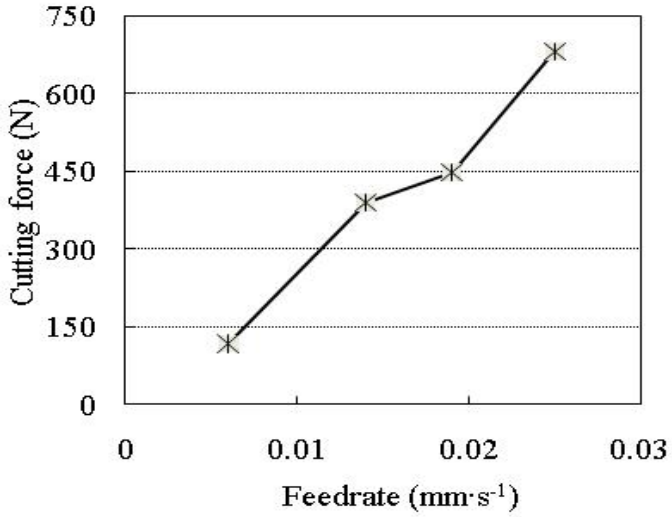

Comparing with Figs. 3.7, 3.9, 3.12, 3.18, and 3.21, it can be seen that the trends of predicted influences of input variables on cutting force agree well with experimental results except that of diamond grain number. The inconsistence may be due to the following reason. The influences of diamond grain number on cutting force were predicted based on the assumption that everything else was the same when the diamond grain number changed. In experiments, two different tools (or grinding wheels) were used, one with diamond concentration of 80, and the other 100. There was no guarantee that the two wheels were made exactly the same except diamond concentration. Further experimental investigations on the influences of diamond concentration are planned and the results will be reported later.

3.5 Conclusions

A physics-based cutting force model in ultrasonic-vibration-assisted grinding (UVAG) of titanium has been developed. The model was used to predict the influences of input variables on cutting force. These predictive influences were compared with those determined experimentally. The trends of predicted influences of input variables on cutting force agree well with experimental results (except that of diamond concentration). These predicted trends are summarized below.

The cutting force will increase as diamond grain number, diamond grain radius, and feedrate increase. It will decrease as vibration amplitude, vibration frequency, and spindle speed increase.

This model is the first cutting force model in UVAG. It can serve as a useful template for development of cutting force models in UVAG of other materials (such as ceramics and stainless steels) and models to predict torque, cutting temperature, tool wear, and surface roughness in UVAG.

Acknowledgements

The authors would like to thank Dr. X.J. Xin (Department of Mechanical and Nuclear Engineering at Kansas State University) for his assistance with SOLIDWORKS.

References

[68] Froes, F., Allen, P., and Niinomi, M., 1998, "Non-aerospace Application of Titanium: An Overview," *Proc. the 1998 TMS Annual Meeting,* February 16-19, 1998, San Antonio, TX, USA, pp. 3-18.

[69] Aust, E., and Niemann, H., 1999, "Machining of Gamma Ti-Al," Adv. Eng. Mater., **1**(1), pp. 53-57.

[70] Kumar, K., 1991, "Grinding Titanium," Aerospace Engineering, **11**(9), pp. 17-19.

[71] Boyer, R., 1996, "Overview on the Use of Titanium in the Aerospace Industry," Mat. Sci. and Eng. A: Structure Materials: Properties, Microstructure and Processing, **213**(2), pp. 103-114.

[72] Peacock, D., 1988, "Aerospace Applications for Titanium," Sheet Metal Industries, **65**(8), pp. 406-408.

[73] Montgomery, J., and Well, M., 2001, "Titanium Armor Applications in Combat Vehicles," JOM, **53**(4), pp. 9-32.

[74] Lerner, I., 2004, "Titanium Market Recovering on Commercial Military Aircraft," Chemical Market Reporter, **266**(18), pp. 17.

[75] Yamashita, Y., Tkayama, I., Fujii, H., and Yamazaki, T., 2002, "Applications and Features of Titanium for Automotive Industry," Nippon Steel Technical Report No. 85, pp. 11-14.

[76] Farthing, T., 1979, "Application of Titanium in the Chemical Industry," Chemical Age of India, **30**(2), pp. 151-166.

[77] Orr, N., 1982, "Industrial Application of Titanium in the Metallurgical and Chemical Industries," *Proc. Technical Sessions at the 111th American Institute of Mining, Metallurgical and Petroleum Engineers*, J. E. Anderson, ed., The Metallurgical Society of AIME, February 14-18, 1982, Dallas, Texas, pp. 1149-1156.

[78] Froes, F., 2002, "Titanium Sport and Medical Application Focus," Materials Technology, **17**(1), pp. 4-7.

[79] Abdullin, I., Bagautinov, A., and Ibragimov, G., 1988, "Improving Surface Finish for Titanium Alloy Medical Instruments," Biomedical Engineering, **22**(2), pp. 48-50.

[80] Yang, X., and Liu, R., 1999, "Machining Titanium and Its Alloys," Mach. Sci. Tech., **3**(1), pp. 107-139.

[81] Ezugwu, E.Q., 1997, "Titanium Alloys and Their Machinability - A Review," J. Mater. Process. Tech., **68**(3), pp. 262-274.

[82] Churi, N.J., Li, Z.C., Pei, Z.J., and Treadwell, C., 2005, "Rotary Ultrasonic Machining of Titanium Alloy: A Feasibility Study," *Proc. 2005 ASME International Mechanical Engineering Congress and Exposition (IMECE),* November 5-11, 2005, Orlando, FL, Vol. 16-2, pp. 885-892.

[83] Churi, N.J., Li, Z.C., Pei, Z.J., and Treadwell, C., 2006, "Rotary Ultrasonic Machining of Titanium Alloy: Effects of Machining Variables," Mach. Sci. Tech., **10**(3), pp. 301-321.

[84] Churi, N.J., Li, Z.C., Pei, Z.J., and Treadwell, C., 2007, 'Rotary Ultrasonic Machining of Titanium Alloy (Ti-6Al-4V): Effects of Tool Variables," Int. J. of Precision Technology, **1**(1), pp. 85-96.

[85] Churi, N.J., Li, Z.C., Pei, Z.J., and Treadwell, C., 2007, "Wheel Wear Mechanisms in Rotary Ultrasonic Machining of Titanium," *Proc. 2007 ASME International Mechanical Engineering Congress and Exposition (IMECE),* November 11-15, 2007, Seattle, WA, Vol. 3, pp. 399-407.

[86] Stinton, D., 1988, "Assessment of the State of the Art Machining and Surface Preparation of Ceramics," ORNL/TM Report No. 10791, Oak Ridge National Laboratory, Oak Ridge, TN.

[87] Legge, P., 1966, "Machining without Abrasive Slurry," Ultrasonics, **2**, pp. 157-162.

[88] Kubota, M., Tamura, Y., and Shimamura, N., 1977, "Ultrasonic Machining with a Diamond Impregnated Tool," Bull. Jpn. Soc. Precis. Eng., **11**(3), pp. 127-132.

[89] Markov, A., 1977, "Ultrasonic Drilling and Milling of Hard Non-Metallic Materials with Diamond Tools," Machine and Tooling, **48**(9), pp. 45-47.

[90] Pei, Z.J., Prabhakar, D., Ferreira, P.M., and Haselkorn, M., 1995, "Rotary Ultrasonic Drilling and Milling of Ceramics," Ceram Trans, **48**, pp. 185-196.

[91] Petrukha, P., 1970, "Ultrasonic Diamond Drilling of Deep Holes in Brittle Materials," Russ. Eng. J., **50**(10), pp. 70-74.

[92] Prabhakar, D., 1992, "Machining Advanced Ceramic Materials Using Rotary Ultrasonic Machining Process," MS Thesis, University of Illinois at Urbana-Champaign, Illinois, USA.

[93] Prabhakar, D., Ferreira, P.M., and Haselkorn, M., 1992, "An Experimental Investigation of Material Removal Rates in Rotary Ultrasonic Machining," Transactions of the North American Manufacturing Research Institute of SME, **10**, pp. 211-218.

[94] Wang, H., and Lin, L., 1993, "Improvement of Rotary Ultrasonic Deep Hole Drilling of Glass Ceramics-Zerodur," *Proc. 7th International Precision Engineering Seminar,* The Japan Society of Applied Physics, Kobe, Japan, pp. 719-730.

[95] Pei, Z.J., and Ferreira, P.M., 1998, "Modeling of Ductile-Mode Material Removal in Rotary Ultrasonic Machining," Int. J. Mach. Tool. Manufact., **38**(10-11), pp. 1399-1418.

[96] Pei, Z.J., Prabhakar, D., Ferreira, P.M., and Haselkorn, M., 1995, "A Mechanistic Approach to the Prediction of Material Removal Rates in Rotary Ultrasonic Machining," J. Eng. for Industry, **177**(2), pp. 142-151.

[97] Zhang, Q.H., Wu, C.L., Sun, J.L., and Jia, Z.X., 2000, "Mechanism of Material Removal in Ultrasonic Drilling of Engineering Ceramics," *Proc. Institution of Mechanical Engineers, Part B: Journal of Engineering Manufacture,* **214**(9), pp. 805-810.

[98] Chao, C.L., Chou, W.C., Chao, C.W., and Chen, C.C., 2007, "Material Removal Mechanisms Involved in Rotary Ultrasonic Machining of Brittle Materials," Key Engineering Materials, **329**, pp. 391-396.

[99] Prabhakar, D., Pei, Z.J., Ferreira, P.M., and Haselkorn, M., 1993, "A Theoretical Model for Predicting Material Removal Rates in Rotary Ultrasonic Machining of Ceramics," Transactions of the North American Manufacturing Research Institute of SME, **21**, pp. 167-172.

[100] Shaw, M.C., 1996, *Principles of Abrasive Processing,* Oxford University Press, New York, p. 112.

[101] Wu, Y.B., Nomura, M., Feng, Z.J., and Kato, M., 2004, "Modeling of Grinding Force in Constant-Depth-of-Cut Ultrasonically Assisted Grinding," Mater. Sci. Forum, **471-472**, pp. 101-106.

[102] Younis, M., Sadek, M.M., and EI-Wardani, T., 1987, "New Approach to Development of a Grinding Force Model," J. Eng. for Industry, **109**(4), pp. 306-313.

[103] Li, L.C., and Fu, J., 1980, "Study of Grinding Force Mathematical Model," Annals of the CIRP, **29**(1), pp. 245-249.

[104] Lortz, W., 1979, "A Model of the Cutting Mechanism in Grinding," Wear, **53**(1), pp. 115-128.

[105] Wener, G., 1978, "Influence of Work Material on Grinding Force," Annals of the CIRP, **27**(1), pp. 243-248.

[106] Collins, J.A., 1981, *Failure of Materials in Mechanical Design*, John Wiley & Sons, New York, p. 591.

Chapter 4 - Cutting force model for brittle materials

The content of this chapter has been published in a conference paper.

Paper Title:

Ultrasonic-vibration-assisted grinding of brittle materials: a mechanistic model for cutting force

Published in:

Proceedings of the ASME 2011 International Manufacturing Science and Engineering Conference, June 13-17, 2011, Corvallis, Oregon, USA.

Authors' Names:

Na Qin [a, c,] W. L. Cong [a], Z. J. Pei[a], C. Treadwell [b], D. M. Guo[c]

Authors' Affiliation:

[a]Department of Industrial and Manufacturing Systems Engineering, Kansas State University, Manhattan, KS 66506, USA

[b]Sonic-Mill, 7500 Bluewater Road N.W., Albuquerque, NM 87102, USA

[c]School of Mechanical Engineering, Dalian University of Technology, Dalian, Liaoning 116024, China

Abstract

A mechanistic model for cutting force in ultrasonic-vibration-assisted grinding (UVAG) (also called rotary ultrasonic machining) of brittle materials is proposed for the first time. Fundamental assumptions include: (1) brittle fracture is the dominant mechanism of material removal, and (2) the removed volume by each diamond grain in one vibration cycle can be related to its indentation volume in the workpiece through a mechanistic parameter. Experiments with UVAG of silicon are conducted to determine the mechanistic parameter for silicon. With the developed model, influences of six input variables on cutting force are predicted. These predicted influences are also compared with those determined experimentally for silicon and several other brittle materials.

Keywords: Brittle material; Cutting force; Grinding; Machining; Silicon; Ultrasonic vibration.

4.1 Introduction

Ultrasonic-vibration-assisted grinding (UVAG), also known as rotary ultrasonic machining (RUM), is illustrated in Figure 4.1. A rotary core drill with metal-bonded diamond grains vibrates at an ultrasonic frequency and is fed towards the workpiece. Coolant pumped through the core of the drill washes away the swarf, prevents jamming of the drill and keeps it cool.

Figure 4.1 Illustration of ultrasonic-vibration-assisted grinding (after [1])

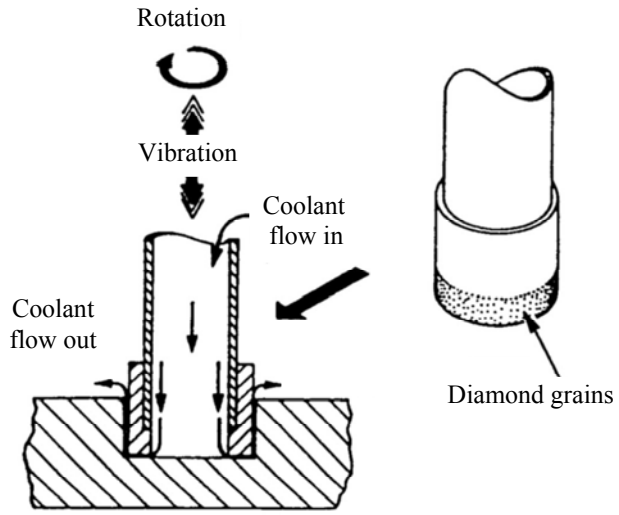

Reported experimental studies on UVAG of brittle materials [2-16] are primarily focused on relationships between input variables (diamond concentration, grain size, and type; bond type; vibration amplitude and frequency; spindle speed; feedrate; coolant type and pressure) and output variables (cutting force, material removal rate, edge chipping, and surface roughness). Reported modeling work on UVAG of brittle materials [17-20] is concentrated on predicting material removal rate (MRR). In the literature, there exist no models to predict cutting force for UVAG of brittle materials.

This paper presents a mechanistic model for cutting force in UVAG of brittle materials using silicon as an example. It first describes the model development step by step. Afterwards, with the developed model, influences of six input variables (diamond grain number and grain diameter, vibration amplitude and frequency, spindle speed, and feedrate) on cutting force (and

on intermediate variables used in some steps of the model development) are predicted. Then, the predicted influences are compared with those determined experimentally for silicon and several other brittle materials.

4.2 Model development

4.2.1 Model assumptions and simplification

Ultrasonic-vibration-assisted grinding (UVAG) is a hybrid machining process that combines the material removal mechanisms of ultrasonic machining and diamond grinding. In the model presented in this paper, ultrasonic machining was considered as the dominant process and brittle fracture was the dominant mode of material removal. Effects of the rotating motion of the tool were taken into consideration via its effects on the indentation volume by each diamond grain into the workpiece. Development of the model started with an analysis of single diamond grain. The cutting force for individual diamond grain was obtained first. Then the total cutting force was derived by summing up the forces on all diamond grains taking part in cutting. Similar approaches were followed by others to develop grinding force models [21-26].

1) The model was based on the following assumptions and simplifications:
2) Diamond grains were rigid spheres of same size;
3) Diamond grains located on the tool end surface had the same height of extrusion, and all of them took part in cutting during each ultrasonic vibration cycle;
4) The workpiece material was an ideally brittle material.

Additional assumptions were also used and will be presented in subsequent sections.

4.2.2 Relation between maximum contact force on individual diamond grain F_c/n and maximum indentation depth δ

During UVAG, the tool is fed into the workpiece with a constant feedrate, but the tool is not in continuous contact with the workpiece due to its oscillatory motion. In each vibration cycle of the tool, a diamond grain on the end surface of the tool will make contact with the workpiece for a certain period of time (called effective contact time). When a diamond grain penetrates into the workpiece to maximum indentation depth δ, maximum contact force on the diamond grain will be F_c/n (and maximum contact force on all diamond grains on the end surface of the tool is F_c).

Figure 4.2 Indentation of a diamond grain into the workpiece

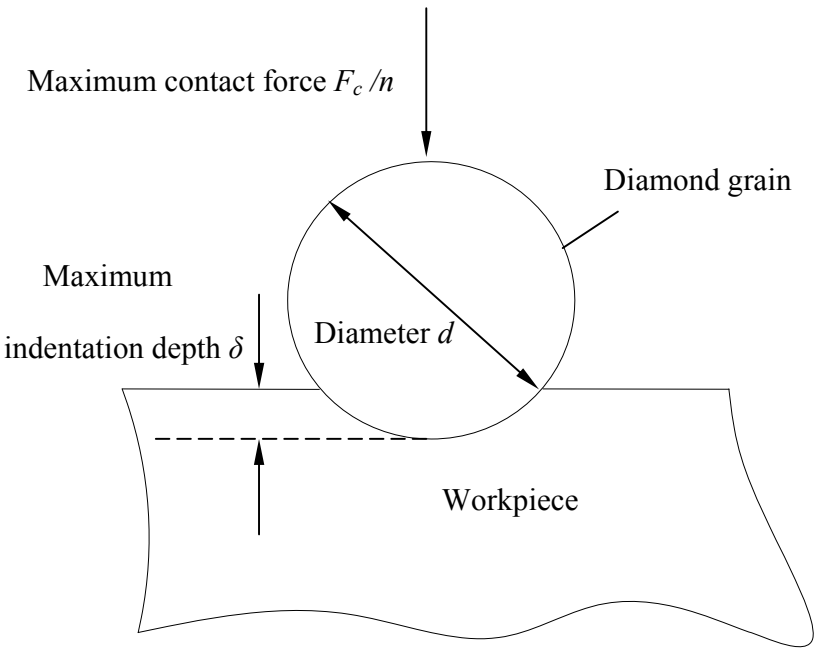

Hertz equation [27] was used to relate maximum contact force F_c/n to maximum indentation depth δ. Hertz equation is strictly applicable only up to the point of initial surface fracture. However, according to Sheldon and Finnie [28], even after cracking occurred, Hertz equation might be used to predict the indentation depth of a grain into a surface within certain ranges. Therefore, maximum contact force F_c/n on individual grain can be expressed as follows [29]:

$$\frac{F_c}{n} = \left(\frac{8}{9} \left(\frac{E}{1-\upsilon^2} \right)^2 d\delta^3 \right)^{\frac{1}{2}} \tag{1}$$

where E and ν are Young's modulus and Poisson's ratio of workpiece material, respectively, n is the number of diamond grains taking part in cutting, d is diamond grain diameter, and δ is maximum indentation depth, as illustrated in Figure 4.2. δ is the only unknown parameter on the right side of Eq. (1). It can be related to the indentation volume of a diamond grain into the workpiece, as discussed in the next section.

4.2.3 Relation between maximum indentation depth δ and indentation volume U

Maximum indentation depth δ can be related to U, the indentation volume of a diamond grain into the workpiece in one vibration cycle. During each vibration cycle, the diamond grain moves a distance of L while in contact with the workpiece due to the rotating motion of the tool, and the indentation depth of a diamond grain into the workpiece changes from 0 to δ, and then changes back to 0. In the mean time, the contact width between a diamond grain and the workpiece surface also changes from 0 to some maximum value and then back to 0. Consequently, the indentation volume will be a shape of part of an ellipsoid. As shown in Figure 4.3, the cross section of the indentation volume in plane XY (the plane that is parallel to the

workpiece surface) is an ellipse with semimajor axis of $\frac{d+L}{2}\sqrt{\left(1-\left(\frac{2z}{d}\right)^2\right)}$ and semiminor axis of $\frac{d}{2}\sqrt{\left(1-\left(\frac{2z}{d}\right)^2\right)}$, where z is the z-coordinate of this cross-section. So the indentation volume can be calculated by integration:

$$U=\int_{-\frac{d}{2}}^{-\left(\frac{d}{2}-\delta\right)}\pi\left(\frac{d+L}{2}\right)\left(\frac{d}{2}\right)\left(1-\left(\frac{2z}{d}\right)^2\right)dz \tag{2}$$

Figure 4.3 Illustration for calculation of indentation volume

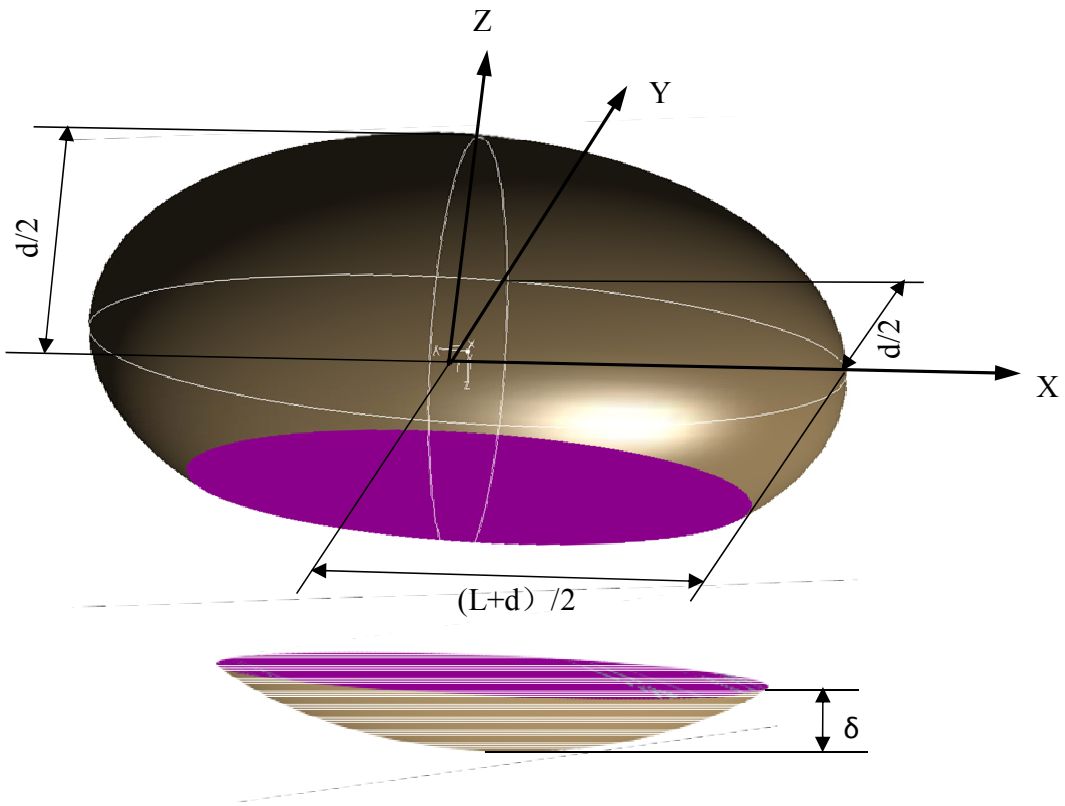

The result of the integration is:

$$U = \pi\delta^2\left(\frac{d}{2} + \frac{L}{2} - \frac{L\delta}{3d} - \frac{\delta}{3}\right) \tag{3}$$

The distance L moved by a diamond grain while in contact with the workpiece can be expressed as:

$$L = \frac{\pi D_o S \Delta t}{60} \tag{4}$$

where D_o is the outer diameter of the cutting tool, S is spindle speed in rpm (revolution per minute), Δt is effective contact time (i.e., the period of time during which the diamond grain has penetrated into the workpiece). Δt can be obtained as follows.

The motion of each diamond grain (on the tool end surface) could be considered as sinusoidal. The diamond grain oscillates with an amplitude A and a frequency f. The position of each diamond grain relative to its mean position at any given time t can be described by the following equation:

$$z = A \cdot \sin(2\pi f t) \tag{5}$$

The equation can be expressed in a different way:

$$t = \frac{1}{2\pi f}\arcsin\frac{z}{A} \tag{6}$$

As illustrated in Figure 4.24, it would take $\frac{\Delta t}{2}$ for a diamond grain to move from $z = -(A - \delta)$ to $z = -A$. So, $z = -A$, Δt can be calculated as:

$$\Delta t = 2(t_2 - t_1) = \frac{1}{\pi f} \times \left\{\frac{3\pi}{2} - \arcsin\left(\frac{\delta}{A} - 1\right)\right\} \tag{7}$$

Figure 4.4 Calculation of effective contact time *Δt*

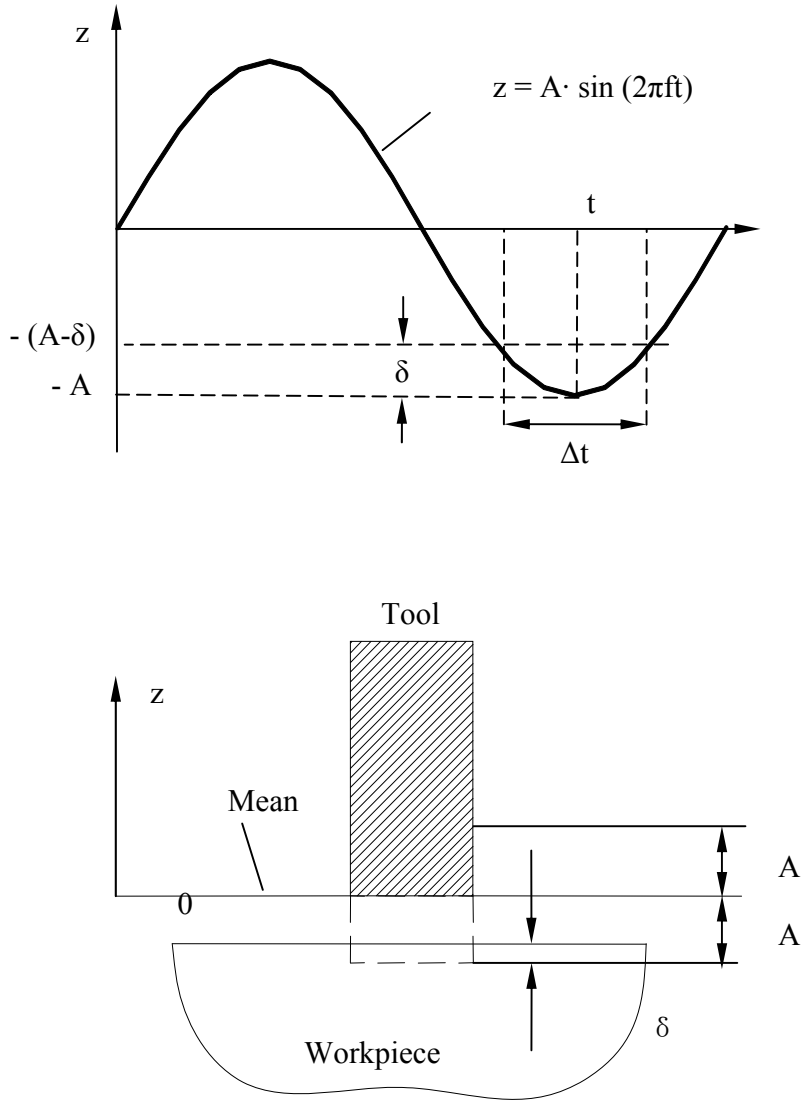

Substituting Eqs. (4) and (7) into Eq. (3), the relation between U and δ can be obtained as:

$$U = \pi\delta^2\left[1 + \frac{D_o S}{60df}\left(\frac{3\pi}{2} - \arcsin\left(\frac{\delta}{A} - 1\right)\right)\left(\frac{d}{2} - \frac{\delta}{3}\right)\right] \tag{8}$$

This equation relates δ to U, the indentation volume of a diamond grain into the workpiece in one vibration cycle. As shown in the following sections, U can be obtained from input variables.

4.2.4 Relation between indentation volume U and removed volume W

Let W denotes the removed volume by one diamond grain during one vibration cycle. It is assumed that W and U have the following relation:

$$W = kU \tag{9}$$

where k is a mechanistic parameter that would include multiple considerations. For example, it may take more than one vibration cycles to remove the indentation volume U. Furthermore, since the cracks responsible for material removal may initiate and propagate outside the indentation volume, the removed volume may be larger than the indentation volume. This parameter k has to be determined experimentally for a specific workpiece material. The procedure to obtain k experimentally will be illustrated in section 3.

4.2.5 Relation between removed volume W and input variables

If W is the volume removed by a diamond grain in a vibration cycle, material removal rate (MRR) will be given by:

$$MRR = nfw \tag{10}$$

where n is the number of diamond grains taking part in cutting and f is the frequency of the vibration.

MRR can also be calculated from input variables:

$$MRR = \frac{v\left(\pi D_o^2 - \pi D_i^2\right)}{4} \tag{11}$$

where V is feedrate, D_i and D_o are the inner and outer diameters of cutting tool.

The relation between W and input variables can be obtained by substituting Eq. (10) into Eq. (11).

$$w = \frac{\pi v\left(D_o^2 - D_i^2\right)}{4nf} \tag{12}$$

2.6 Cutting force of individual diamond grain $\frac{\mathrm{F}}{\mathrm{n}}$

Since diamond grains are assumed incompressible, the impulse in terms of maximum contact force for individual diamond grain F_c/n during one vibration cycle is:

$$\text{Impulse} = \int_{cycle} \frac{F_c}{n} dt \approx \frac{F_c}{n} \Delta t \tag{13}$$

The impulse in terms of the cutting force for individual diamond grain F/n during one vibration cycle is:

$$\text{Impulse} = \frac{F}{nf} \tag{14}$$

By equating the two impulses in Eqs. (13) and (14), the following relation can be obtained:

$$\frac{F}{n} = \frac{F_c}{n} f\Delta t \tag{15}$$

Substituting Eqs. (1) and (7) to Eq. (15), the cutting force of individual diamond grain F/n can be expressed as:

$$\frac{F}{n} = \left(\frac{8}{9}\left(\frac{En}{1-\upsilon^2}\right) d\delta^3\right)^{\frac{1}{2}} \cdot \frac{1}{\pi}\left\{\frac{3\pi}{2} - \arcsin\left(\frac{\delta}{A} - 1\right)\right\} \tag{16}$$

4.2.6 Cutting force F

The cutting force F observed during experiments can be obtained if multiplying the cutting force for individual diamond grain F/n by the number of the diamond grains taking part in cutting n.

$$\begin{aligned} F &= F_c f \Delta t \\ &= \left(\frac{8}{9} \left(\frac{En}{1-\upsilon^2} \right) d\delta^3 \right)^{\frac{1}{2}} \cdot \frac{1}{\pi} \left\{ \frac{3\pi}{2} - \arcsin\left(\frac{\delta}{A} - 1 \right) \right\} \end{aligned} \tag{17}$$

On the right side of this equation, every item except δ is known once input variables are known. δ is maximum indentation depth of a diamond grain into the workpiece. As discussed in sections 4.3.3 and 4.3.4, δ can be calculated from the indentation volume of a diamond grain U, and U is related to W (the removed volume by a diamond grain within one vibration cycle) through a mechanistic parameter k. This k has to be determined by experiments.

4.3 Determination of mechanistic parameter k using experiments

4.3.1 Experiment set up

A rotary ultrasonic machine of Sonic Mill Series 10 (Sonic-Mill, Albuquerque, NM, USA) was used to perform the experiments. The workpiece material was silicon and the size was 10 mm × 10 mm × 0.84 mm. Each workpiece was cut from silicon wafers that had a diameter of 200 mm. For silicon, Yong's modulus E = 126 GPa, Poisson ratio ν = 0.3.

The diamond cutting tool was provided by N.B.R. Diamond Tool Corp. (LaGrangeville, NY, USA). The mesh size of the diamond grains was 80/100. The outer and inner diameters of the cutting tool were D_o= 9.6 mm and D_i = 7.8 mm, respectively. Water-soluble Quakercool

6010 cutting fluid (Murdock Industrial Supply Co., Wichita, KS, USA) was used as the coolant (diluted with water at 1:14 ratio). The cutting force was measured using a Kistler 9272 piezoelectric dynamometer (Kistler Instrument Corp, Amherst, NY, USA).

4.3.2 Design of experiments

A 2^3 (three variables, two levels) full factorial design was employed. Table 4.1 shows the values of low and high levels of three variables. There were eight different combinations and two replicated tests were conducted for each combination, bringing the total number of tests to 16, as shown in Table 4.2. Commercial software Minitab 14 (Minitab, Inc., State College, PA, USA) was used to generate a random order for these tests as well as to assist in processing the experimental data.

Table 4.1 Low level and high level of process variables

Variable	Unit	Low level	High level
Vibration amplitude *A*	mm	0.008	0.015
Spindle speed *S*	rpm	2000	4000
Feedrate *V*	$mm \cdot s^{-1}$	0.013	0.026

Vibration amplitude was determined by ultrasonic power. A series of experiments were conducted to establish the relationship between ultrasonic power and vibration amplitude and the results will be published in a separate paper [30]. Vibration amplitudes were 0.008 mm with 25% ultrasonic power (for the low level) and 0.015 mm with 50% ultrasonic power (for the high level).

Diamond grain number n was measured with a microscope DVM-1 (Olympus American, Inc., Melville, NY, USA). Four areas having about the same size of 0.6 mm $\times$ 0.6 mm at different locations on the tool surface were observed. The number of diamond grains on each of these areas was counted. The average was 3. The total area of the tool end surface was $\pi\left(\frac{D_o^2}{4}-\frac{D_i^2}{4}\right)$, and D_o= 9.6 mm, D_i = 7.8 mm. Therefore the number of diamond grains on the tool end surface was approximately 65.

4.3.3 Experiment results

Experimental results on cutting force are presented in 4.2. Table 4.2 also includes values of mechanistic parameter k for each test.

For each test, the measured value of cutting force F and the values of input variables were used to calculate δ using Eq. (17), U using Eq. (8), and W using Eq. (12). The ratio of W/U was taken as the value of mechanistic parameter k. Since there were 16 k tests, 16 values of k were obtained from the experiments. Figure 4.5 shows a plot of these 16 values vs. maximum indentation depth δ. It shows that k is dependent on maximum indentation depth δ and feedrate V. The plot also indicates the following possible relation:

$$k = a\delta^{\alpha}V^{\beta} \tag{18}$$

Table 4.2 Experimental results on cutting force *F* and mechanistic parameter *k*

Order	A (mm)	S (rpm)	V ($mm \cdot s^{-1}$)	F (N)	k
1	0.008	2000	0.013	50.4	1.44
2	0.008	2000	0.013	53.2	1.35
3	0.008	4000	0.013	42.0	1.74
4	0.008	4000	0.013	37.8	1.99
5	0.015	2000	0.013	58.8	1.11
6	0.015	2000	0.013	56.0	1.18
7	0.015	4000	0.013	43.4	1.58
8	0.015	4000	0.013	40.6	1.72
9	0.008	2000	0.026	84.0	1.53
10	0.008	2000	0.026	75.6	1.74
11	0.008	4000	0.026	42.0	3.49
12	0.008	4000	0.026	39.2	3.80
13	0.015	2000	0.026	103.6	1.09
14	0.015	2000	0.026	106.4	1.05
15	0.015	4000	0.026	44.8	3.04
16	0.015	4000	0.026	47.6	2.81

Figure 4.5 Relationship between mechanistic parameter *k* and maximum indentation depth δ

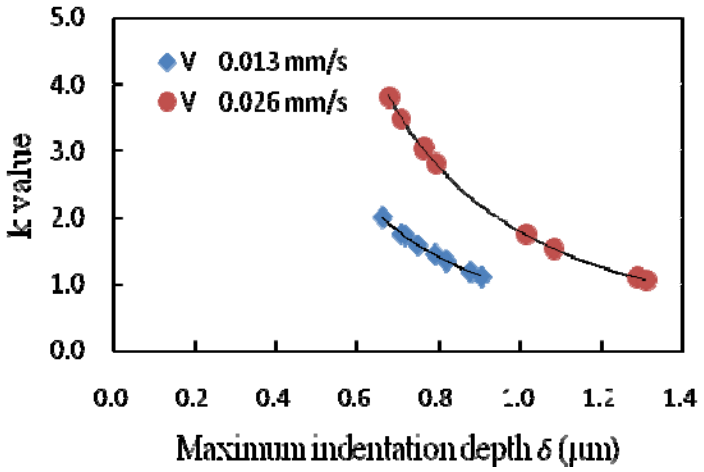

Multiple linear regression of experimental data was used to obtain the estimates of a, α and β. First, Eq. (18) was converted into a linear equation using the log function. Then, the multiple linear regression method [31] was used with one dependent variable (k) and two independent variables (δ and V). The estimates of a, α and β were found to be 1.03×10^{-4}, -1.93, and 0.97, respectively.

Figure 4.6 is another plot of the 16 k values against $(1.03\times10^{-4}\delta^{-1.93}V^{0.97})$. It indicates that Eq. (18) (together with the obtained estimates of a, α and β) fits the experiment data well.

In the previous sections, a mechanistic model was developed for the cutting force in UVAG of brittle materials using silicon as an example. In this section, the developed model is used to predict how individual input variable influence the cutting force. Material properties and mechanistic parameter k of silicon were used in the predictions.

Figure 4.6 Relationship between mechanistic parameter *k* and maximum indentation depth δ and feedrate *V*

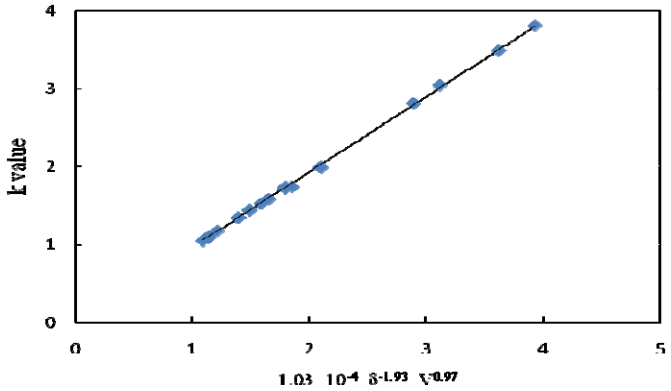

4.4 Influences of input variables on cutting force

4.4.1 Diamond grain number n

Predicted relationships between cutting force F and diamond grain number n are plotted in Figure 4.7. Figure 4.8 shows changes of intermediate variables with diamond grain number n. if diamond grain number n increases, since feedrate V keeps constant, the material removal rate (MRR) also keeps constant, so maximum indentation depth δ should decrease to keep the same MRR. The decrease in maximum indentation depth δ will result in a decrease in maximum contact force F_c/n of individual diamond grain (according to Eq. (1)) and in effective contact time Δt (according to Eq. (7)). Because maximum indentation depth δ decreases at a much faster rate than the rate at which the diamond grain number n increases, maximum contact force F_c on all diamond grains decreases. In Eq. (17), $F = F_c f \Delta t$, if diamond grain number n increases and vibration frequency f remains unchanged, maximum contact force F_c and effective contact time Δt will decrease and, therefore, cutting force F will decrease.

Figure 4.7 Relation between diamond grain number and cutting force

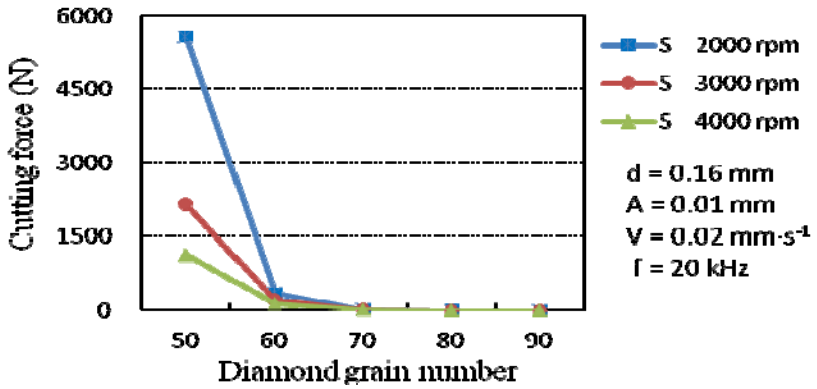

Figure 4.8 Influences of diamond grain number

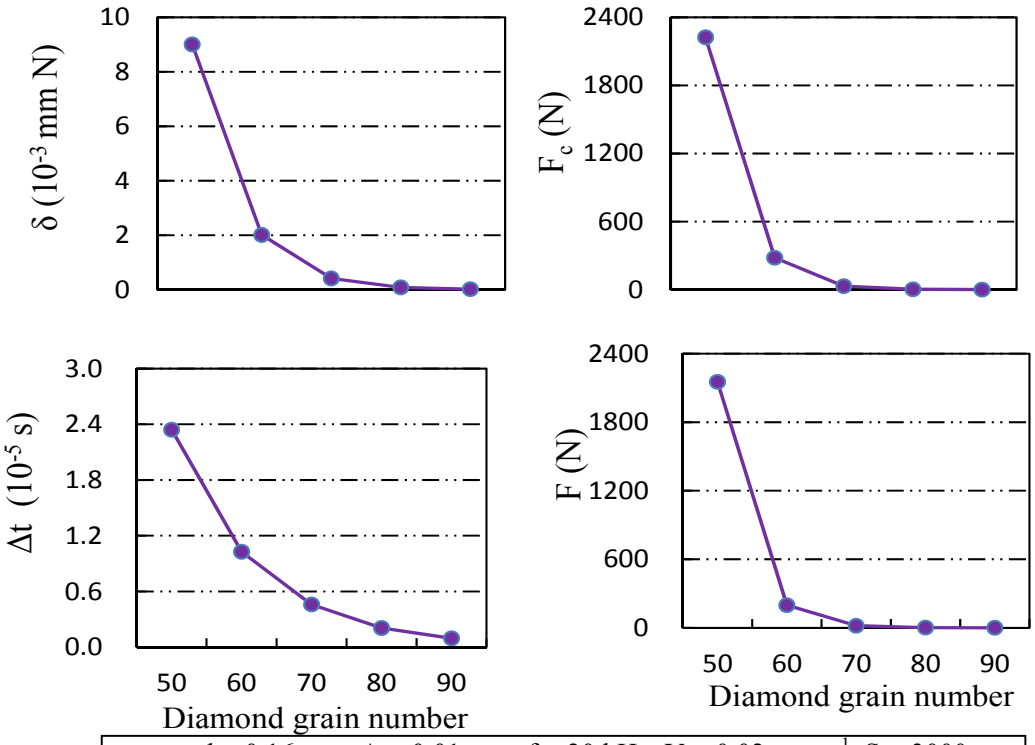

4.4.2 Diamond grain diameter d

Figure 4.9 Relation between diamond grain diameter and cutting force

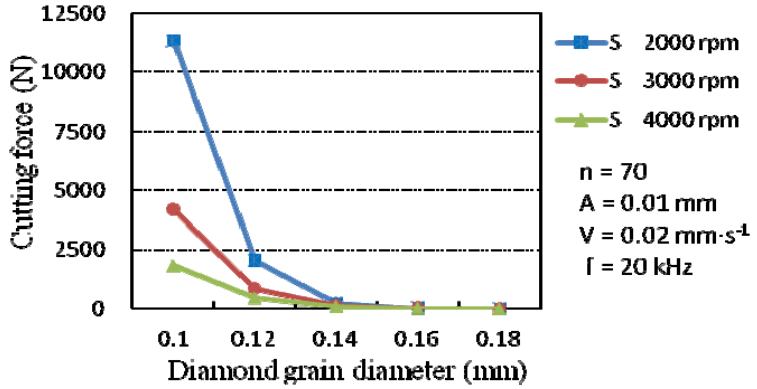

Figure 4.10 Influences of diamond grain diameter

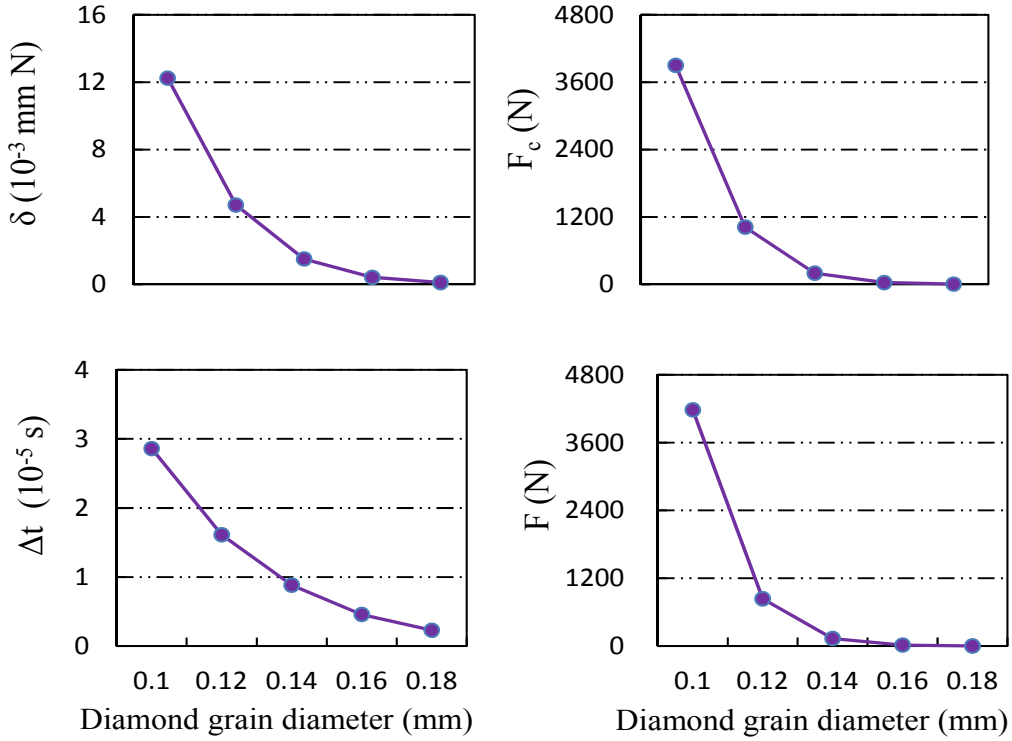

n = 70, A = 0.01 mm, f = 20 kHz, V = 0.02 mm·s^{-1}, S = 3000 rpm

Figure 4.9 shows the predicted relationships between diamond grain diameter d and cutting force F. The changes of intermediate variables with diamond grain diameter n are shown in Figure 4.10. If the diamond grain diameter d increases and feedrate V remains unchanged (i.e. MRR will not change), maximum indentation depth δ should decrease to keep MRR unchanged. The decrease of maximum indentation depth δ will result in a decrease in maximum contact force F_c and in effective contact time Δt. According to Eq. (17), $F = F_c f \Delta t$, if diamond grain diameter d increases and vibration frequency f remains unchanged, maximum contact force F_c and effective contact time Δt will decrease and, therefore, cutting force F will decrease.

4.4.3 Vibration amplitude A

Predicted relationships between cutting force F and vibration amplitude A are plotted in Figure 4.11. Figure 4.12 shows changes of intermediate variables with vibration amplitude A. If vibration amplitude A increases, MRR and removed volume W will not change. Since k is not a function of vibration amplitude A, indentation volume U will not change either. To keep U unchanged, indentation depth δ has to increase. The increase in maximum indentation depth δ will result in an increase in maximum contact force F_c and decrease in effective contact time Δt. But the increasing rate of maximum contact force F_c is higher than the decreasing rate of effective contact time Δt. In Eq. (17), $F = F_c f \Delta t$, if vibration amplitude A increases and vibration frequency f remains unchanged, cutting force F will increase.

Figure 4.11 Relation between vibration amplitude and cutting force

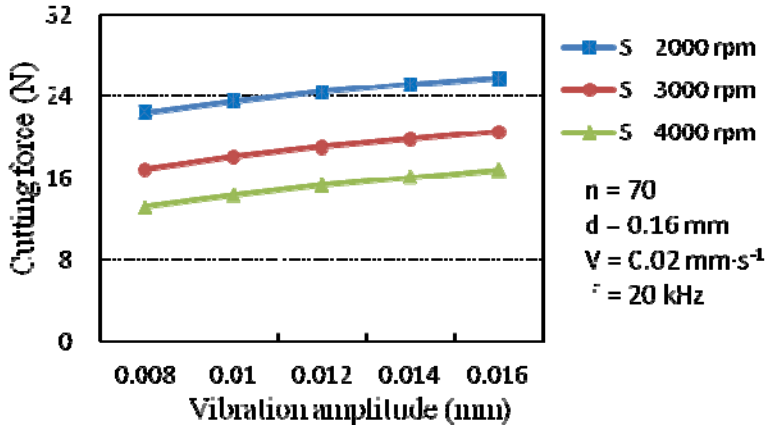

Figure 4.12 Influences of vibration amplitude

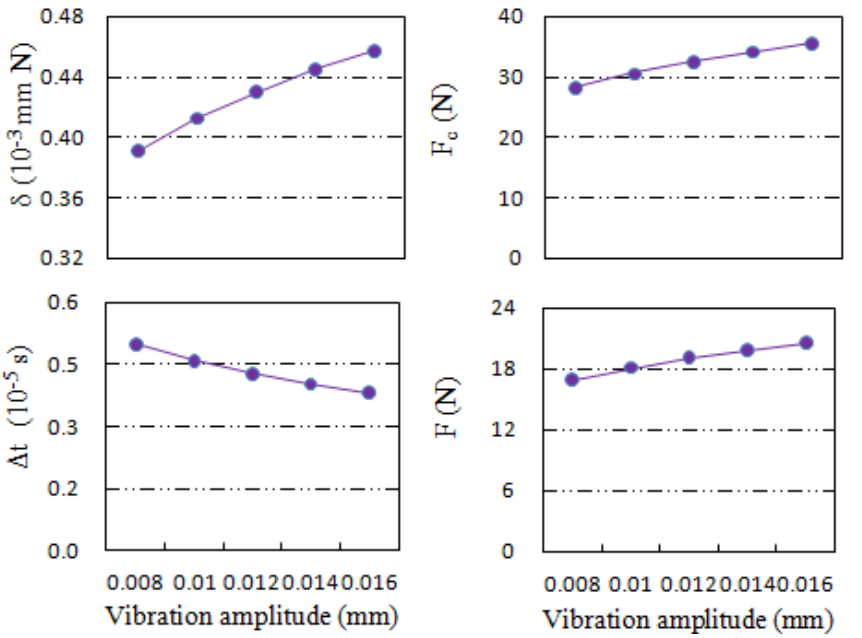

n = 70, d = 0.16 mm, f = 20 kHz, V = 0.02 mm·s^{-1}, S = 3000 rpm

4.4.4 Vibration frequency f

Figure 4.13 Relation between vibration frequency and cutting force

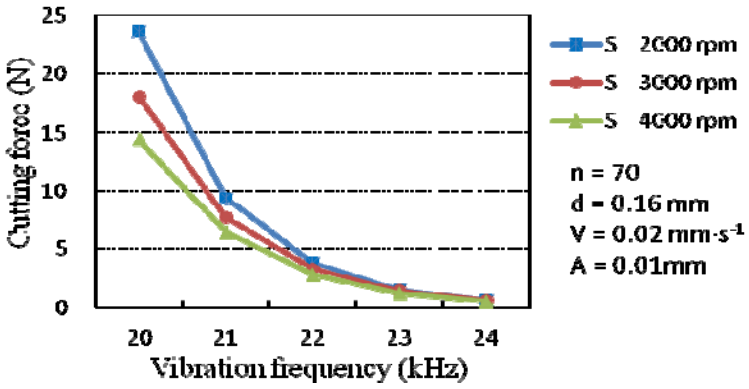

Figure 4.14 Influences of vibration frequency

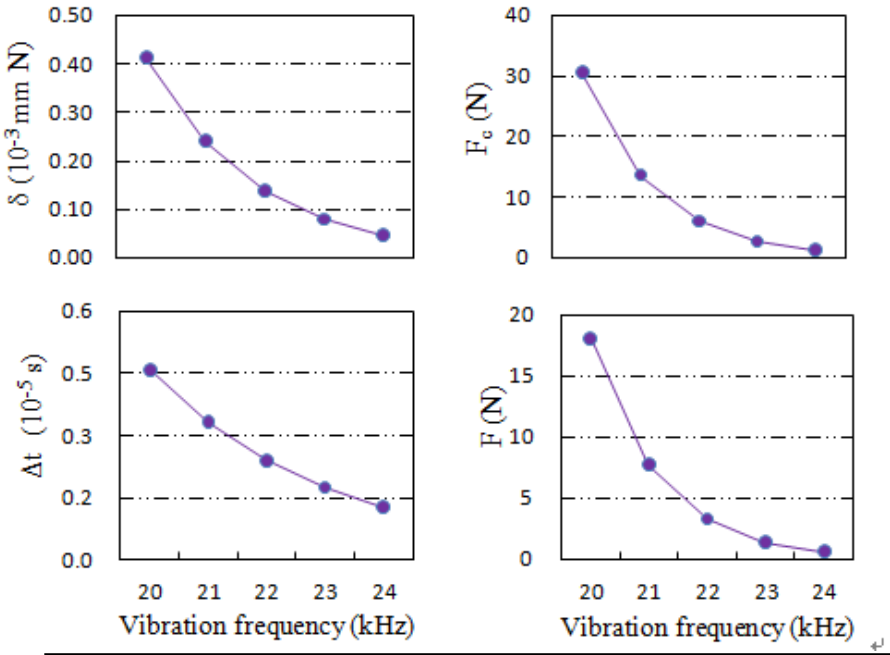

n = 70, d = 0.16 mm, A = 0.01 mm, V = 0.02 mm·s^{-1}, S = 3000 rpm

Figure 4.13 shows the predicted relationships between vibration frequency f and cutting force F. The changes of intermediate variables with vibration frequency f are shown in Figure 4.14. If the vibration frequency f increases, the MRR will not change according to Eq. (11). Based on Eq. (10), removed volume W has to decrease to keep MRR unchanged. Since k is not a function of f, indentation volume U will decrease too. Therefore, maximum indentation depth δ should decrease. The decrease of maximum indentation depth δ will result in a decrease in maximum contact force Fc and effective contact time Δt. According to Eq. (17) $F = F_c f \Delta t$, if vibration frequency f increases, the decreasing rate of maximum contact force Fc and effective contact time Δt is larger than the increasing rate of vibration frequency f, so cutting force F will decrease.

4.4.5 Spindle speed S

Predicted relationships between cutting force *F* and spindle speed *S* are plotted in Figure 4.15. Figure 4.16 shows changes of intermediate variables with spindle speed *S*. If spindle speed *S* increases, MRR (and hence *W* and *U*) will not change, but *L* will increase. Maximum indentation depth δ should decrease to keep indentation volume *U* the same. The decrease in maximum indentation depth δ will result in a decrease in maximum contact force F_c and decrease in effective contact time Δt. From Eq. (17), $F = F_c f \Delta t$, if spindle speed *S* increases and vibration frequency *f* remains unchanged, both maximum contact force F_c and effective contact time Δt will decrease, so cutting force *F* will decrease.

Figure 4.15 Relation between spindle speed and cutting force.

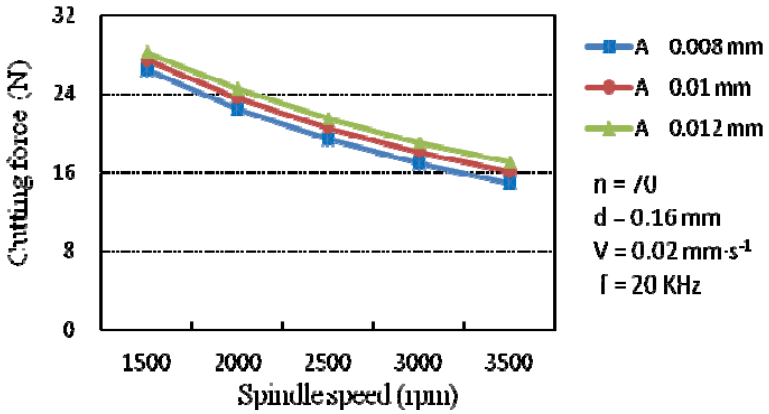

Figure 4.16 Influences of spindle speed

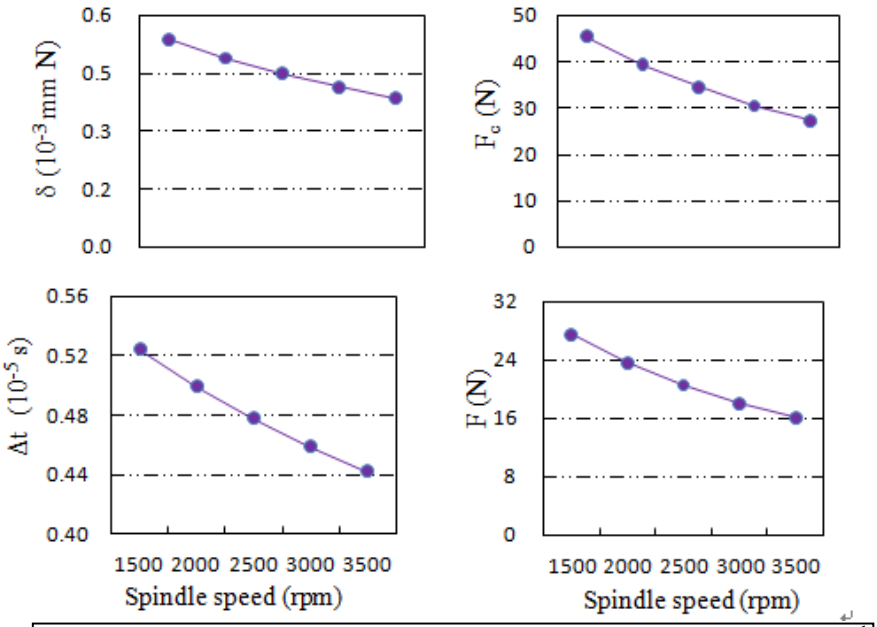

4.4.6 Feedrate V

Figure 4.17 Relation between feedrate and cutting force

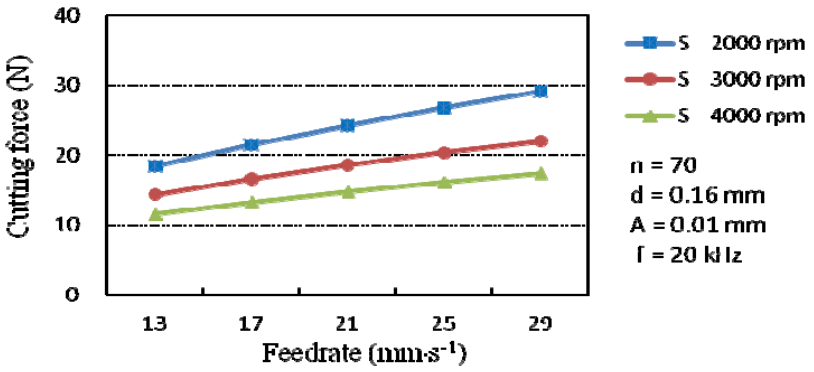

Figure 4.18 Influences of feedrate

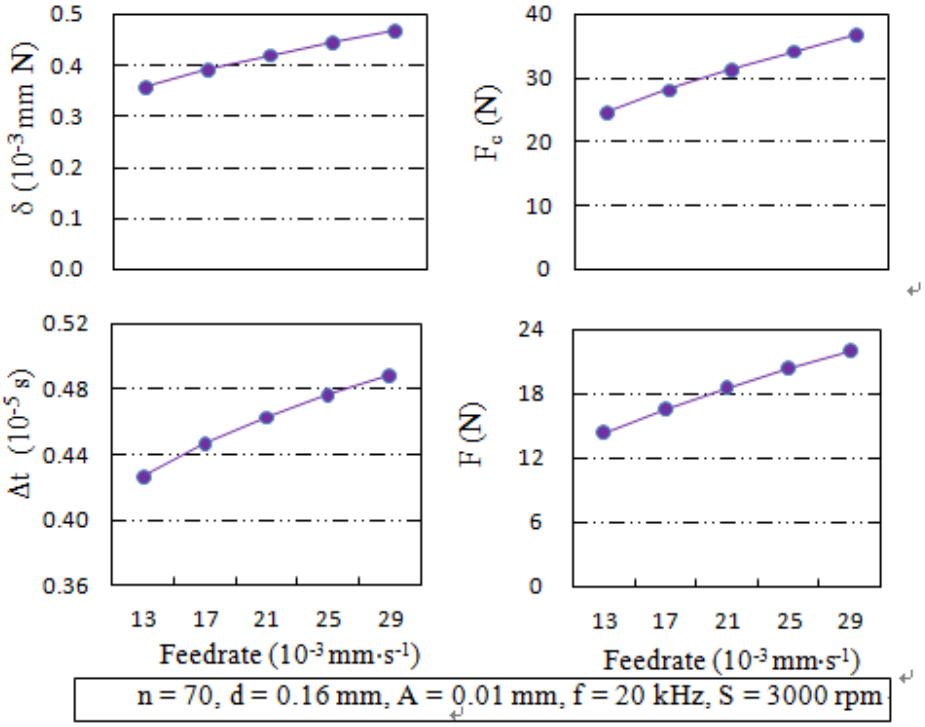

Predicted relationships between cutting force F and feedrate V are plotted in Figure 4.17. Figure 4.18 shows changes of intermediate variables with feedrate V. If feedrate V increases, MRR (and hence W) will increase. Consequently, maximum indentation depth δ should increase. The increase in maximum indentation depth δ will result in an increase in maximum contact force F_c and an increase in effective contact time Δt. From Eq. (17), $F = F_c f \Delta t$, if feedrate V increases and vibration frequency f remains unchanged, maximum contact force F_c and effective contact time Δt will increase, so cutting force F will increase.

4.5 Comparison with experimental results

In this section, predicted relations between input variables and cutting force are compared with the experimental results from the tests conducted on silicon to obtain its mechanistic parameter k. They are also compared with published results on cutting forces in UVAG of other brittle materials.

Figure 4.19 Experimental relation between diamond grain size and cutting force when UVAG of silicon carbide (after [2])

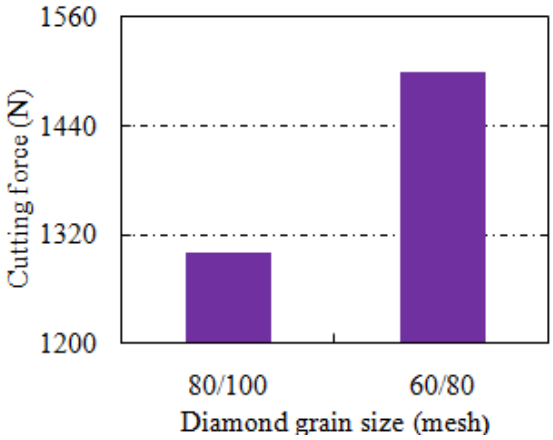

Figure 4.20 Experimental relation between ultrasonic power and cutting force

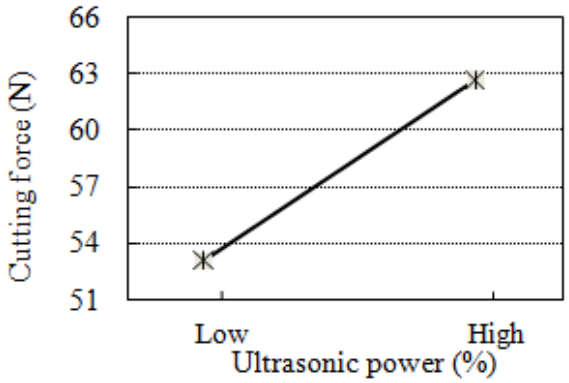

(a) Silicon

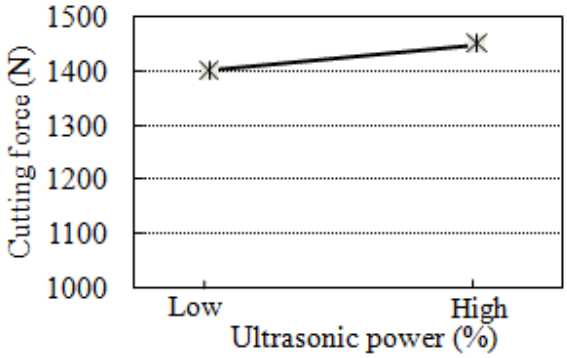

(b) Silicon carbide (after [2])

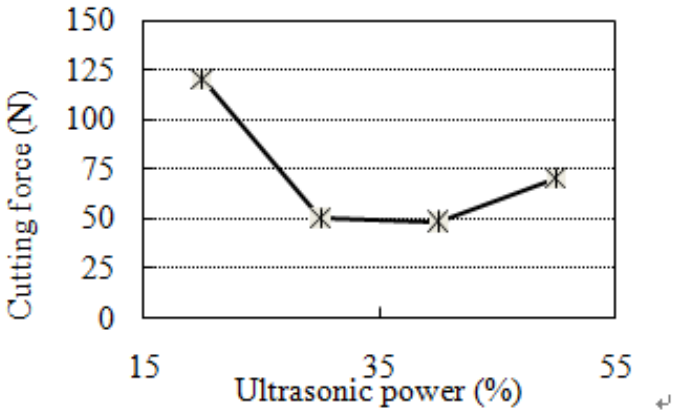

(c) Dental ceramics (after [3])

Figure 4.21 Experimental relation between spindle speed and cutting force

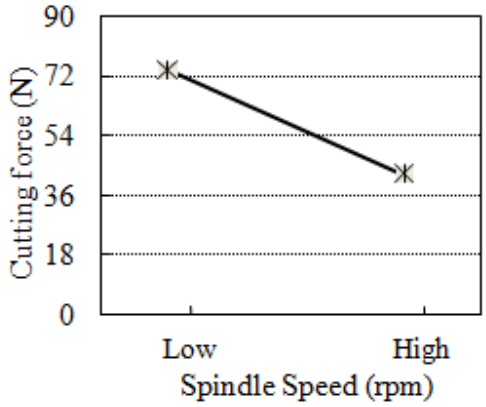

(a) Silicon

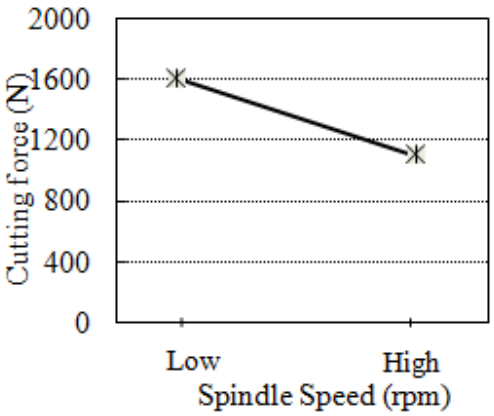

(b) Silicon carbide (after [2])

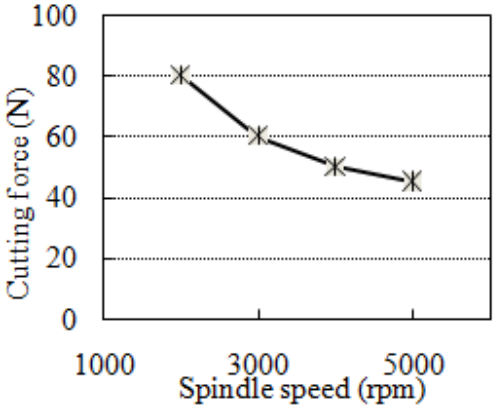

(c) Dental ceramics (after [3])

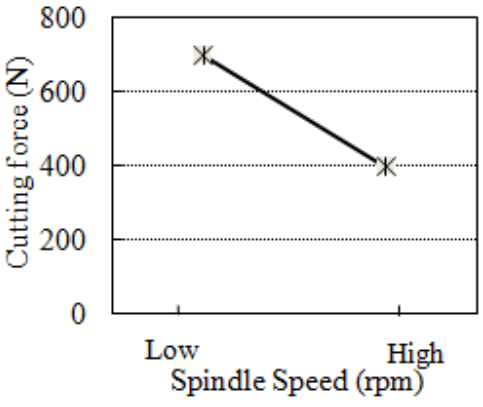

(d) Aluminum oxide (after [4])

Figure 4.19 shows the experimentally determined relation between diamond grain size and cutting force when UVAG of silicon carbide. As can be seen, when diamond grain size

increased (from mesh 80/100 to mesh 60/80), cutting force increased. This result is different from the predicted influence of diamond grain size on cutting force, as shown in Figure 4.9. The inconsistence may be due to the following reason. The predicted influence of diamond grain diameter on cutting force was based on the assumption that everything else (including the number of diamond grains) was the same when the diamond grain diameter changed. In experiments, two different tools (i.e. grinding wheels) were used: one with diamond grain size of mesh 60/80, and the other of mesh 80/100. There was no guarantee that the two grinding wheels were made exactly the same except diamond grain diameter. In fact, in order to keep the same diamond concentration, the number of diamond grains would decrease when using a larger diamond grain diameter, resulting in higher cutting force, as predicted in Figure 4.7.

The model predicted that cutting force will increase as vibration amplitude increases (see Figure 4.11). This predicted trend agrees with the experimental results on silicon as shown in Figure 4.20 (a), those on silicon carbide as shown in Figure 4.20 (b), and those on dental ceramics as shown in Figure 4.20 (c).

The predicted trends of spindle speed's influence on cutting force (as shown in Figure 3.15) and feedrate's influence (as shown in Figure 4.17) are consistent with the experimental results on silicon and on other materials reports in the literature (as shown in Figure 4.21 and Figure 4.22).

Figure 4.22 Experimental relation between feedrate and cutting force

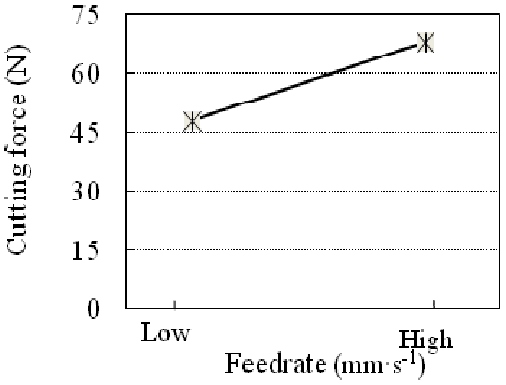

(a) Silicon

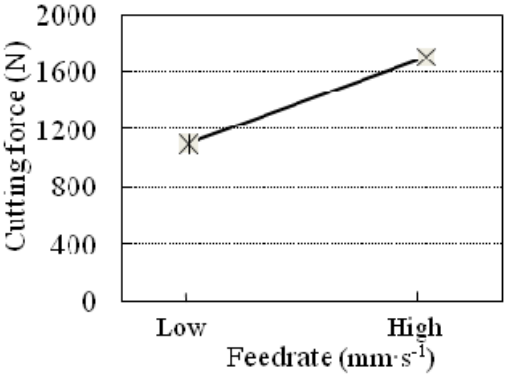

(b) Silicon carbide (after [2])

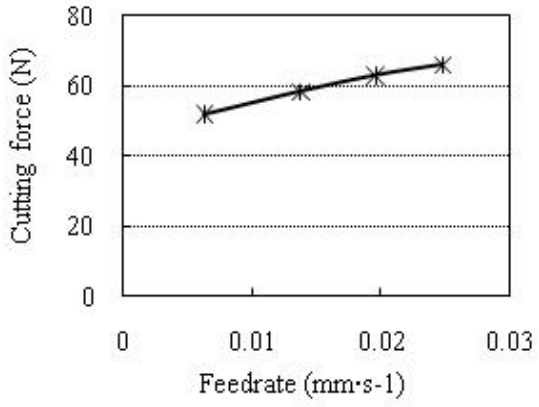

(c) Dental ceramics (after [3])

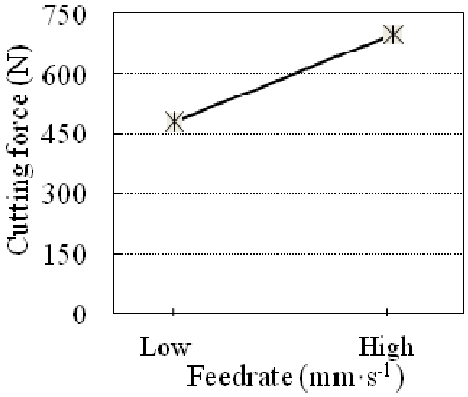

(d) Aluminum oxide (after [4])

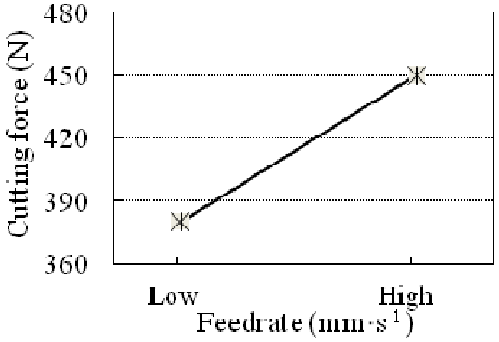

(e) Ceramic matrix composite (after [5])

4.6 Conclusions

A mechanistic model for cutting force in ultrasonic-vibration-assisted grinding (UVAG) of brittle materials has been developed using silicon as an example. The model was used to predict influences of input variables on cutting force. These predicted influences were compared with those determined experimentally. The trends of predicted influences of input variables on cutting force agree well with experimental results (except that of diamond grain diameter). Based on model predictions, cutting force will increase as vibration amplitude and feedrate increase, but decrease as diamond grain number, vibration frequency, and spindle speed increase.

Acknowledgements

The work was supported by the National Science Foundation through Award CMMI-0900462. The authors would like to thank Mr. Bruno Renzi at NBR Diamond Tool Corporation for providing the diamond tool and Mr. Timothy Denies at Kansas State University for providing technical assistance in making fixture and setting up the RUM machine.

References

[1] D. Stinton, Assessment of the state of the art machining and surface preparation of ceramics, ORNL/TM Report No. 10791, Oak Ridge National Laboratory, Oak Ridge, TN, 1988.

[2] N.J. Churi, Z.J. Pei, D.C. Shorter, C. Treadwell, Rotary ultrasonic machining of silicon carbide: designed experiments, International Journal of Manufacturing Technology and Management 12 (1-3) (2007) 284-298.

[3] N.J. Churi, Z.J. Pei, C. Treadwell, D.C. Shorter, Rotary ultrasonic machining of dental ceramics, International Journal of Machining and Machinability of Materials 6 (3-4) (2009) 270-284.

[4] Y. Jiao, P. Hu, Z.J. Pei, C. Treadwell, Rotary ultrasonic machining of ceramics: design of experiments, International Journal of Manufacturing Technology and Management 7 (2-4) (2005) 192-206.

[5] Z.C. Li, Y. Jiao, T.W. Deines, Z.J. Pei, C. Treadwell, Rotary ultrasonic machining of ceramic matrix composites: feasibility study and designed experiments, International Journal of Machine Tools and Manufacture 45 (2005) 1402-1411.

[6] W.M. Zeng, Z.C. Li, X.P. Xu, Z.J. Pei, J.D. Liu, J. Pi, Experimental investigation of intermittent rotary ultrasonic machining, Key Engineering Materials 359-360 (2008) 425-430.

[7] Z.C. Li, L.W. Cai, Z.J. Pei, C. Treadwell, Edge-chipping reduction in rotary ultrasonic machining of ceramics: finite element analysis and experimental verification, International Journal of Machine Tools and Manufacture 46 (2006) 1469-1477.

[8] W.M. Zeng, X.P. Xu, Z.J. Pei, Rotary ultrasonic machining of advanced ceramics, Materials Science Forum 532-533 (2006) 361-364.

[9] Z.C. Li, Y. Jiao, T.W. Deines, Z.J. Pei, C. Treadwell, Development of an innovative coolant system for rotary ultrasonic machining, International Journal of Manufacturing Technology and Management 7 (2-4) (2005) 318-328.

[10] M. Kubota, Y. Tamura, and N. Shimamura, Ultrasonic machining with a diamond impregnated tool, Bulletin Japan Society of Precision Engineering 11 (3) (1977) 127-132.

[11] A.I. Markov et al., Ultrasonic drilling and milling of hard non-metallic materials with diamond tools, Machine and Tooling 48 (9) (1977) 45-47.

[12] Z.J. Pei, D. Prabhakar, P.M. Ferreira, M. Haselkorn, Rotary ultrasonic drilling and milling of ceramics, Ceramic Transactions 49 (1995) 185-196.

[13] P.G. Petrukha et al., Ultrasonic diamond drilling of deep holes in brittle materials, Journal of Russian engineering 50 (10) (1970) 70-74.

[14] D. Prabhakar, Machining Advanced Ceramic Materials Using Rotary Ultrasonic Machining Process, MS Thesis, University of Illinois at Urbana-Champaign, Illinois, USA, 1992.

[15] D. Prabhakar, P.M. Ferreira, M. Haselkorn, An experimental investigation of material removal rates in rotary ultrasonic machining, Transactions of the North American Manufacturing Research Institute of SME 20 (1992) 211-218.

[16] H. Wang, L. Lin, Improvement of rotary ultrasonic deep hole drilling of glass ceramics-zerodur, Proceedings of the 7th International Precision Engineering Seminar, The Japan Society of Applied Physics, Kobe, Japan (1993) 719-730.

[17] Z.J. Pei, D. Prabhakar, P.M. Ferreira, M. Haselkorn, A mechanistic approach to the prediction of material removal rates in rotary ultrasonic machining, Journal of Engineering for Industry 117 (2) (1995) 142-151.

[18] Q.H. Zhang, C.L. Wu, J.L. Sun, Z.X. Jia, Mechanism of material removal in ultrasonic drilling of engineering ceramics, Proceedings of Institution of Mechanical Engineers, Part B: Journal of Engineering Manufacture 214 (9) (2000) 805-810.

[19] C.L. Chao, W.C. Chou, C.W. Chao, C.C. Chen, Material removal mechanisms involved in rotary ultrasonic machining of brittle materials, Key Engineering Materials 329 (2007) 391-396.

[20] D. Prabhakar, Z.J. Pei, P.M. Ferreira, M. Haselkorn, A theoretical model for predicting material removal rates in rotary ultrasonic machining of ceramics, Transactions of the North American Manufacturing Research Institute of SME 21 (1993) 167-172.

[21] M.C. Shaw, Principles of Abrasive Processing, Oxford University Press, New York, 1996.

[22] Y.B. Wu, M. Nomura, Z.J. Feng, M. Kato, Modeling of grinding force in constant-depth-of-cut ultrasonically assisted grinding, Materials Science Forum 471-472 (2004) 101-106.

[23] M. Younis, M.M. Sadek, T. EI-Wardani, New approach to development of a grinding force model, Journal of Engineering for Industry 109 (4) (1987) 306-313.

[24] L.C. Li, J. Fu, Study of grinding force mathematical model, Annals of the CIRP 29 (1) (1980) 245-249.

[25] W. Lortz, A model of the cutting mechanism in grinding, Wear 53 (1) (1979) 115-128.

[26] G. Wener, Influence of work material on grinding force, Annals of the CIRP 27 (1) (1978) 243-248.

[27] K.L. Johnson, Contact Mechanics, Cambridge University Press, New York, 1985.

[28] G. L. Sheldon, I. Finnie, The mechanism of material removal in the erosive cutting of brittle materials, Journal of Engineering for Industry (1966) 393-399.

[29] S. Timoshenko, J. N. Goodier, Theory of Elasticity, third ed., McGraw-Hill, New York, 1970.

[30] W.L. Cong, Z.J. Pei, E.V. Vleet, N. Mohanty, C. Treadwell, Vibration amplitude in rotary ultrasonic machining: a novel measurement method and effects of process variables, submitted to International Journal of Machine Tools and Manufacture.

[31] D.C. Montgomery, G.C. Runger, Applied Statistics and Probability for Engineers, second ed., John Wiley & Sons, Inc., New York, 1999.

Chapter 5 - Cutting force modeling with design of experiments for ductile materials

The content of this chapter has been published in a conference paper.

Paper Title:

Ultrasonic-vibration-assisted grinding of Titanium: cutting force modeling with design of experiments

Published in:

Proceedings of the ASME International Manufacturing Science & Engineering Conference, 2009, 2: 619-624.

Authors' Names:

Na Qin[a,b], Z. J. Pei[a], D. M. Guo[b]

Authors' Affiliation:

[a]Department of Industrial and Manufacturing Systems Engineering, Kansas State University, Manhattan, KS 66506, USA

[b]School of Mechanical Engineering, Dalian University of Technology, Dalian, Liaoning 116024, China

Abstract

Titanium and its alloys (Ti) have wide applications in industry. However, since Ti is notorious for its poor machinability, their applications have been hindered by the high cost and low efficiency. Ultrasonic-vibration-assisted grinding (UVAG) is a hybrid machining process that combines the material removal mechanisms of diamond grinding and ultrasonic machining, and it is a cost-effective machining process for Ti. The relations between cutting force and input variables have been investigated and reported. But these relations have been studied by changing one variable at time. Therefore, the interactions between cutting force and input variables have not been revealed. In this paper, a two-level five-factor full factorial design is used to study the relations between cutting force and input variables based on a cutting force model for UVAG of Ti. The main effects of these variables, and two-factor interactions and three-factor interactions of these variables are also revealed.

Keywords: Cutting force, Design of experiment, Grinding, Titanium, Ultrasonic vibration

5.1 Introduction

Titanium and its alloys (Ti) are attractive for many applications due to their superior properties [1]. These properties include high strength-to-weight ratio [2,3], creep strength, fatigue strength, fracture toughness, fabricability [1], heat and corrosion resistance at elevated temperature, and shock resistance [2,3]. Besides the aerospace industry that uses 60% of the Ti [4,5], Ti is also used in such industries as military [6,7], automotive [8], chemical [9,10], medical [11,12], and sporting goods [13].

Many Ti components require drilling operations. However, Ti is notorious for its poor machinability [14], resulting in high cost and low efficiency with current drilling methods. Increasing use of Ti/composite stacks in the aerospace industry presents even greater challenges. Therefore, there is a critical need to develop more cost-effective Ti drilling processes.

Figure 5.1 Illustration of ultrasonic-vibration-assisted grinding (after [19])

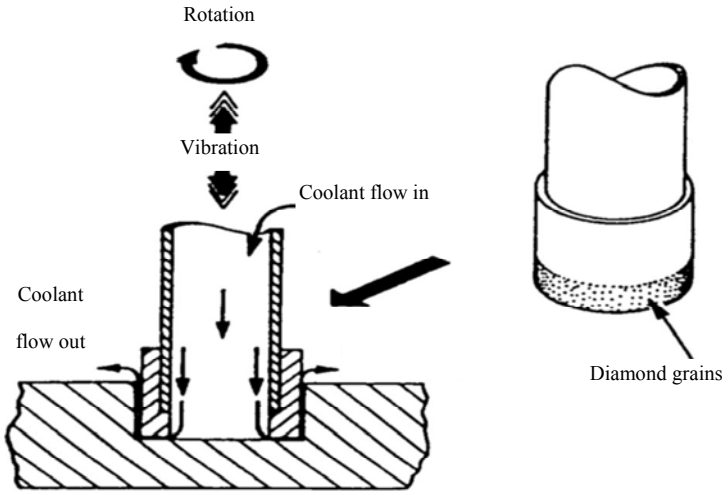

Ultrasonic-vibration-assisted grinding, also called rotary ultrasonic machining (RUM), has been used to drill Ti recently [15-18]. Figure 5.1 is the schematic illustration of UVAG. A rotary core drill with metal-bonded diamond grains ultrasonically vibrates in its axial direction and is fed towards the workpiece. Coolant pumped through the core of the drill washes away the swarf, prevents jamming of the drill and keeps it cool.

Since it was invented in 1960's [20], UVAG has been used primarily to drill brittle materials. Effects of input variables (diamond grain number, grain size, and type; bond type;

vibration amplitude and frequency; spindle speed; coolant type and pressure) on output variables (cutting force, material removal rate, and surface roughness) in UVAG of brittle materials have been investigated experimentally [21-27].

Churi et al. [15-18] were the first to perform feasibility experiments on UVAG of Ti. They also investigated effects of

input variables (diamond concentration, diamond grain size, vibration power, spindle speed, and feedrate) on four output variables (cutting force, material removal rate, tool wear, and surface roughness) in UVAG of Ti.

Qin et al. [28] derived a physics-based model to predict cutting force in UVAG of Ti. Using this model, they also investigated the effects of number of diamond grains, diamond grain size, vibration amplitude, spindle speed, and federate on cutting force.

However, the interactions of these input variables on the cutting force in UVAG of Ti have not been reported. This paper, for the first time, reports the results of a systematic study on the cutting force in UVAG of Ti using the physics-based model derived by Qin et al. In this paper, a-two level, five-factor full factorial design is used to investigate the relationship between the cutting force and the process variables. This study provides the main effects of these variables, the effects of two-factor interactions and three-factor interactions among these variables.

5.2 Brief introduction of the physics-based model and design of experiments

5.2.1 Physics-based model for cutting force in UVAG

The relation between cutting force F and the five process variables is as follows [28]:

$$F = n\sigma_y \delta(2r - \delta)\left\{\frac{\pi}{2} - arcsin\left(1 - \frac{\delta}{A}\right)\right\} \quad (1)$$

where, n is the number of diamond grains, r the diamond grain radius, A the vibration amplitude, and δ the penetration depth of diamond grains into workpiece. δ not only relates to the process variables existing in the above formula, but also relates to spindle speed and feedrate. With given process variables, δ can be obtained using commercial software Solidworks, and then the cutting force will be obtained from the above formula. For more details, please refer to the paper on this physics-based model [28].

5.2.2 Design of experiments

The mechanical properties of workpiece are given in Table 5.1. A 2^5 full factorial design is employed. This means five factors, each at two levels (high and low) as shown in Table 5.2. Table 5.3 shows the matrix with total of 32 treatment combinations. Commercial software called Minitab (version 14, Minitab Inc., State College PA, USA) is used to assist in data processing.

Table 5.1 Mechanical properties of Ti

Property	Unit	Value
Elastic modulus	MPa	105,000
Poission ratio		0.37
Mass density	Kg/m^3	4510
Tensile Strength	MPa	344
Thermal conductivity	W/m·k	16.4

Table 5.2 Low and high levels of processes variables

Process variable	Unit	Low level (-)	High level (+)
Diamond grain number		100	300
Grain size	mm	0.15	0.2
Spindle speed	rpm	2000	3000
Feedrate	mm/s	0.03	0.05
Vibration amplitude	mm	0.02	0.04

Table 5.3 Design matrix and results

Diamond number	Grain radius	Spindle speed	Feed-rate	Vibration amplitude	Cutting force (N)
-	-	-	-	-	253
+	-	-	-	-	347
-	+	-	-	-	311
+	+	-	-	-	406
-	-	+	-	-	204
+	-	+	-	-	287
-	+	+	-	-	253
+	+	+	-	-	354
-	-	-	+	-	378
+	-	-	+	-	502
-	+	-	+	-	438
+	+	-	+	-	599

-	-	+	+	-	298
+	-	+	+	-	411
-	+	+	+	-	364
+	+	+	+	-	503
-	-	-	-	+	219
+	-	-	-	+	298
-	+	-	-	+	260
+	+	-	-	+	356
-	-	+	-	+	174
+	-	+	-	+	240
-	+	+	-	+	211
+	+	+	-	+	290
-	-	-	+	+	320
+	-	-	+	+	298
-	+	-	+	+	382
+	+	-	+	+	507
-	-	+	+	+	253
+	-	+	+	+	344
-	+	+	+	+	306
+	+	+	+	+	411

5.3 Results and discussion

5.3.1 Main effects

The main effects of each process variable are shown in Figure 5.2 (a) - (e) respectively. It can be seen that cutting force increases as the diamond grain number, diamond grain size, and feedrate increase, and as the spindle speed and vibration amplitude decrease. These main effects in UVAG are consistent with those observed experimentally by Churi et al. [16,17] except for the diamond grain number. The inconsistence may be due to the following reason. The predicted

influences of diamond grain number on cutting force were based on the assumption that everything else was the same when the diamond grain number changed. In experiments, two different tools (or grinding wheels) were used, one with diamond concentration of 80, and the other 100. There was no guarantee that the two wheels were made exactly the same this except concentration. Further experimental investigations on the influences of diamond concentration are planned and the results will be reported later.

Figure 5.2 Main effects of process variables

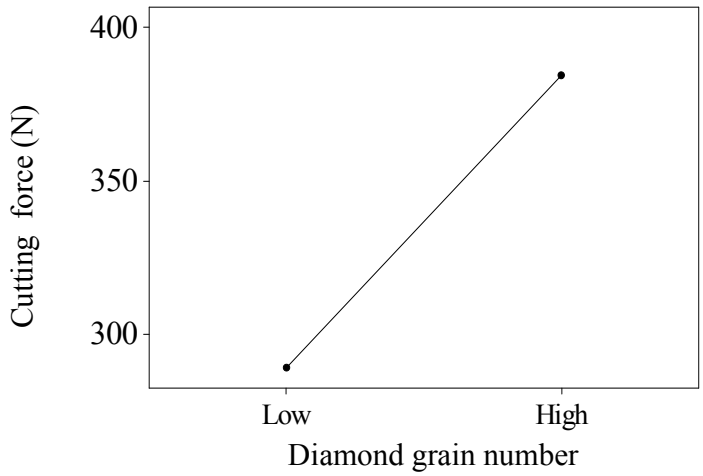

(a)

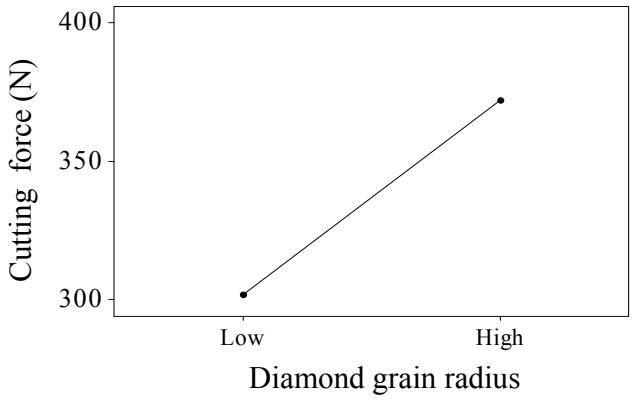
400
350
300
Cutting force (N)
Low
High
Diamond grain radius

(b)

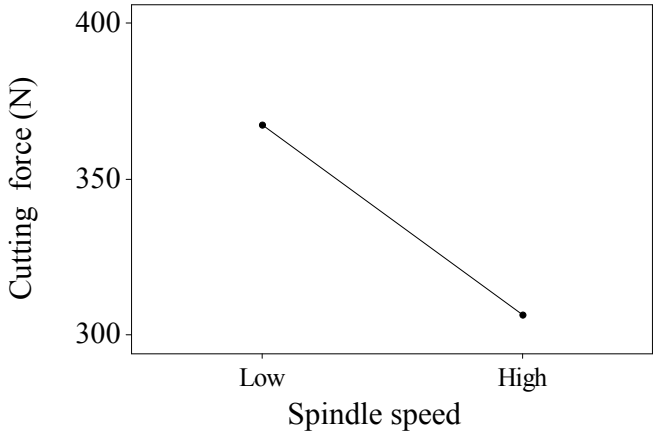
400
350
300
Cutting force (N)
Low
High
Spindle speed

(c)

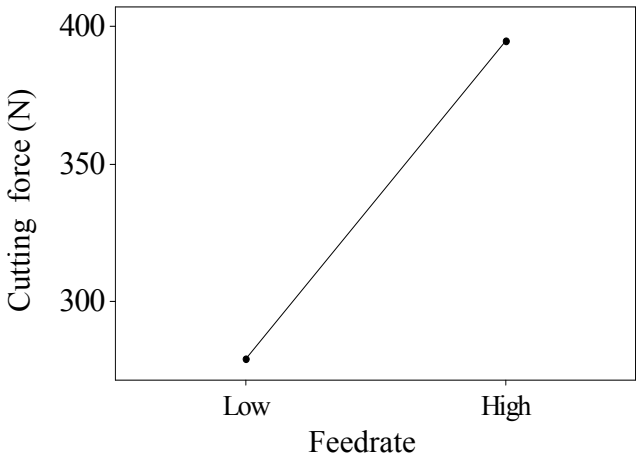
400
350
300
Cutting force (N)
Low
High
Feedrate

(d)

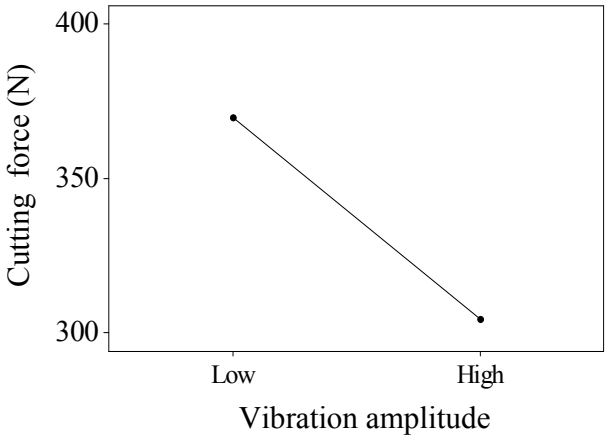

(e)

5.3.2 Two-factor interactions

Figure 5.3 provides all two-factor interaction effects of five variables. For the interaction between diamond grain number and diamond grain radius, at the high level of diamond grain number, the change in grain size causes a larger change in the cutting force than at the low level of diamond grain number. For the interaction between diamond grain number and spindle speed, with different level of diamond grain number, the change in spindle speed does not make obvious change in cutting force, For the interaction between diamond grain number and feedrate, at the high level of diamond grain number, the change in feedrate causes a larger change in the cutting force than at the low level of diamond grain number. For the interaction between diamond grain number and vibration amplitude, at the high level of diamond grain number, the change in vibration amplitude causes a larger change in the cutting force than at the low level of diamond grain number.

For the interaction between diamond grain radius and spindle speed, at the high level of diamond grain radius, the change in spindle speed causes a larger change in cutting force than at the low level of spindle speed. For the interaction between diamond grain radius and vibration amplitude, with different levels of diamond grain radius, the change in vibration does not cause significant change in cutting force.

For the interaction between spindle speed and feedrate, at different levels of spindle speed, the change of feedrate does not cause significant change in cutting force. For the interaction between spindle speed and vibration amplitude, at the high level of spindle speed, the change of vibration amplitude causes smaller change in cutting force than at the low level of spindle speed.

Figure 5.3 Two-factor interactions of process variables

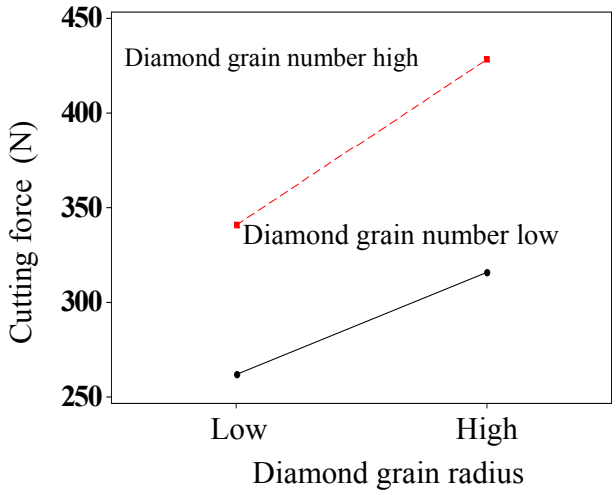

(a)

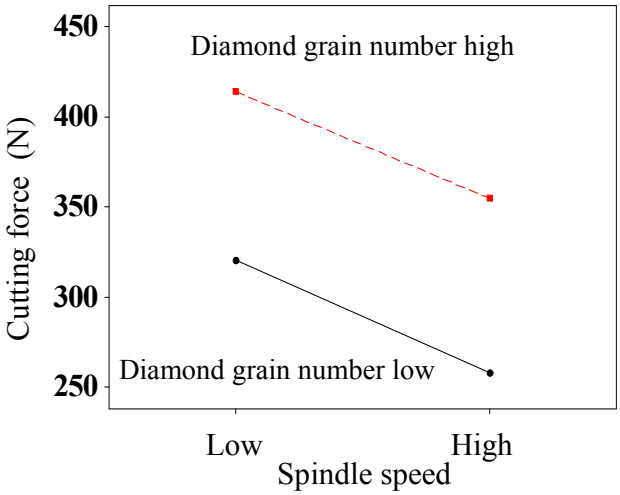
450
400
350
300
250
Cutting force (N)
Diamond grain number high
Diamond grain number low
Low
High
Spindle speed

(b)

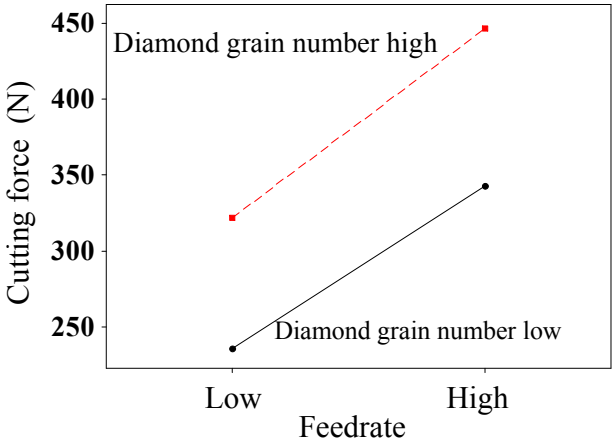
450
400
350
300
250
Cutting force (N)
Diamond grain number high
Diamond grain number low
Low
High
Feedrate

(c)

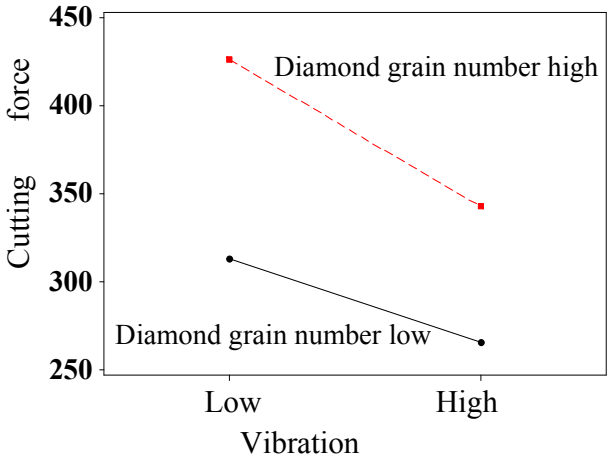
450
400
350
300
250
Cutting force
Diamond grain number high
Diamond grain number low
Low
High
Vibration

(d)

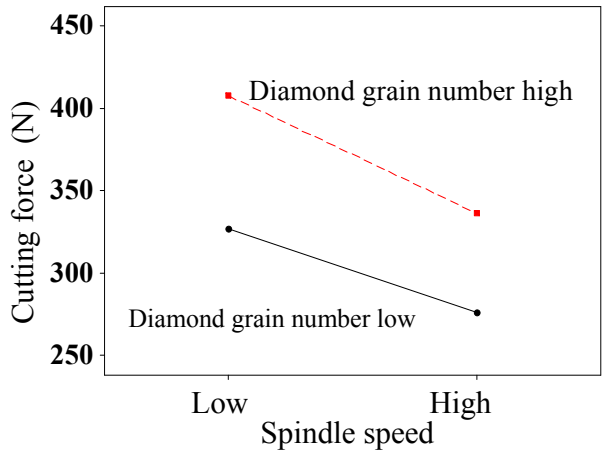
450
400
350
300
250
Cutting force (N)
Diamond grain number high
Diamond grain number low
Low
High
Spindle speed

(e)

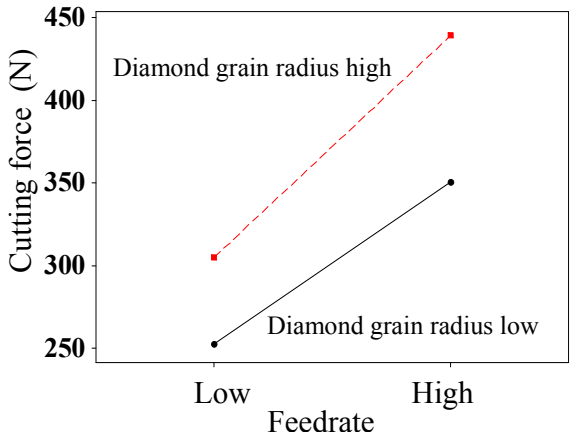
450
400
350
300
250
Cutting force (N)
Diamond grain radius high
Diamond grain radius low
Low
High
Feedrate

(f)

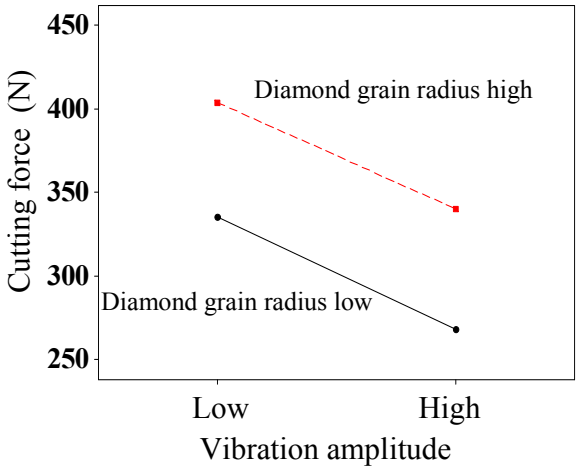
450
400
350
300
250
Cutting force (N)
Diamond grain radius high
Diamond grain radius low
Low
High
Vibration amplitude

(g)

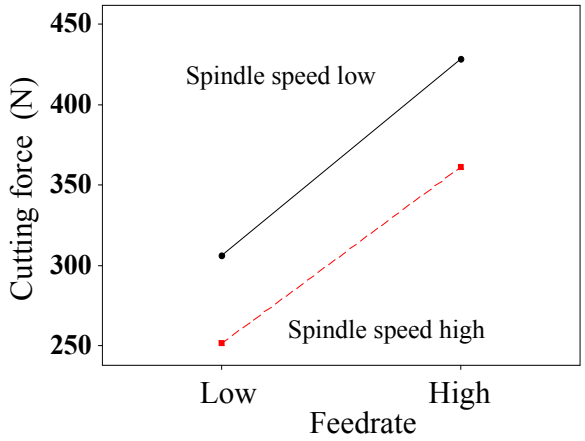
450
400
350
300
250
Cutting force (N)
Spindle speed low
Spindle speed high
Low
High
Feedrate

(h)

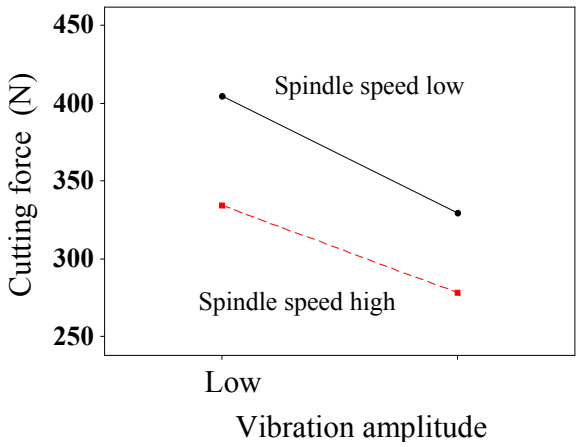

(i)

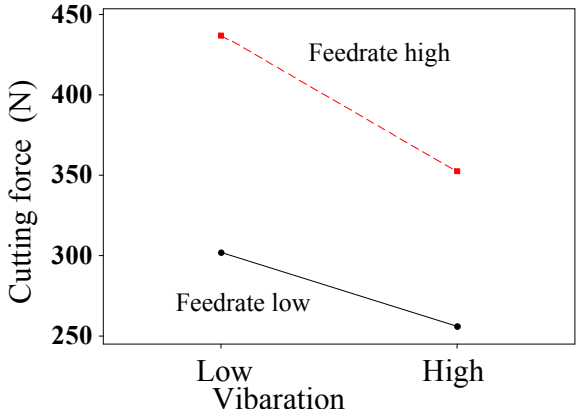

(j)

5.3.3 Three-factor interactions

Figure 5.4 shows four three-factor interactions on cutting force. The first three-factor interaction as shown in (a) is among diamond grain number, diamond grain radius, and spindle speed. It can be observed that at the combination of high level of diamond grain number, high level of diamond grain radius, and low level of spindle speed, cutting force is the highest. The second three-factor interaction as shown in (b) is among feedrate, vibration amplitude, and

spindle speed. At the combination of high level of feedrate, high level of vibration amplitude, and low level of spindle speed, cutting force is the highest. The third three-factor interaction as show in (c) is among diamond grain number, vibration amplitude, and spindle speed. It can be seen that at the combination of high level of diamond grain number, high level of vibration amplitude, and low level of spindle speed, cutting force is the highest. The last three-factor interaction as shown in (d) is among feedrate, diamond grain radius, and spindle speed. It can be observed that the combination of high level of feedrate, high level of diamond grain radius, and low level of spindle speed, will result in the highest cutting force.

Figure 5.4 Three-factor interactions of process variables

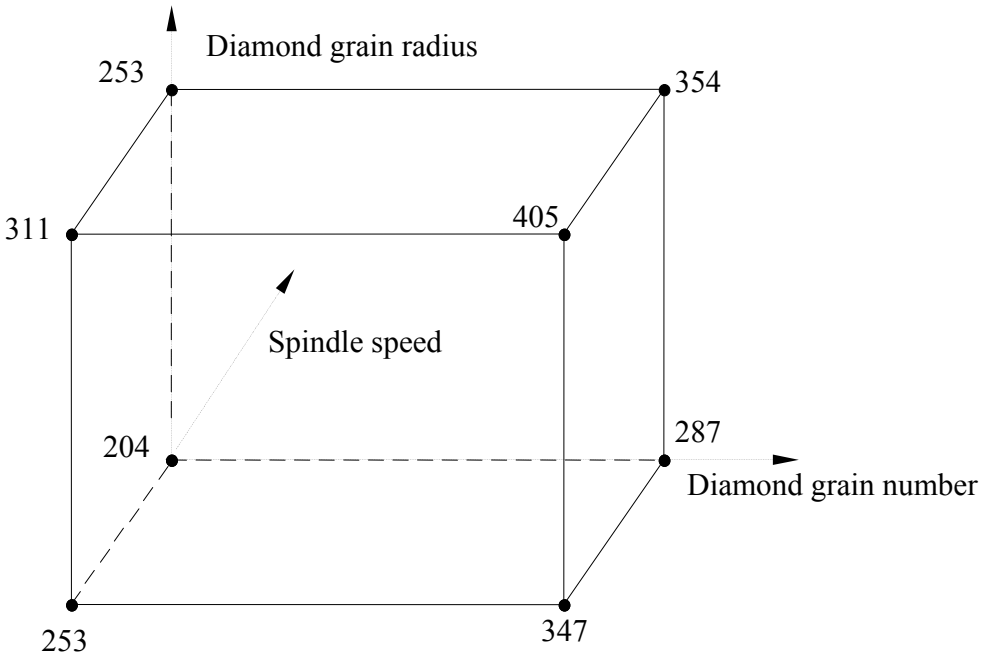

(a)

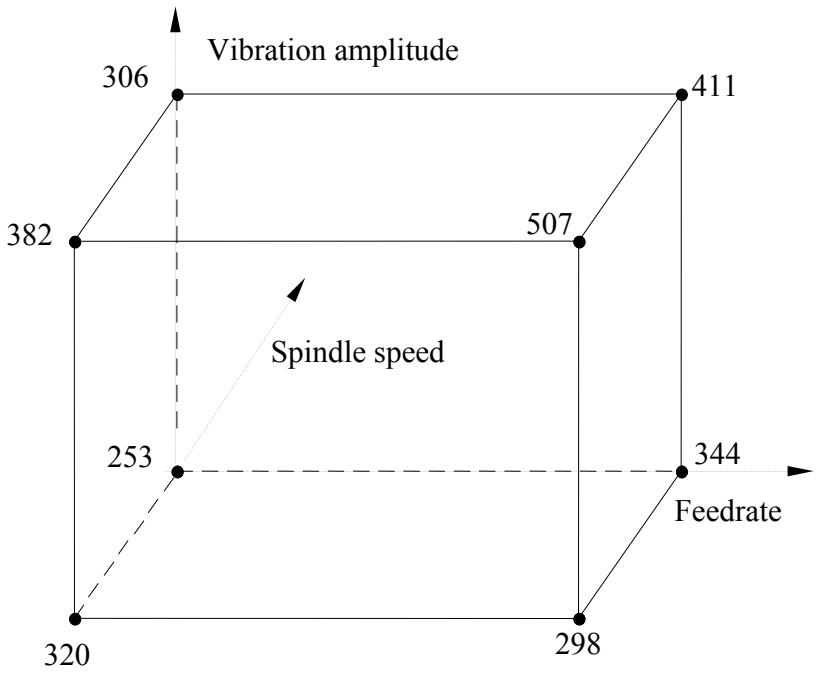
Vibration amplitude
306
411
382
507
Spindle speed
253
344
Feedrate
320
298

(b)

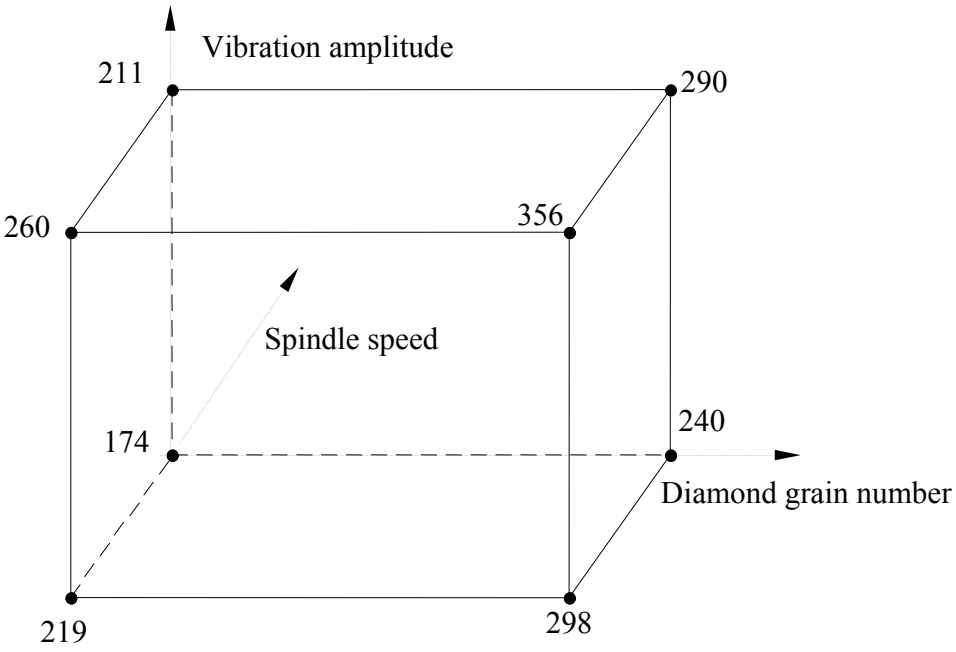
Vibration amplitude
211
290
260
356
Spindle speed
174
240
Diamond grain number
219
298

(c)

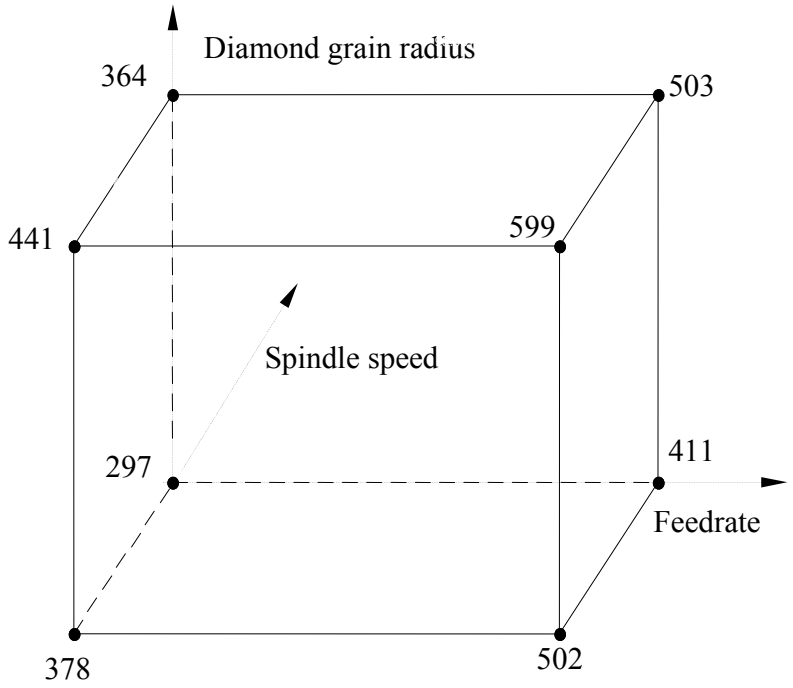

(d)

5.4 Conclusions

In this paper, a 2^5 full factorial design is employed to study the relations between five process variables (diamond grain number, diamond grain size, spindle speed, feedrate, and vibration amplitude) and cutting force in UVAG of Ti, using the physics-based predictive model for cutting force in UVAG of Ti. For the first time, interactions effects of process variables on the cutting force in UVAG of Ti are performed and reported.

References

[1] Froes, F., Allen, P., and Niinomi, M., 1998, "Non-Aerospace Application of Titanium: an Overview," Proceedings of Minerals, Metals and Materials Meeting, Minerals, Metals and Materials Society, Warrendale, PA, pp. 89-97.

[2] Aust, E., and Niemann, H., 1999, "Machining of Gamma Ti-Al," Advanced Engineering Materials, **1** (1), pp. 53-57.

[3] Kumar, K., 1991, "Grinding Titanium," Aerospace Engineering, **11** (9), pp. 17-19.

[4] Boyer, R., 1996, "Overview on the Use of Titanium in the Aerospace Industry," Materials Science and Engineering A: Structure Materials: Properties, Microstructure and Processing, **213** (2), pp. 103-114.

[5] Peacock, D., 1988, "Aerospace Applications for Titanium," Sheet Metal Industries, **65** (8), pp. 406-408.

[6] Montgomery, J., and Well, M., 2001, "Titanium Armor Applications in Combat Vehicles," Journal of Machining 53 (4), pp. 9-32.

[7] Lerner, I., 2004, "Titanium Market Recovering on Commercial Military Aircraft," Chemical Market Reporter, **266** (18), pp. 17.

[8] Yamashita, Y., Tkayama, I., Fujii, H., and Yamazaki, T., 2002, "Applications and Features of Titanium for Automotive Industry," Nippon Steel Technical Report No. 85, pp. 11-14.

[9] Farthing, T., 1979, "Application of Titanium in the Chemical Industry," chemical Age of India, **30** (2), pp. 151-166.

[10] Orr, N., 1982, "Industrial Application of Titanium on the Metallurgical Industries, and Chemical Light Metals," Proceedings of Technical Sessions at the 111th American

Institute of Mining, Metallurgical and Petroleum Engineers, Annual Meeting, AIME, Warrendale, PA.

[11] Froes, F., 2002, "Titanium Sport and Medical Application Focus," Materials Technology, **17** (1), pp. 4-7.

[12] Abdullin, I., Bagautinov, A., and Ibragimov, G., 1988, "Improving Surface Finish for Titanium Alloy Medical Instruments," Biomedical Engineering, **22** (2), pp. 48-50.

[13] Yang, X., and Liu, R., 1999, "Machining Titanium and Its Alloys," Machining Science and Technology 3 (1), pp. 107-139.

[14] Ezugwu, E.Q., 1997, "Titanium Alloys and Their Machinability - A Review," Journal of Materials Processing Technology, **68** (3), pp. 262-274.

[15] Churi, N.J., Li, Z.C., Pei, Z.J., and Treadwell, C., 2005, "Rotary Ultrasonic Machining of Titanium Alloy: A Feasibility Study," Proceedings of International Mechanical Engineering Congress and Exposition (IMECE), Orlando, FL, pp. 885-892.

[16] Churi, N.J., Pei, Z.J., and Treadwell, C., 2006, "Rotary Ultrasonic Machining of Titanium Alloy: Effects of Machining Variables," Machining Science and Technology, **10** (3), pp. 301-321.

[17] Churi, N.J., Pei, Z.J., and Treadwell, C., 2007, "Rotary ultrasonic machining of titanium alloy (Ti-6Al-4V): effects of tool variables," International Journal of Precision Technology, **1** (1), pp. 85-96.

[18] Churi, N.J., Pei, Z.J., and Treadwell, C., 2007, "Wheel Wear Mechanisms in Rotary Ultrasonic Machining of Titanium," Proceedings of International Mechanical Engineering Congress and Exposition (IMECE), Seattle, WA, pp. 399-407.

[19] Stinton, D., 1988, “Assessment of the State of the Art Machining and Surface Preparation of Ceramics,” ORNL/TM- Report 10791, Oak Ridge National Laboratory, Oak Ridge, TN.

[20] Legge, P., 1966, “Machining without abrasive slurry,” Ultrasonics, **2**, pp. 157-162.

[21] Kubota, M., Tamura, Y., and Shimamura, N., 1977, “Ultrasonic Machining with a Diamond Impregnated Tool,” Bulletin of Japan Society of Precision Engineering, **11** (3), pp.127-132.

[22] Markov, A., 1977, “Ultrasonic Drilling and Milling of Hard Non-Metallic Materials with Diamond Tools,” Machine and Tooling, **48** (9), pp. 45-47.

[23] Pei, Z.J., Prabhakar, D., Ferreira, P.M., and Haselkorn, M., 1995, “Rotary ultrasonic drilling and milling of ceramics, Ceramic Transactions," Manufacture of Ceramic Components, American Ceramic Society, **49**,Westerville, OH, pp. 185-196.

[24] Petrukha, P., 1970, “Ultrasonic Diamond Drilling of Deep Holes in Brittle Materials,” Russian Engineering Journal **50** (10), pp.70-74.

[25] Prabhakar, D., 1992, “Machining Advanced Ceramic Materials Using Rotary Ultrasonic Machining Process,” MS Thesis, University of Illinois at Urbana-Champaign.

[26] Prabhakar, D., Ferreira, P.M., and Haselkorn, M., 1992, “An Experimental Investigation of Material Removal Rates in Rotary Ultrasonic Machining,” Transactions of the North American Manufacturing Research of SME, **10**, pp. 211-218.

[27] Wang, H., Lin, L., 1993, “Improvement of Rotary Ultrasonic Deep Hole Drilling of Glass Ceramics-Zerodur,” Proceedings of Seminar of the 7th International Precision Engineering, Kobe, Japan, pp. 719-730.

[28] Qin, N., Pei, Z. J., Treadwell, C., and Guo, D. M., 2009, "Physics-Based Predictive Cutting Force Model in Ultrasonic-Vibration-Assisted Grinding for Titanium Drilling," Journal of Manufacturing Science and Engineering, **131** (4), pp. 041011-1-041011-9.

Chapter 6 - Cutting force modeling with design of experiments for brittle materials

The content of this chapter has been published in a conference paper.

Paper Title:

UVAG of brittle materials: DOE with a cutting force model

Published in:

Proceedings of the 2010 Industrial Engineering Research Conference, 2010.

Authors' Names:

Na Qin[a,b], Z.J., Pei[a], D.M. Guo[b], W.L. Cong[a]

Authors' Affiliation:

[a]Department of Industrial and Manufacturing Systems Engineering, Kansas State University, Manhattan, KS 66506, USA

[b]School of Mechanical Engineering, Dalian University of Technology, Dalian, Liaoning 116024, China

Abstract

Ultrasonic-vibration-assisted grinding (UVAG) combines the material removal mechanisms of diamond grinding and ultrasonic machining. Models have been presented to predict material removal rate and edge chipping and many experiments have also been conducted. However, there were no models on cutting force in UVAG of brittle materials until the authors developed one. Based on this developed model, this paper reports a systematic study on cutting force in UVAG of brittle materials using a 2^6 factorial design. The main effects, two-factor and three-factor interaction effects on cutting force are revealed and compared with those obtained experimentally.

Keywords: Brittle material, cutting force, design of experiment, ultrasonic-vibration-assisted grinding

6.1 Introduction

Brittle materials (such as silicon carbide and ceramics matrix composite) have broad applications in industry due to their high strength, high stiffness, and resistance to wear [1-8]. However, these superior properties also make it very difficult to shape and machine these materials into a precise size and shape [9].

Reported machining methods for these brittle materials include laser processing [10], electrical-discharge machining (EDM) [11,12], ultrasonic machining (USM) [13], and ultrasonic-vibration-assisted grinding (UVAG) (also called rotary ultrasonic machining, RUM) [14-17]. Among these non-traditional machining processes, UVAG is a relatively cost-effective process due to its high material removal rate (MRR) [15], better capability to drill deep and accurate holes [18-20], low tool pressure, and superior surface finish [9,18,21].

Figure 6.1 is the schematic illustration of UVAG. A rotary core drill with metal-bonded diamond grains is vibrated ultrasonically and fed towards the workpiece. Coolant pumped through the core of the drill washes away the swarf, prevents jamming of the drill and keeps it cool.

Many experiments on UVAG of brittle materials have been conducted to study the relationships between input variables and output variables (including cutting force, surface roughness, edge chipping, and material removal rate). Models have been presented to predict material removal rate and edge chipping. However, there were no models on cutting force in UVAG of brittle materials.

Qin et al. [22] developed a mechanistic model to predict cutting force in UVAG of brittle materials. Using this model, they also studied the effects of six input variables on cutting force. However, no systematic studies have been published about the interaction effects of these input variables on cutting force in UVAG of brittle materials. For the first time, a systematic study on the cutting force in UVAG of brittle materials using the mechanistic model is conducted and reported in this paper. A 2^6 (two-level six-factor) full factorial design is utilized. The main effects, two-factor interaction effects as well as three-factor interaction effects of these variables on cutting force are revealed.

Figure 6.1 Illustration of UVAG [9]

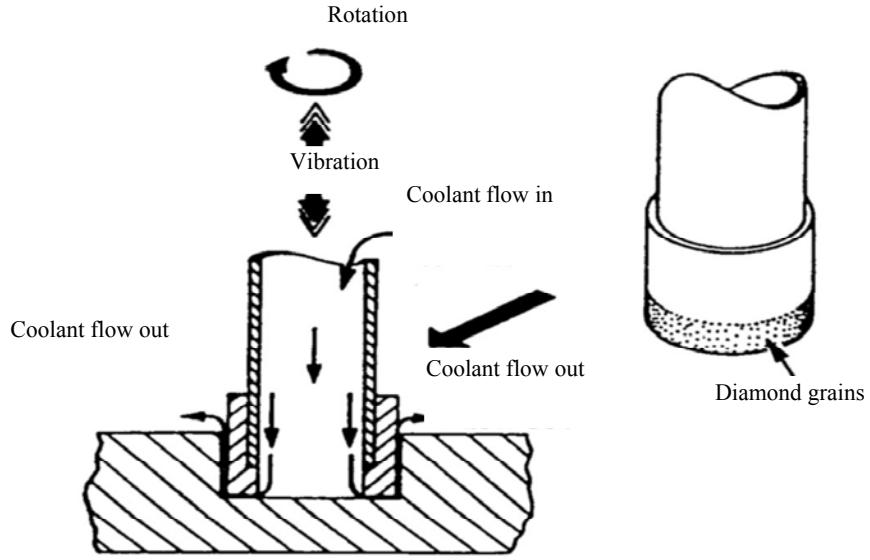

Figure 6.2 Main effects of input variables

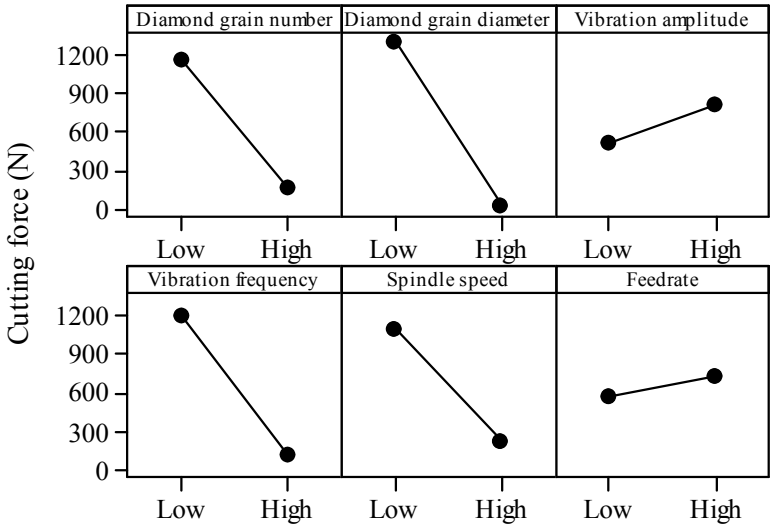

6.2 Brief description of the mechanistic model

UVAG is a hybrid machining process that combines the material removal mechanisms of ultrasonic machining and diamond grinding. In the mechanistic model, ultrasonic machining with an amplitude A and a frequency f was taken as the primary process and brittle fracture is the dominant mode of material removal. Effects of the rotating motion of the tool were taken into consideration via its effects on the indentation volume by each diamond grain into the workpiece. As most researchers did when developing cutting force models for grinding [23-29], the cutting force for individual diamond grain F/n was derived first, and then, the total cutting force could be obtained by summing up the forces on all diamond grains taking part in cutting,

In the model, the maximum contact force on individual diamond grain, F_c/n, was expressed as follows [30]:

$$\frac{F_c}{n} = \left(\frac{8}{9} \left(\frac{E}{1-\upsilon^2} \right)^2 d\delta^3 \right)^{\frac{1}{2}} \tag{1}$$

where F_c is the maximum contact force on all diamond grains taking part in cutting, n is the number of diamond grains taking part in cutting, E and v are Young's modulus and Poisson's ratio of workpiece material, respectively, d is diamond grain diameter, and δ is maximum indentation depth into the workpiece by a diamond grain.

In the above equation, δ was the only unknown parameter, and could be calculated from indentation volume U:

$$U = \pi\delta^2\left[1+\frac{D_o S}{60df}\left(\frac{3\pi}{2}-\arcsin\left(\frac{\delta}{A}-1\right)\right)\left(\frac{d}{2}-\frac{\delta}{3}\right)\right] \tag{2}$$

where D_o is the outer diameter of the cutting tool, S is spindle speed, f is ultrasonic frequency, and A is ultrasonic amplitude.

For UVAG of brittle materials, more than one vibration cycles may be needed to remove the indentation volume U. In addition, the removed volume W may be larger than the indentation volume U because the cracks responsible for material removal may initiate and propagate outside the indentation volume. So a mechanistic parameter k was utilized to relate W and U:

$$W = kU \tag{3}$$

A serial of experiments with UVAG of silicon were conducted to determine this mechanistic parameter:

$$k = (1.03\times10^{-4}\,\delta^{-1.93}V^{0.97}) \tag{4}$$

Furthermore, W could be obtained by input variables as follows:

$$w = \frac{\pi v\left(D_o^2 - D_i^2\right)}{4nf} \tag{5}$$

where V is feedrate and D_i is the inner diameter of the cutting tool.

Using two impulses in terms of F_c/n and F/n during one vibration cycle, the relationship between F_c/n and F/n could be written as:

$$\frac{F}{n} = \frac{F_c}{n} f\Delta t \tag{6}$$

Where Δt is effective contact time (i.e., the period of time during which the diamond grain has penetrated into the workpiece).

Consequently, the cutting force F can be expressed as:

$$F = \left(\frac{8}{9}\left(\frac{En}{1-\upsilon^2}\right)d\delta^3\right)^{\frac{1}{2}} \cdot \frac{1}{\pi}\left\{\frac{3\pi}{2} - \arcsin\left(\frac{\delta}{A} - 1\right)\right\} \tag{7}$$

For further details of the mechanistic model, please refer to the paper by Qin et al. [22].

6.3 Design of experiments

Since the cutting force model was developed by using silicon as an example of brittle materials, the silicon is also used in this paper. Elastic modulus of silicon is E = 125.6 GPa and Poisson's ratio is ν = 0.3. A 2^6 full factorial design is employed to study the effects of six input variables (diamond grain number n and diameter d, vibration amplitude A and frequency f, spindle speed S, and feedrate V). There are two levels (high and low) for each of the input variables. The values of the corresponding high and low levels are determined according to preliminary experiments and presented in Table 6.1. The design matrix and results of cutting

force are shown in Table 6.2. Commercial software Minitab (version 14, Minitab Inc., State College PA, USA) was used to process the data and obtain the main effects, and two-factor interaction effects, as well as three-factor interaction effects.

Table 6.1 Low and high levels of input variables

Input variable	Unit	High level (-)	Low level (+)
Diamond grain number		60	70
Diamond grain diameter	mm	0.13	0.18
Vibration amplitude	mm	0.008	0.015
Vibration frequency	kHz	20	24
Spindle speed	rpm	2000	4000
Feedrate	$mm \cdot s^{-1}$	0.013	0.029

Table 6.2 Design matrix and results

n	d	A	f	S	V	Force (N)
-	-	-	-	-	-	6466.36
+	-	-	-	-	-	512.76
-	+	-	-	-	-	60.34
+	+	-	-	-	-	6.53
-	-	+	-	-	-	6759.39
+	-	+	-	-	-	713.81
-	+	+	-	-	-	67.38
+	+	+	-	-	-	6.87
-	-	-	+	-	-	378.60
+	-	-	+	-	-	47.13
-	+	-	+	-	-	3.75
+	+	-	+	-	-	0.36
-	-	+	+	-	-	495.75
+	-	+	+	-	-	53.39
-	+	+	+	-	-	3.88
+	+	+	+	-	-	0.36
-	-	-	-	+	-	736.76
+	-	-	-	+	-	186.07
-	+	-	-	+	-	35.74
+	+	-	-	+	-	4.92
-	-	+	-	+	-	1300.62
+	-	+	-	+	-	275.75
-	+	+	-	+	-	43.74
+	+	+	-	+	-	5.51
-	-	-	+	+	-	152.99
+	-	-	+	+	-	27.23
-	+	-	+	+	-	3.02
+	+	-	+	+	-	0.32
-	-	+	+	+	-	216.45
+	-	+	+	+	-	33.83
-	+	+	+	+	-	3.28
+	+	+	+	+	-	0.34
-	-	-	-	-	+	4279.55
+	-	-	-	-	+	780.23
-	+	-	-	-	+	97.56
+	+	-	-	-	+	10.80
-	-	+	-	-	+	11366.31
+	-	+	-	-	+	1149.71

-	+	+	-	-	+	111.02
+	+	+	-	-	+	11.48
-	-	-	+	-	+	595.37
+	-	-	+	-	+	75.81
-	+	-	+	-	+	6.28
+	+	-	+	-	+	0.60
-	-	+	+	-	+	823.15
+	-	+	+	-	+	87.67
-	+	+	+	-	+	6.54
+	+	+	+	-	+	0.61
-	-	-	-	+	+	986.73
+	-	-	-	+	+	260.40
-	+	-	-	+	+	54.24
+	+	-	-	+	+	7.81
-	-	+	-	+	+	1824.80
+	-	+	-	+	+	398.25
-	+	+	-	+	+	67.91
+	+	+	-	+	+	8.88
-	-	-	+	+	+	219.96
+	-	-	+	+	+	41.05
-	+	-	+	+	+	4.88
+	+	-	+	+	+	0.54
-	-	+	+	+	+	321.79
+	-	+	+	+	+	52.22
-	+	+	+	+	+	5.38
+	+	+	+	+	+	0.56

6.3.1 Main effects

Figure 6.2 shows the main effects of six input variables on cutting force. Cutting force decreases as the diamond grain number and diameter, vibration frequency and spindle speed increase, and as the vibration amplitude and feedrate decrease.

The main effects of diamond grain diameter, spindle speed and feedrate are consistent with those observed experimentally in UVAG of other brittle materials and reported in the literature [14-16,31]. For the main effect of diamond grain number, the modeling prediction was not consistent with experimental results reported by Churi et al. [16]. The inconsistence may be

due to the following reasons. The influences of diamond grain number on cutting force in the model were predicted based on the assumption that everything else was the same when the diamond grain number changed. In experiments, two different tools (or grinding wheels) were used, one with diamond concentration of 80, and the other 100. There was no guarantee that the two wheels were made exactly the same except diamond concentration. Further experimental investigations on the influences of diamond concentration are planned and the results will be reported later.

For the main effect of vibration amplitude, experiments on UVAG of silicon carbide show that cutting force decreases first and then increases as the vibration amplitude increases [16]. The second half of the experiments results agrees with the model prediction. The reason for this phenomenon will be provided in the next section.

6.3.2 Two-factor interaction effects

Figure 6.3 shows all the two-factor interaction effects of input variables on cutting force. It can be seen that, among the five interaction effects between feedrate and other input variables, only one is significant: the interaction effect between vibration amplitude and feedrate. Therefore, in the following discussion, only the interaction effect between vibration amplitude and feedrate will be discussed for feedrate.

Figure 6.3 Two-factor interaction effects

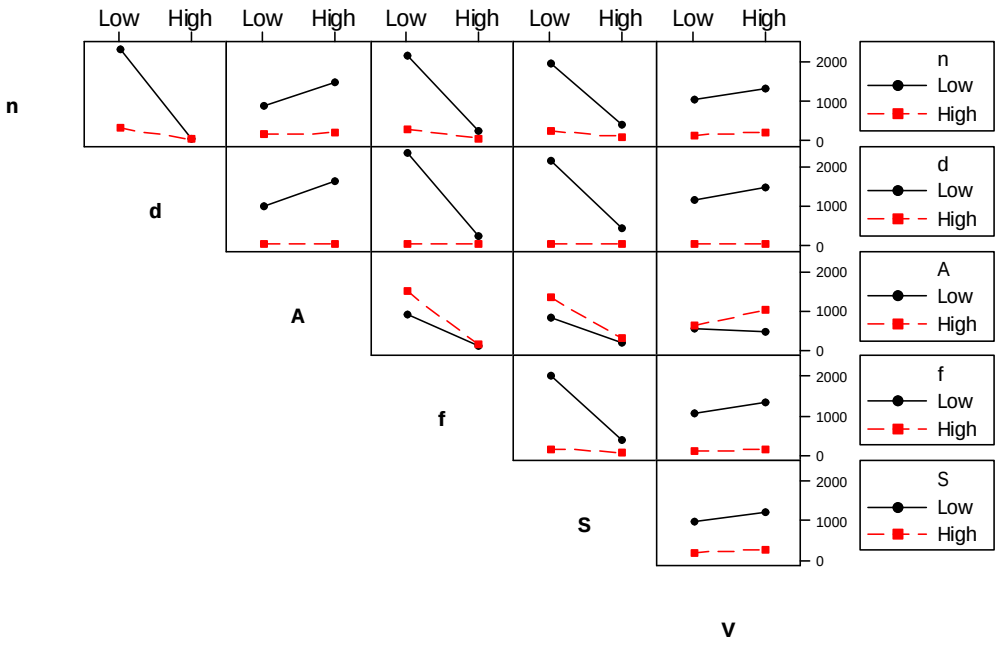

For the interaction effects between diamond grain number and other four variables (diamond grain diameter, vibration amplitude, vibration frequency, and spindle speed), at the low level of diamond grain number, the changes in the four variables cause larger changes in the cutting force than at the high level of grain number. The same situation can be observed for the interaction effects between diamond grain diameter and other three variables (vibration amplitude, vibration frequency, and spindle speed) as shown in Figure 6.3.

For the interaction effects between vibration amplitude and vibration frequency and spindle speed, the changes of vibration frequency and spindle speed at the high level of vibration amplitude causes larger changes in cutting force than at the low level of vibration amplitude. Note that for interaction effects between vibration amplitude and feedrate, with different levels

of vibration amplitude, the change in feedrate has opposite effects on cutting force. At the high level of vibration amplitude, the cutting force increases as the feedrate increases, but at the low level of vibration amplitude, the cutting force decreases as the feedrate increases. In the experiments conducted by Churi et al. [16], the low level and high level of feedrate were 0.008 mms^{-1} and 0.015 mms^{-1}, respectively. In the model predictions, the low level of feedrate was 0.013 mms^{-1} while the high level of feedrate was 0.026 mms^{-1}. It can be seen that even the low level of the feedrate in the model predictions is close to the high level of the feedrate in the experiments [16]. This is why the predicted main effect of vibration amplitude on cutting force agrees with only the second half of the experiment results.

For the interaction effects between vibration frequency and spindle speed, at the low level of vibration frequency, the change in spindle speed causes a larger change in cutting force.

6.3.3 Three-factor interaction effects

Figure 6.4 shows four three-factor interaction effects on cutting force. For interaction effects among diamond grain number, diamond grain diameter, and vibration amplitude, as shown in Figure 6.4 (a), at the high level of grain number,high level of grain diameter, and low level of vibration amplitude, the cutting force is the lowest. For interaction effects among diamond grain number, diamond grain diameter, and vibration frequency, as shown in Figure 6.4 (b), at the high level of grain number, high level of grain diameter and high level of vibration frequency, the cutting force is the lowest. For interaction effects among diamond grain number, diamond grain diameter, and spindle speed, as shown in Figure 6.4 (c), at the high level of grain number, high level of grain diameter, and high level of spindle speed, the cutting force is the lowest. For interaction effects among diamond grain number, diamond grain diameter and

federate, as shown in Figure 6.4 (d), at the high level of grain number, high level of grain diameter, and low level of feedrate, the cutting force is the lowest. The same analysis can be applied to other three-factor interaction effects.

Figure 6.4 Three-factor interaction effects

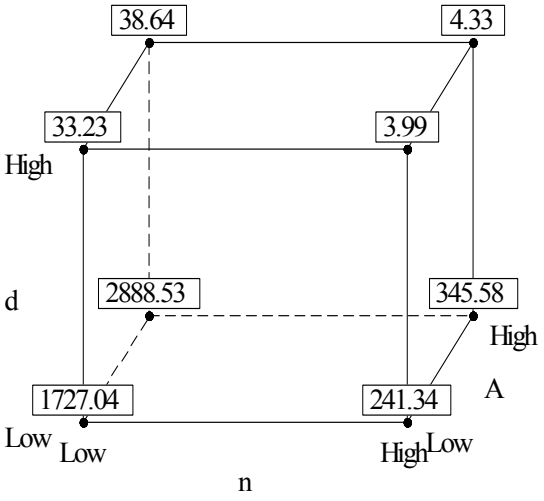

(a)

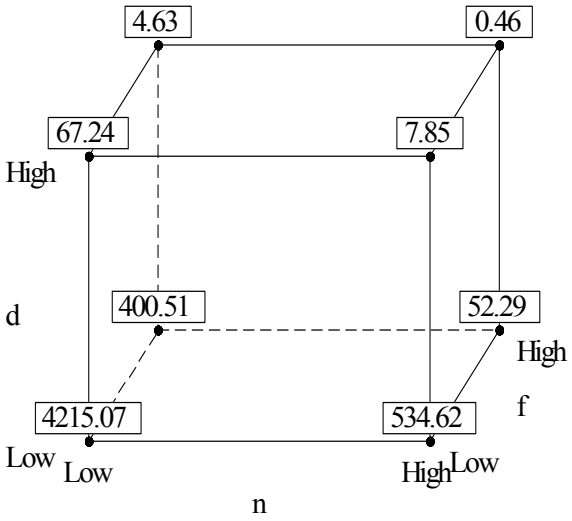

(b)

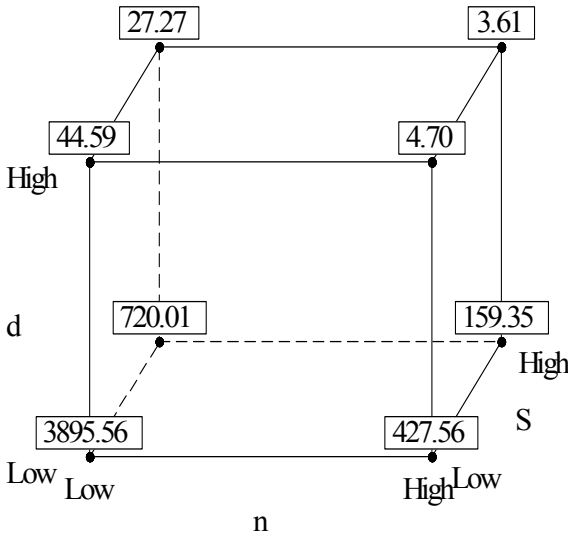

(c)

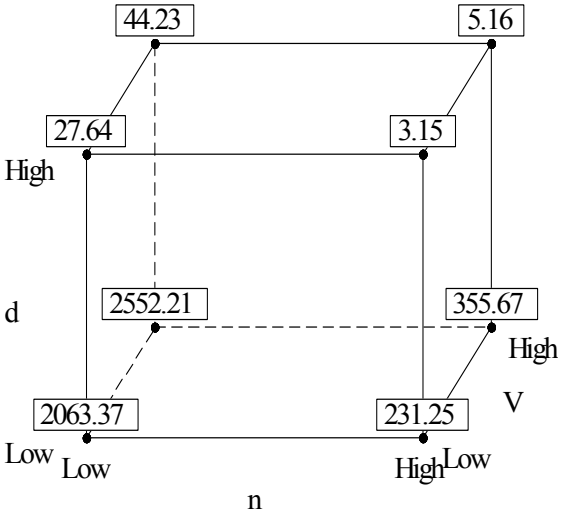

(d)

6.4 Conclusions

Using the mechanistic model of cutting force in UVAG of brittle materials developed by the authors, a 2^6 full factorial design is employed to study the relations between six input

variables (diamond grain number, diamond grain diameter, vibration amplitude, vibration frequency, spindle speed, and feedrate) and cutting force in UVAG of brittle materials. For the first time, interaction effects of input variables on the cutting force in UVAG of brittle materials are studied systematically.

Acknowledgements

The work was supported in part by the National Science Foundation through Award CMMI-0900462.

References

[1] Richerson, D.W., 1997, Ceramic Matrix Composites, Chapter 19 in Composite Engineering Handbook, Marcel Dekker Inc., New York.

[2] Okamura, K., 1995, "Ceramic Matrix Composites (CMC)," Journal of the Japan Society of Composite Materials, 4 (3), 247-259.

[3] Freitag, D.W., and Richerson, D.W., 1998, "Ceramic Matrix Composites in Opportunities for Advanced Ceramics to Meet the Needs of the Industries of the Future," Advanced Ceramic Association and Oak Ridge National Laboratory, Oak Ridge, Tennessee.

[4] Anonymous, 1966, "An Improved Ultrasonic Machine Tool for Glass and Ceramics," Industry Diamond Review, 26 (308), 274-278.

[5] Datta, M., Bandyopadhyay, A., and Chaudha, B., 2004, "Preparation of Nano A-Silicon Carbide Crystalline Particles by Attrition Grinding," International Ceramic Review, 53 (4), 242-244.

[6] Datta, M., and Chaudhari, B., 2003, “Preparation of Nano B-Silicon Carbide Crystalline Particles by Attrition Grinding,” International Ceramic Review, 52 (6), 340-343.

[7] Kibble, K., and Phelps, L., 1995, “Influence of Grinding Variables on Strength of Reaction Bonded Silicon Carbide,” British Ceramic Transactions, 94 (5), 209-216.

[8] Yin, L., Vancoille, E., Lee, L., Huang, H., Ramesh, K., and Liu, X., 2004, “High-Quality Grinding of Polycrystalline Silicon Carbide Spherical Surfaces,” Wear, 256 (1-2), 197-207.

[9] Stinton, D., 1988, “Assessment of the State of the Art Machining and Surface Preparation of Ceramics,” ORNL/TM- Report 10791, Oak Ridge National Laboratory, Oak Ridge, Tennessee.

[10] Zhang, C., Quick, N. R., and Kar, A., 2006, “Laser Drilling of Single Crystal Silicon Carbide Substrates,” Proc. of ICALEO 2006 - 25th International Congress on Applications of Laser and Electro-Optics, October 30, November 2, Scottsdale, Arizona, 42-48.

[11] Luis, C., Puertas, I., and Villa, G., 2005, “Material Removal Rate and Electrode Wear Study on the EDM of Silicon Carbide,” Journal of Materials Processing Technology, 164-165 (2), 889-896.

[12] Puertas, I., and Perez, C., 2003, “Modeling the Manufacturing Variables in Electrical Discharge Machining of Siliconized Silicon Carbide,” Proceedings of the Institution of Mechanical Engineers, Part B, Journal of Engineering Manufacture, 217 (6), 791-803.

[13] Ramulu, M., 2005, “Ultrasonic Machining Effects on the Surface Finish and Strength of Silicon Carbide Ceramics,” International Journal of Manufacturing Technology and Management, 7 (2-4), 107-126.

[14] Zeng, W.M., Li, Z.C., Xu, X.P., Pei, Z.J., Liu, J.D., and Pi, J., 2008, "Experimental Investigation of Intermittent Rotary Ultrasonic Machining," Key Engineering Materials, 359-360, 425-430.

[15] Li, Z.C., Jiao, Y., Deines, T.W., Pei, Z.J., and Treadwell, C., 2005, "Rotary Ultrasonic Machining of Ceramic Matrix Composites: Feasibility Study and Designed Experiments," International Journal of Machine Tools and Manufacture, 45, 1402-1411.

[16] Churi, N.J., Pei, Z.J., Treadwell, C., and Shorter, D., 2007, "Rotary Ultrasonic Machining of Silicon Carbide: Designed Experiments," International Journal of Manufacturing Technology and Management, 12 (1-3), 284-298.

[17] Cleave, D.V., 1976, "Ultrasonic Gets Bigger Jobs in Machining and Welding," Iron Age, 218 (11), 69-72.

[18] Graff, K.F., 1975, "Ultrasonic Machining," Ultrasonics, 13 (3), 103-109.

[19] Tyrrell, W.R., 1970, "Rotary Ultrasonic Machining," SME Technical Paper, MR70-516.

[20] Petrukha, P.G. et al., 1970, "Ultrasonic Diamond Drilling of Deep Holes in Brittle Materials," Russian Engineering Journal, 50 (10), c70-74.

[21] Spur, G., Uhlmann, E., Holl, S.E., and Daus, N.A., 1999, "Influences on Surface and Subsurface During Ultrasonic Assisted Grinding of Advanced Ceramics," Proc. of the 14th Annual Meeting, the American Society for Precision Engineering, October 31 - November 5, Monterey, California, 481-484.

[22] Qin, N., Cong, W.L., Pei, Z.J., Treadwell, C., and Guo, D.M., 2009, Ultrasonic-Vibration-Assisted Grinding of Brittle Materials: A Mechanistic Model for Cutting Force (submitted).

[23] Pei, Z.J., Prabhakar, D., Ferreira, P.M., and Haselkorn, M., 1995, "A Mechanistic Approach to the Prediction of Material Removal Rates in Rotary Ultrasonic Machining," Journal of Engineering for Industry, 117 (2), 142-151.

[24] Shaw, M.C., 1996, Principles of Abrasive Processing, Oxford University Press, New York.

[25] Wu, Y.B., Nomura, M., Feng, Z.J., and Kato, M., 2004, "Modeling of Grinding Force in Constant-Depth-of-Cut Ultrasonically Assisted Grinding," Materials Science Forum, 471-472, 101-106.

[26] Younis, M., Sadek, M.M., and EI-Wardani, T., 1987, "New Approach to Development of a Grinding Force Model," Journal of Engineering for Industry, 109 (4), 306-313.

[27] Li, L.C., and Fu, J., 1980, "Study of Grinding Force Mathematical Model," Annals of the CIRP, 29 (1), 245-249.

[28] Lortz, W., 1979, "A Model of the Cutting Mechanism in Grinding," Wear, 53 (1), 115-128.

[29] Wener, G., 1978, "Influence of Work Material on Grinding Force," Annals of the CIRP, 27 (1), 243-248.

[30] Johnson, K.L., 1985, Contact Mechanics, Cambridge University Press, New York.

[31] Jiao, Y., Hu, P., Pei, Z.J., and Treadwell, C., 2005, "Rotary Ultrasonic Machining of Ceramics: Design of Experiments," International Journal of Manufacturing Technology and Management, 7 (2-4), 192-206.

Chapter 7 - Effects of tool design on edge chipping

The content of this chapter has been published in a conference paper.

Paper Title:

Effects of tool design on edge chipping in ultrasonic-vibration-assisted grinding

Published in:

Proceedings of the 2010 ASME International Manufacturing Science and Engineering Conference, 2010, Erie, Pennsylvania, USA.

Authors' Names:

Na Qin[a,b], Z.J., Pei[a], D.M. Guo[b], W.L. Cong[a]

Authors' Affiliation:

[a]Department of Industrial and Manufacturing Systems Engineering, Kansas State University, Manhattan, KS 66506, USA

[b]School of Mechanical Engineering, Dalian University of Technology, Dalian, Liaoning 116024, China

Abstract

Edge chipping is an important quality parameter in ultrasonic-vibration-assisted grinding (UVAG) of advanced ceramics. In this paper, the effects of cutting tool design, including three different tool angles at tool end surface and wall thickness of the cutting tool (core drills), and process variables on edge chipping are investigated using a finite element analysis (FEA) model. Experiments are also conducted to verify the FEA predicted effects of process variables on edge chipping for the three cutting tools.

Keywords: Advanced ceramics, Cutting tool design, Edge-chipping thickness, Edge chipping size, Finite element analysis, Ultrasonic-vibration-assisted grinding

7.1 Introduction

Advanced ceramics, like functional ceramics, structure ceramics, bioceramics, ceramics coatings, special glasses, represent an important category of materials which has considerable impact for a lot of industries, branches and markets. They have a potential to deliver high-value contributions for solving the challenges of our life [1].

Thousands of engineering components have benefited from advanced ceramics [2] due to their high wear resistance, high hardness and strength at elevated temperature, and low thermal conductivity, etc, providing considerable lifetime increases over conventional metal components [2].

However, the high cost and variable performance (reliability) impede the rapid application of advanced ceramic components [3]. The world-wide market for advanced ceramics is forecast to arrive at $ 40 billion in 2009 [1]. Their machining, which is considered as an essential step in the fabrication of ceramic components, often accounts for more than 75% even up to 90%, of the

final cost of the components [3]. Therefore, cost-effective and reliable machining processes for advanced ceramics are crucially desired.

Ultrasonic machining (USM) is considered as probably the most frequently used machining method for advanced ceramics [4], but it has very low material removal rate (MRR), difficulty to drill deep hole and limited accuracy [5].

Ultrasonic-vibration-assisted grinding (UVAG), which combines the material removal mechanisms of diamond grinding and USM, is another process applicable to advanced ceramic materials [5-14]. Comparing to USM, it achieves higher material removal rates while maintaining low cutting pressures [5], it is easier to drill deep holes and improved hole accuracy [15]. In addition, UVAG is an environmentally benign process because the slurry in USM is replaced with abrasives bonded to the tool.

Figure 7.1 is a schematic illustration of UVAG. A rotary core drill with metal-bonded diamond grains vibrates at an ultrasonic frequency and is fed towards the workpiece. Coolant pumped through the core of the drill washes away the swarf, prevents jamming of the drill and keeps it cool.

Reported experimental studies on UVAG [7,9,12-14,16-25] are primarily focused on relationships between input variables (diamond concentration, grain size, and type; bond type; vibration amplitude and frequency; spindle speed; feedrate; coolant type and pressure) and output variables (material removal rate, cutting force, surface roughness, and tool wear). Reported modeling work on UVAG includes predicting material removal rate (MRR) [6,26-28], cutting force using brittle fracture model and ductile model [29,30], and tool wear mechanisms [31, 32].

Figure 7.1 Schematic illustration of UVAG

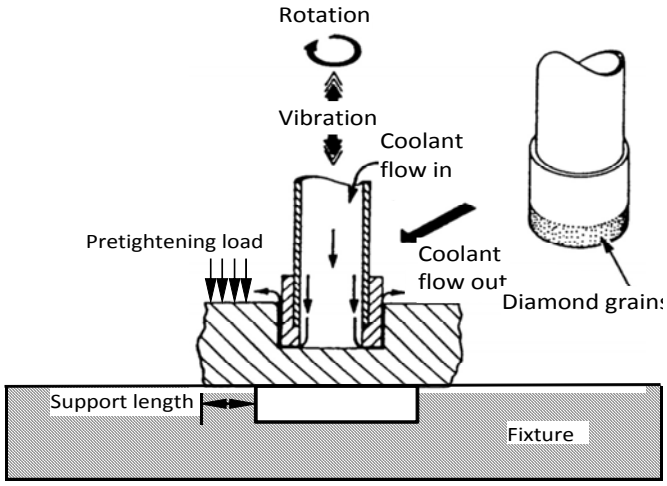

One of the remaining challenges for UVAG is edge chipping when it comes to drill hard and brittle materials like advance ceramics [13,33, 34].

There are several investigations dealing with the machining induced edge chipping in milling [35-37] and grinding [38] of brittle materials. But little research on edge chipping in UVAG of hard and brittle materials has been reported. Jiao et al. [33] studied the main and interaction effects of process variables on edge chipping in UVAG of advanced ceramics through an integrated way combining experimental design and finite element method. They concluded that the edge-chipping thickness could be reduced by using higher spindle speed and lower feedrate. Li et al. [13] developed a 3-D FEA model to study the effects of cutting depth, support length and pretightening load on the initiation of edge chipping in UVAG of advanced ceramics and verified the model predictions by experiments. They concluded that edge-chipping thickness could be reduced by increasing the support length.

However, there are no reports on the effects of cutting tool design, for example, tool angle and wall thickness of the cutting tool, on edge chipping initiation in UVAG of advanced ceramics.

This paper first develops an FEA model to investigate the edge-chipping thickness with three different cutting tools, and the effects of tool angle, wall thickness of tool, and process variables on edge chipping. Furthermore, the simulation results are verified by experimental results of UVAG of advanced ceramics.

7.2 Development of the model

In order to reduce the computation cost significantly, the machining process will be modeled as a static problem. Only static stress distribution in the region of the edge chipping initiation is concerned. The dynamic nature is not taken into account in this paper.

7.2.1 Geometry creation and mesh generation

The commercial software Solidworks 2009 SP4.0 (SolidWorks Corp, Concord, Massachusetts, USA) is utilized to create the model. The mechanical properties of the ceramic are listed in Table 7.1. The workpiece is assumed to have a cylinder shape with a radius of 16 mm and thickness of 6 mm. Due to the symmetry of workpiece and fixture geometry as well as load conditions, with two axisymmetric planes, one quarter of a 3-D solid model of the workpiece is constructed as shown in Figure 7.2. The cutting tool has a hollow cylinder with outer diameter of 9.6 mm and inner diameter of 7.8 mm. The elements are refined progressively on the cutting surface and the fillets as well as the walls, with default mesh for other parts of the

model as shown in Fig 2. The length of pretightening load is 8 mm, equal to the length of the supporting by the fixture as shown in Figure 7.1.

Table 7.1 Mechanical properties of the ceramic

Property	Unit	Value
Elastic modulus	GPa	190
Poisons's ratio		0.25
Density	kg/m^3	3500
Tensile strength	MPa	130
Compressive strength	MPa	1750

Figure 7.2 A 3-D FEA model of the workpiece

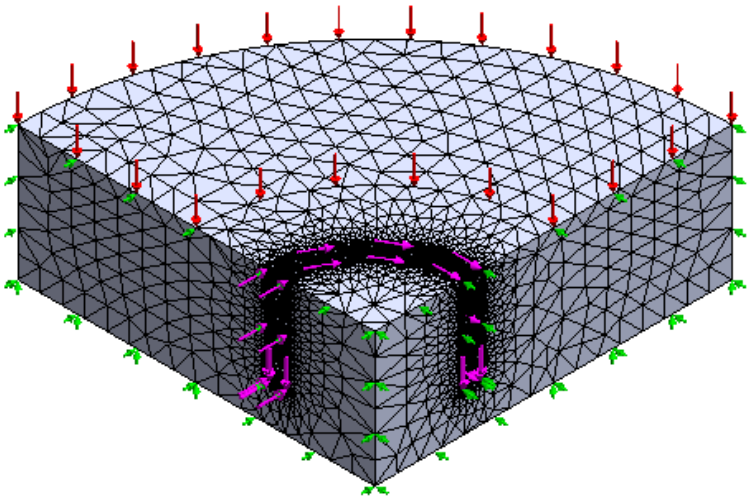

7.2.2 Boundary conditions and loading

The bottom of the workpiece (supported portion) which is in contact with fixture is constrained from moving in vertical direction, so roller constraints are chosen in Solidworks to fix the supported portion of the workpiece. The two axisymmetric planes are fixed by symmetric constraints in Solidworks as shown in Figure 7.2.

A uniform pretightening load of 3.7 MPa is applied on the top surface of the workpiece to tighten it. A vertical cutting force is applied to the contact surface between the workpiece and the end surface of cutting tool. Due to rotation of cutting tool, there is a torque between the contact areas of cutting tool and workpiece, but it turns out the torque is too small to get the accurate value during experiments. In order to simulate the real machining process as much as possible, a torque of 0.5 *N.m* is applied on the contact areas between cutting tool and workpiece. The contact area consists of two fillets of 0.1 mm on both sides and a middle horizontal contact surface between the fillets. The simulation results show that the effect trends of different input variables keep the same under different fillets. So in the following, all the results are obtained by using 0.1 mm fillets. The cutting force is calculated according to a mechanistic model for brittle material [30].

7.2.3 Failure criterion of edge chipping

The tensile stresses of the ceramic are of the primary concern because the compressive strength of the workpiece is much higher than the tensile strength as listed in Table 7. 1. The maximum normal stress criterion is applied to predict the edge-chipping thickness. It is assumed that edge chipping initiates at a critical cutting depth where the maximum normal equivalent stress reaches the tensile strength of the workpiece material.

Therefore, when the maximum normal stress reaches the tensile strength of the workpiece at one cutting depth, this depth is the critical depth. The edge-chipping thickness can be obtained by using the total thickness of the workpiece (6 mm) subtracting the critical cutting depth. For more detail of the calculation of the edge-chipping thickness, please refer to Li et al. [13].

7.3 Simulation results

There are three cutting tools as shown in Figure 7.3. They are normal tool (equal length for both outer and inner sides), inner tool (length of inner side is smaller than that of outer side), outer tool (length of outer side is smaller than that of inner side). For each of them, two tool parameters (tool angle and wall thickness) and five process variables (diamond grain number, diamond grain diameter, vibration amplitude, spindle speed, and federate) are investigated for edge-chipping thickness in UVAG of advanced ceramics.

Figure 7.3 Schematic illustration of angle for three cutting tools

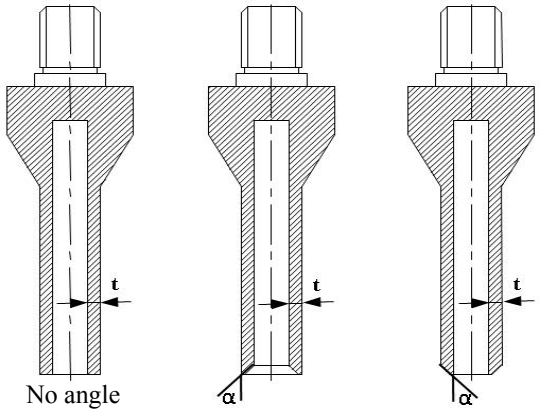

(a) Normal tool (b) Inner tool (c) Outer tool

7.3.1 Effects of tool angle on edge-chipping thickness

The tool angle is defined by α, which is the intersection angle between the oblique side and the longer side of the tool as shown in Figure 7.3 (b) and (c). Five angles are chosen for both inner tool and outer tool as shown in Figure 7.4. When the tool angle increases from 45° to 84°, the edge-chipping thickness increases for both inner tool and outer tool. In addition, with the same angle, at different tool angles, all the edge-chipping thicknesses drilled by outer tool are smaller than those drilled by inner tool.

Figure 7.4 Effects of tool angle on edge-chipping thickness

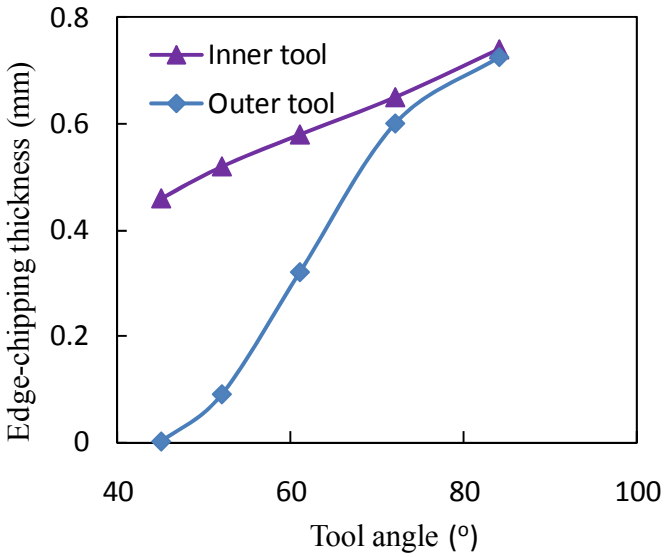

7.3.2 Effects of wall thickness on edge-chipping thickness

The wall thickness of the cutting tool t is one half of the difference between the outer diameter and inner diameter as shown in Figure 7.3. The simulation results are shown in Figure

7.5. Five thicknesses are chosen to study the effects of wall thickness on edge-chipping thickness. The edge-chipping thickness increases as wall thickness increases for normal tool and inner tool and as the wall thickness decreases for outer tool. In addition, with the same wall thickness, at different wall thicknesses, the outer tool produces the lowest edge-chipping thickness, followed by inner tool and normal tool.

Figure 7.5 Effects of wall thickness on edge-chipping thickness

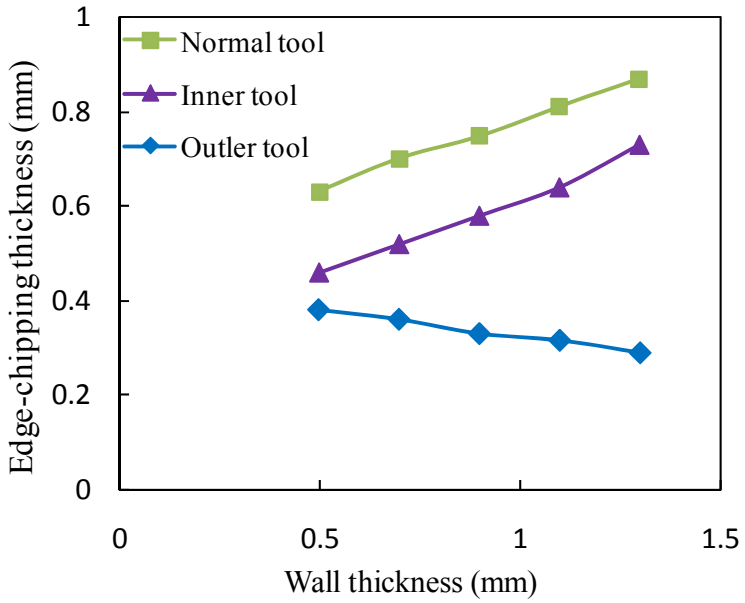

7.3.3 Effects of process variables on edge-chipping thickness

Five process variables are investigated in UVAG of the ceramic in the simulation: diamond grain number, diamond grain diameter, vibration amplitude, spindle speed, and feedrate. In a mechanistic model developed by Qin et al. [31], they provided a relationship between the five

process variables and cutting force in UVAG of brittle materials. According to these relationships, the change trends of cutting force could be obtained for these process variables. The results are shown in Figure 7.6 (a) - (e). According to these graphs, edge-chipping thickness decreases with an increase in the diamond grain number and diameter, vibration amplitude and spindle speed, and as a decrease in the feedrate. In addition, for all the five variables, the edge-chipping thickness drilled by the outer tool is the lowest, followed by inner tool and normal tool, if the cutting force is the same.

Figure 7.6 Simulation results about effects of process variables on edge-chipping thickness

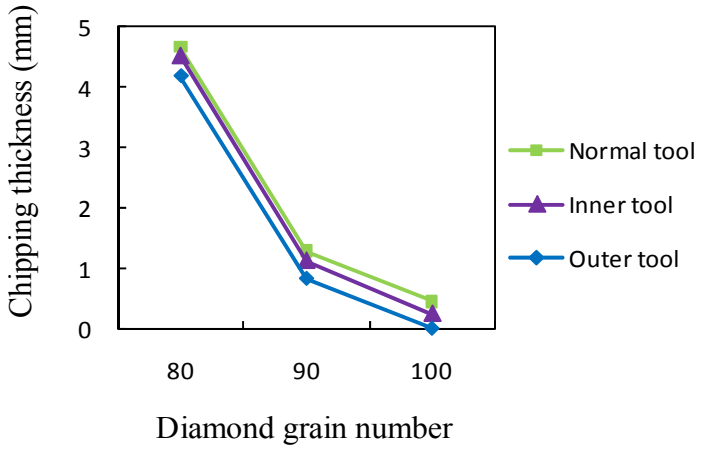

(a)

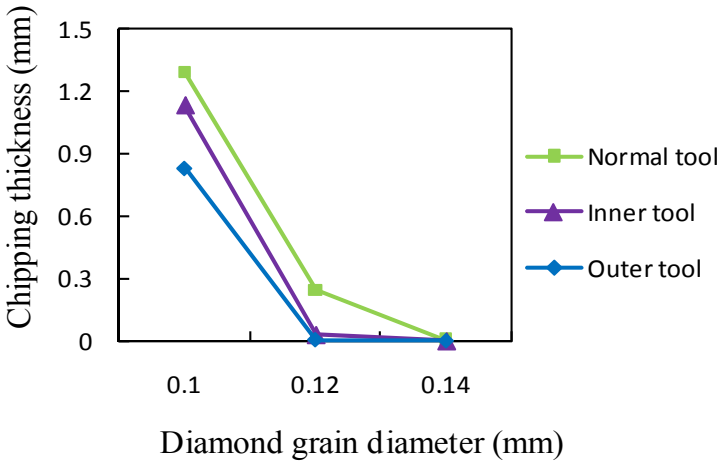
Chipping thickness (mm)
1.5
1.2
0.9
0.6
0.3
0
0.1
0.12
0.14
Normal tool
Inner tool
Outer tool
Diamond grain diameter (mm)

(b)

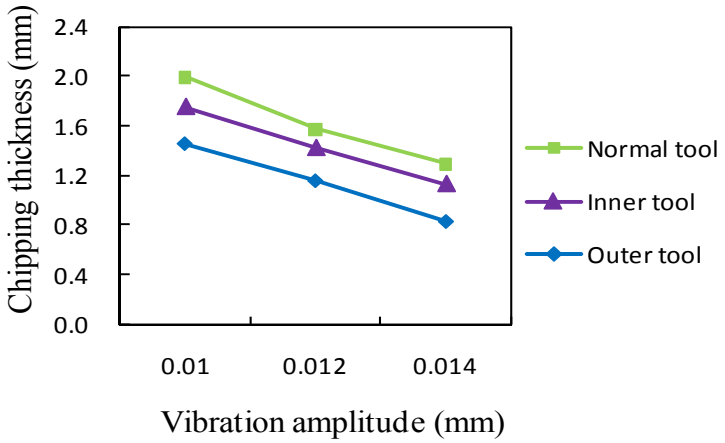
Chipping thickness (mm)
2.4
2.0
1.6
1.2
0.8
0.4
0.0
0.01
0.012
0.014
Normal tool
Inner tool
Outer tool
Vibration amplitude (mm)

(c)

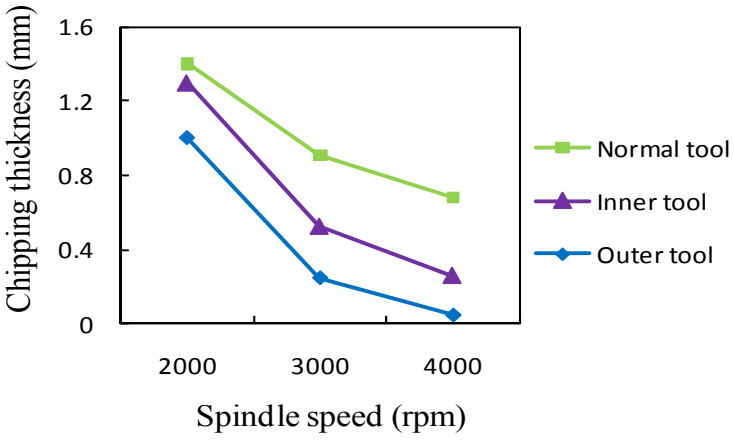
Chipping thickness (mm)
1.6
1.2
0.8
0.4
0
2000
3000
4000
Normal tool
Inner tool
Outer tool
Spindle speed (rpm)

(d)

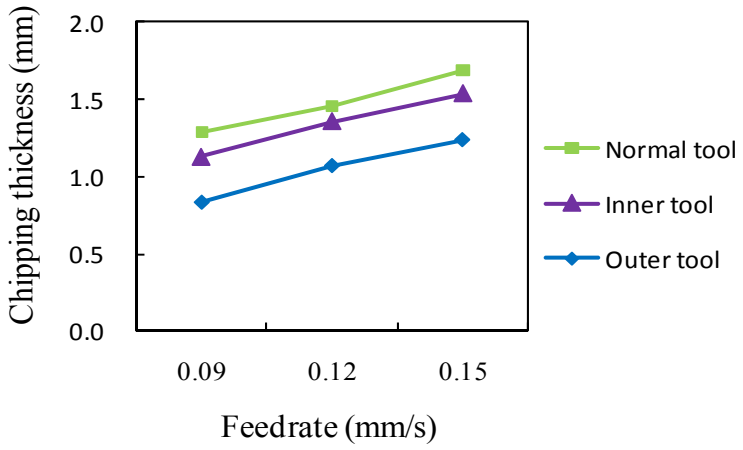

(e)

7.4 Pilot experimental verification

In the experimental verification, effects of the three process variables: vibration power, spindle speed and feedrate on edge-chipping thickness will be verified. And the edge-chipping size will be also measured to estimate the effects of the three process variables for the three cutting tools.

7.4.1 Experimental set-up and conditions

In UVAG of the ceramic, a blind hole is drilled in the fixture under the workpiece to receive the rod, as shown in Figure 7.1. An ultrasonic-vibration-assisted grinding machine of Sonic Mill Series 10 (Sonic-mill®, Albuquerque, NM, USA) was used to perform the experiments. The workpiece material was 92% Al_2O_3 sintered (Ferro-ceramic Grinding, Inc., Wakefield, MA, USA) and the size was 25 mm ×25 mm×6 mm.

Table 7.2 Experimental conditions

Process variable	Unit	Value
Vibration power	%	30, 45
Spindle speed	rpm	2000, 3500
Feedrate	$mm \cdot s^{-1}$	0.15, 0.075

Figure 7.7 Three cutting tools

(a) Normal tool (b) Inner tool (c) Outer tool

The metal-bonded diamond cutting tools were provided by N.B.R. Diamond Tool Corp. (LaGrangeville, NY, USA) as shown in Figure 7.7. The mesh size of the diamond grains was 80/100. The outer and inner diameters of the cutting tool were D_o = 9.6 mm and D_i = 7.8 mm, respectively. Water-soluble Quakercool 6010 cutting fluid (Murdock Industrial Supply Co.,

Wichita, KS, USA) was used as the coolant (diluted with water at 1:14 ratio). For each tool, there were 4 combinations for process variables and two replicated tests for each combination, bringing the total number of test to 8. So for all the three tools, there are 24 tests. The experimental conditions are listed in Table 7.2.

7.4.2 Measurement of edge-chipping thickness and size

In the literature, only the normal tools were used, and the edge-chipping thicknesses on the machined rod were observed to evaluate the edge-chipping thickness of the workpiece since it is convenient to measure the machined rod and the edge chipping on the machined rod exactly matched the edge chipping on the drilled hole [11,13]. However, for the three cutting tools used in this paper, only the machined rods drilled by normal tool and inner tool have this matching characteristic, while the outer tool does not. For the outer tool, as prior definition, the length of the inner side is longer than that of the outer side, so after drilling, no edge chipping will be observed on the outer side of the rod as shown in Figure 7.8 (c). So in this paper, the drilled holes at the exit side of the workpiece instead of the rods is observed to evaluate the edge-chipping thickness for the three cutting tools. The edge-chipping thickness is shown in Figure 7.9. The chipping size is the average width between the hole edge and the chipping edge away from the hole edge as shown in Figure 7.10.

A digital video microscope (Olympus BX-51, Olympus America, Inc., St. Louis, MO, USA) was utilized to inspect the edge-chipping thickness and size at the hole exit edge. Four points were observed at 90 degree interval for each workpiece. Since each test was conducted twice, the total observed points were 8 for each experimental combination. And the average value for the 8 points will be used to evaluate the edge-chipping thickness for each experimental combination.

Figure 7.8 Workpiece and rod drilled by three cutting tools

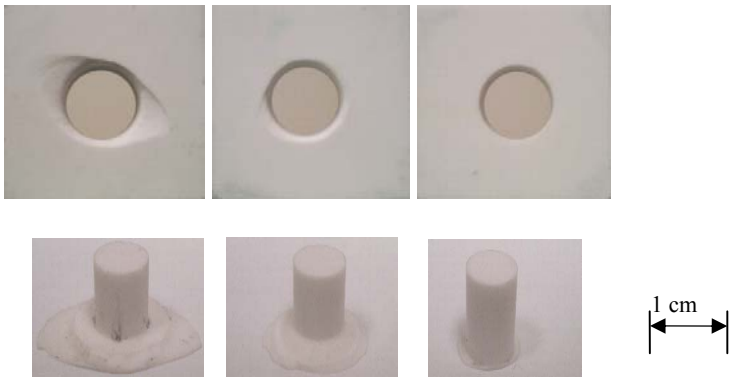

(a) By normal tool (b) By inner tool (c) By outer tool

Figure 7.9 Measurement of edge-chipping thickness on exit hole of workpiece

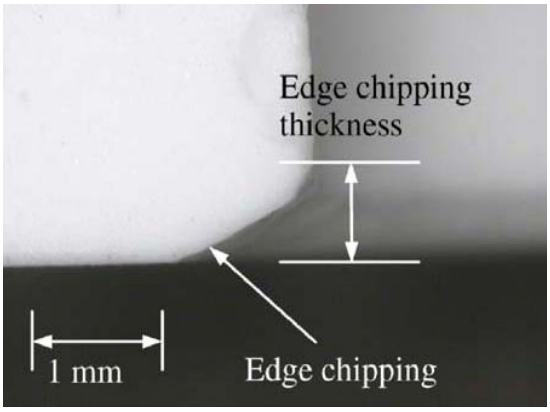

Figure 7.10 Measurement of edge-chipping size

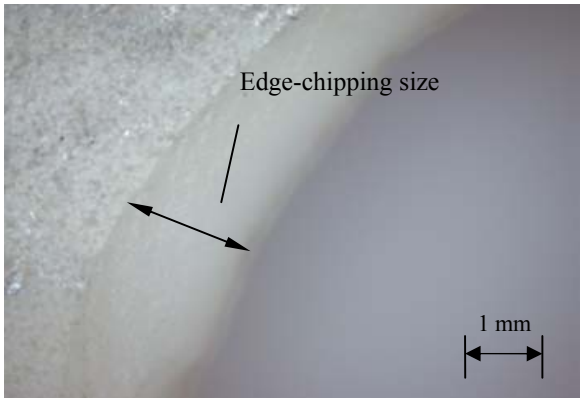

7.4.3 Experimental results and discussion

The experimental data are listed in Table 7.3. As shown in Figure 7.11 and 7.12, the process variables have the same effects on chipping thickness and chipping size. Comparing the simulation results and experimental results for edge-chipping thickness, all the results have similar trends. The chipping thickness and size increase as the spindle speed decreases and vibration power and feedrate increase. This can be explained as below: that larger edge-chipping thickness almost always results from higher cutting force [11], and higher cutting force resulted from lower spindle speed, vibration amplitude and higher feedrate in UVAG of brittle material [30]. Therefore, larger edge-chipping thickness is caused by lower spindle speed and vibration amplitude and higher feedrate.

Table 7.3 Experimental results

	Feedrate ($mm \cdot s^{-1}$)	0.075	0.15	0.15	0.15
	Power (%)	30	30	45	30
	Spindle speed (rpm)	3500	3500	3500	2000
Normal tool	Edge-chipping thickness (mm)	0.67	0.99	0.87	1.11
	Edge-chipping size (mm)	0.91	1.6	1.22	1.88
Inner tool	Edge-chipping thickness (mm)	0.58	0.626	0.51	0.7
	Edge-chipping size (mm)	0.717	0.94	0.83	1.04
Outer tool	Edge-chipping thickness (mm)	0.05	0.075	0.046	0.079
	Edge-chipping size (mm)	0.04	0.125	0.093	0.256

In addition, with same process variables, the lowest edge-chipping thickness was obtained from workpieces drilled by outer tool, followed by inner tool and normal tool, which is consistent with the simulation results.

Figure 7.11 Experimental results about effects of process variables on edge-chipping thickness

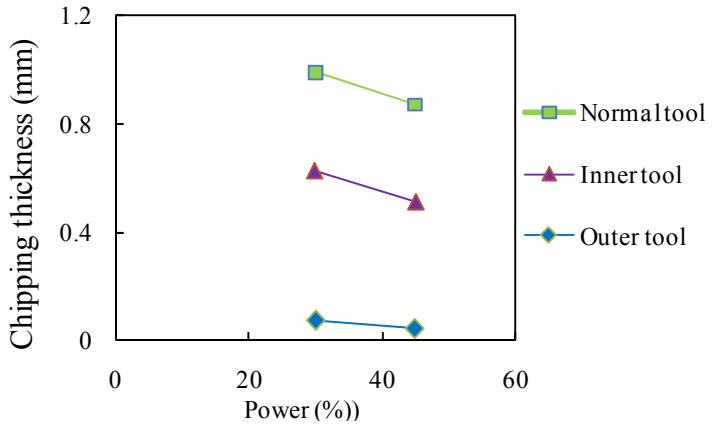

(a)

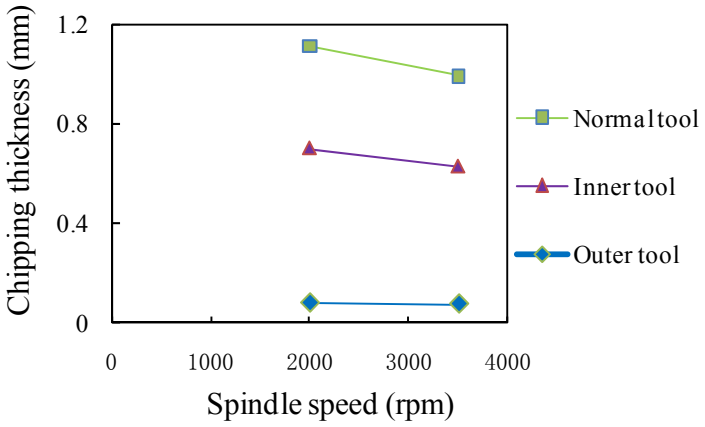

(b)

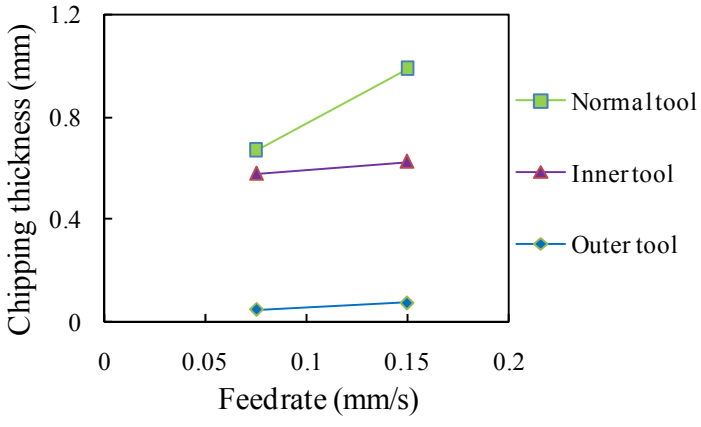

(c)

Figure 7.12 Experimental results about effects of process variables on edge-chipping size

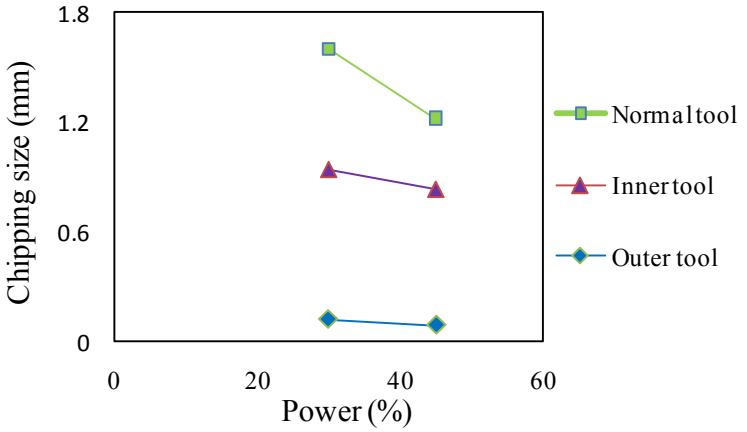

(a)

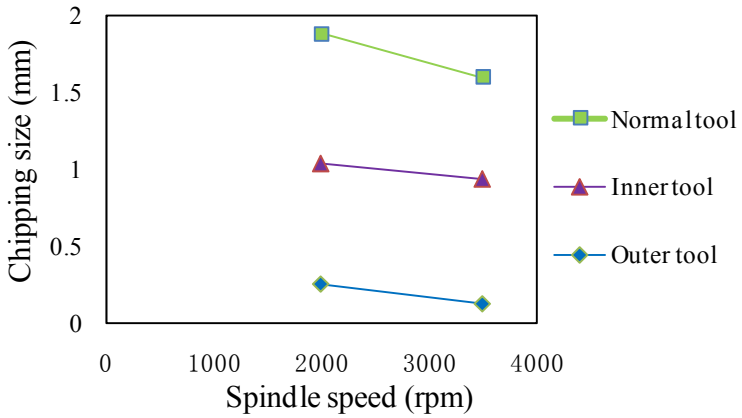

(b)

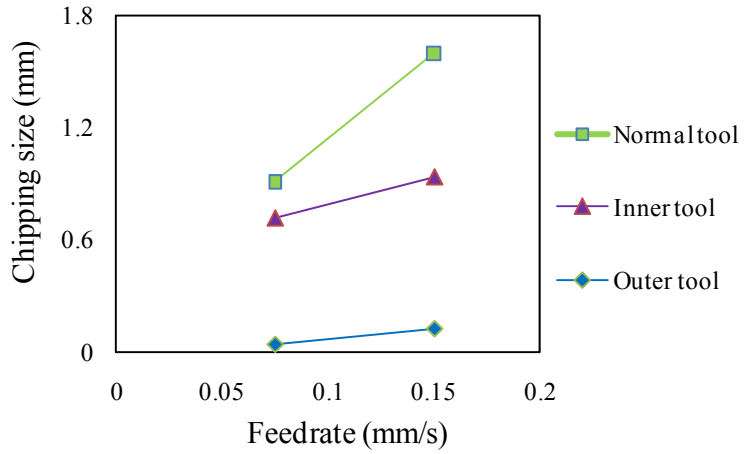

(c)

7.5 Conclusions

This paper provided an investigation into the edge-chipping thickness and size in UVAG of ceramics. A FEA model was developed to study the effects of three cutting tool designs and five process variables on edge-chipping thickness in UVAG of the ceramic. Experiments were conducted to verify the process variables on edge chipping. The main conclusions are as follows:

1. All the five process variables have influences on the edge chipping.
2. The angle and wall thickness and type of cutting tool have influences on edge-chipping thickness.
3. The workpieces drilled by the outer tool has the lowest edge-chipping thickness and size, followed by the inner tool and normal tool.

Acknowledgements

Author would like to thank Dr. X.J. Xin (Department of Mechanical and Nuclear Engineering at Kansas State University) for his assistance with SolidWorks and Sonic-Mill for RUM Machine.

References

[1] Rodel, J., Kounga, A.B.N., and Eibl, M. W., et al., 2009, "Development of A Roadmap for Advanced Ceramics 2010-2025," Journal of the European Ceramic Society, 29 (9), pp. 1549-1560.

[2] Dynamic ceramics, "Applications," 2008, http://www.dynacer.com/applications.htm.

[3] Stinton, D.P., 1988, "Assessment of the State of the Art in Machining and Surface Preparation of Ceramics," ORNL/TM Report 10791, Oak Ridge National Laboratory, Tennessee, pp. 1549-1560,

[4] Jahanmir, S., Ives, L.K, Ruff, A.W., and Peterson, M.B., 1992, "Ceramics Machining: Assessment of Current Practice and Research Needs in the United States," NIST Special Publication 834.

[5] Prabhakar, D., 1992, "Machining Advanced Ceramic Materials Using Rotary Ultrasonic Machining Process," M.S. Thesis, University of Illinois at Urbana-Champaign.

[6] Pei, Z.J., Prabhakar, D., Ferreira, P.M., and Haselkorn, M., 1995, "A Mechanistic Approach to the Prediction of Material Removal Rates in Rotary Ultrasonic Machining," Journal of Engineering for Industry, 117 (2), pp. 142-151.

[7] Pei, Z.J., Prabhakar, D., Ferreira, P.M., and Haselkorn, M., 1995, "Rotary Ultrasonic Drilling and Milling of Ceramics," Ceramic Transactions, 49, pp. 185-196.

[8] Pei, Z.J., Khanna, N., and Ferreira, P.M., 1995, "Rotary Ultrasonic Machining of Structural Ceramics - A Review," Ceramic Engineering and Science Proceedings, 16 (1), pp. 259-278.

[9] Pei, Z.J. and Ferreira, P.M., 1999, "An Experimental Investigation of Rotary Ultrasonic Face Milling," International Journal of Machine Tools & Manufacture, 39, pp. 1327-1344.

[10] Hu, P., Zhang, J.M., Pei, Z.J., and Treadwell, C., 2002, "Modeling of Material Removal Rate in Rotary Ultrasonic Machining: Designed Experiments," Journal of Materials Processing Technology, 129, pp. 339 -344.

[11] Jiao, Y., Hu, P., Pei, Z.J., and Treadwell, C., 2005, "Rotary Ultrasonic Machining of Ceramics: Design of Experiments," International Journal of Manufacturing Technology and Management, 7 (2-4), pp. 192-206.

[12] Li, Z.C., Jiao, Y., Deines, T.W., Pei, Z.J., and Treadwell, C., 2005, "Rotary Ultrasonic Machining of Ceramic Matrix Composites: Feasibility Study and Designed Experiments," International Journal of Machine Tools and Manufacture, 45, pp. 1402-1411.

[13] Li, Z.C., Cai, L.W., Pei, Z.J., and Treadwell, C., 2006, "Edge-Chipping Reduction in Rotary Ultrasonic Machining of Ceramics: Finite Element Analysis and Experimental Verification," International Journal of Machine Tools and Manufacture, 46, pp. 1469-1477.

[14] Zeng, W.M., Xu, X.P., and Pei, Z.J., 2006, "Rotary Ultrasonic Machining of Advanced Ceramics," Materials Science Forum, 532-533, pp. 361-364.

[15] Graff, K.F., 1975, "Ultrasonic Machining," Ultrasonics, 13 (3), pp. 103-109.

[16] Churi, N.J., Pei, Z.J., Shorter, D.C., and Treadwell, C., 2007, "Rotary Ultrasonic Machining of Silicon Carbide: Designed Experiments," International Journal of Manufacturing Technology and Management, 12 (1-3), pp. 284-298.

[17] Churi, N.J., Pei, Z.J., Treadwell, C., and Shorter, D.C., 2009, "Rotary Ultrasonic Machining of Dental Ceramics," International Journal of Machining and Machinability of Materials, 6 (3-4), pp. 270-284.

[18] Zeng, W.M., Li, Z.C., Xu, X.P., Pei, Z.J., Liu, J.D., and Pi, J., 2008, "Experimental Investigation of Intermittent Rotary Ultrasonic Machining," Key Engineering Materials, 359-360, pp.425-430.

[19] Li, Z.C., Jiao, Y., Deines, T.W., Pei, Z.J., and Treadwell, C., 2005, "Development of an Innovative Coolant System for Rotary Ultrasonic Machining," International Journal of Manufacturing Technology and Management, 7 (2-4), pp. 318-328.

[20] Kubota, M., Tamura, Y., and Shimamura, N., 1977, "Ultrasonic Machining with a Diamond Impregnated Tool," Bulletin Japan Society of Precision Engineering, 11 (3), pp. 127-132.

[21] Markov, A.I., et al., 1977, "Ultrasonic Drilling and Milling of Hard Non-Metallic Materials with Diamond Tools," Machine and Tooling, 48 (9), pp. 45-47.

[22] Petrukha, P.G., et al., 1970, "Ultrasonic Diamond Drilling of Deep Holes in Brittle Materials," Journal of Russian engineering, 50 (10), pp. 70-74.

[23] Prabhakar, D., 1992, "Machining Advanced Ceramic Materials Using Rotary Ultrasonic Machining Process," MS Thesis, University of Illinois at Urbana-Champaign, Illinois, USA.

[24] Prabhakar, D., Ferreira, P.M., and Haselkorn, M., 1992, "An Experimental Investigation of Material Removal Rates in Rotary Ultrasonic Machining," Transactions of the North American Manufacturing Research Institute of SME, 20, pp. 211-218.

[25] Wang, H., and Lin, L., 1993, "Improvement of Rotary Ultrasonic Deep Hole Drilling of Glass Ceramics-Zerodur," Proceedings of the 7th International Precision Engineering Seminar, The Japan Society of Applied Physics, Kobe, Japan, pp. 719-730.

[26] Zhang, Q.H., Wu, C.L., Sun, J.L., and Jia, Z.X., 2000, "Mechanism of Material Removal in Ultrasonic Drilling of Engineering Ceramics," Proceedings of Institution of Mechanical Engineers, Part B: Journal of Engineering Manufacture, 214 (9), pp. 805-810.

[27] Chao, C.L., Chou, W.C., Chao, C.W., and Chen, C.C., 2007, "Material Removal Mechanisms Involved in Rotary Ultrasonic Machining of Brittle Materials," Key Engineering Materials, 329, pp. 391-396.

[28] Prabhakar, D., Pei, Z.J., Ferreira, P.M., and Haselkorn, M., 1993, "A Theoretical Model for Predicting Material Removal Rates in Rotary Ultrasonic Machining of Ceramics," Transactions of the North American Manufacturing Research Institute of SME, 21, pp. 167-172.

[29] Qin, N., Pei, Z. J., Treadwell, C., and Guo, D. M., 2009, "Physics-Based Predictive Cutting Force Model in Ultrasonic-Vibration-Assisted Grinding for Titanium Drilling," ASME Transactions Journal of Manufacturing Science and Engineering, 131(4), pp. 041011-1-041011-9.

[30] Qin, N., Cong, W.L., Pei, Z.J., Treadwell, C., and Guo, D.M., 2010, "Ultrasonic-Vibration-Assisted Grinding of Brittle Materials: A Mechanistic Model for Cutting Force, Model," Submitted to ASME Transactions Journal of Manufacturing Science and Engineering.

[31] Spur, G., and Holl, S.E., 1997, "Material Removal Mechanisms During Ultrasonic Assisted Grinding," Production Engineering, 4 (2), pp.9–14.

[32] Zeng, W.M., Li, Z.C., Pei, Z.J., and Treadwell, C., 2005, "Experimental Observation of Tool Wear in Rotary Ultrasonic Machining of Advanced Ceramics," International Journal of Machine Tools and Manufacture, 45 (12–13), pp.1468–1473.

[33] Jiao, Y., Liu, W.J., Pei, Z.J., Xin, X.J., and Treadwell, C., 2005, "Study on Edge Chipping in Rotary Ultrasonic Machining on Ceramics: An Integration of Designed Experiment and FEM Analysis," Journal of Manufacturing Science and Engineering, 127 (4), pp.752-758.

[34] Li, Z.C., Cai, L.W., Pei, Z.J., and Treadwell, C., 2004, "Finite Element Simulation of Rotary Ultrasonic Machining for Advanced Ceramics," Proceedings of ASME International Mechanical Engineering Congress and Exposition, Anaheim, CA, USA.

[35] Ng, S., Le, D., Tucker, S., Zhang, G., 1996, "Control of Machining Induced Edge Chipping on Glass Ceramics," Proceedings of the 1996 ASME International Mechanical Engineering Congress and Exposition, Manufacturing Engineering Division, MED (4), Atlanta, GA, USA, November 17-22, pp. 229-236.

[36] Chiu, W.C., Thouless, M.D., and Endres, W.J., 1998, "An Analysis of Chipping in Brittle Materials," International Journal of Fracture, 90 (4), pp. 287–298.

[37] Cao, Y.Q., 2001, "Failure Analysis of Exit Edges in Ceramic Machining Using Finite Element Analysis," Engineering Failure Analysis, 8 (4), pp. 325–338.

[38] Yoshifumi, O., Tetsuo, M., and Minoru, S., 1995, "Chipping in High Precision Slot Grinding of Mn–Zn Ferrite," Annals of the CIRP, 44 (1), pp. 273–277.

[39] Walter, D., 1997, *Pilkey Peterson's Stress Concentration Factors*, Second ed., Wiley, New York.

Chapter 8- Summary and conclusions

8.1 Summaries of this research

This dissertation studies fundamental mechanisms in UVAG of ductile and brittle materials. In order to study effects of input variables (diamond grain number, diamond grain diameter, vibration amplitude, vibration frequency, spindle speed, and federate) on cutting force, a physics-based predictive cutting force model is developed for UVAG of ductile materials, while a mechanistic predictive cutting force model is developed for UVAG of brittle materials. Based on the developed models, interaction effects of input variables on cutting force are also studied. In addition, since edge chipping is one of the technical challenges in UVAG of brittle materials, an FEA model is developed to study effects of cutting tool design and input variables on edge chipping. Furthermore, some predicted trends from the developed models are verified through experiments.

Below are the main conclusions drawn from this dissertation:

1) A physics-based predictive cutting force model is developed for UVAG of ductile materials. The predicted influences of input variables on cutting force are compared with those determined experimentally. The trends of predicted influences agree well with experimental results. The cutting force will increase as diamond grain number, diamond grain radius, and feedrate increase. It will decrease as vibration amplitude, vibration frequency, and spindle speed increase.
2) A mechanistic model for cutting force in UVAG of brittle materials has been developed using silicon as an example. The predicted influences of input variables on cutting force are compared with those determined experimentally. The trends of predicted influences

agree well with experimental results. Based on model predictions, cutting force will increase as vibration amplitude and feedrate increase, but decrease as diamond grain number, vibration frequency, and spindle speed increase.

3) Based on the developed models for UVAG of ductile and brittle materials, full factorial design is employed to study the main effects and interaction effects of input variables on cutting force in UVAG of Ti and silicon. There are no significant interaction effects among the input variables in UVAG of ductile materials. However, there are significant interaction effects among input variables in UVAG of brittle materials.

4) Three cutting tool designs are used to study their effects on edge chipping. Finite element analysis is utilized to study effects of tool design and process variables on edge chipping for brittle materials. The simulation results from the FEA model are verified through experiments. It is shown that, with increase of feedrate, the edge-chipping thickness and size increase; with increase of spindle speed and ultrasonic vibration amplitude, edge-chipping thickness and size decrease; with increase of tool angle, the edge-chipping thickness increases; with increases of wall thickness of tool, the edge-chipping thickness changes differently for three cutting tools.

8.2 Contributions of this research

The contributions of this research are:

1) For the first time in public domain, this study has developed a physics-based predictive cutting force model for UVAG of ductile materials and the predicted results are verified through experiments. This research has filled a gap in the literature on fundamental mechanisms in UVAG under the condition of constant feedrate.

2) For the first time in public domain, this study has developed a mechanistic predictive cutting force model for UVAG of brittle materials and the predicted results are verified through experiments. The stated results in this dissertation help to understand mechanisms in UVAG of brittle materials.

3) The developed models can serve as useful templates for development of models to predict torque, cutting temperature, tool wear, and surface roughness in UVAG.

4) The interaction effects of input variables on cutting force are studied systematically.

5) For the first time, effects of cutting tool designs on edge chipping are studied. The results in this dissertation can provide guidance for choosing reasonable process variables and designing diamond cutting tools.

Appendix A - Publications during Ph.D. study

Journal and conference publications

1. Qin, N., Pei, Z.J., Treadwell, C., and Guo, D.M.. Physics-based predictive cutting force model in ultrasonic-vibration-assisted grinding for titanium drilling, Journal of Manufacturing Science and Engineering, 2009, 131 (4): 041011-1-041011-9.
2. Qin, N., Pei, Z.J., Fisher, G.R., and Liu, J.. Simultaneous double-side grinding of silicon wafers: a review and analysis of experimental investigations, Machining Science and Technology, 2009, 13 (3): 285-316.
3. Qin, N., Pei, Z.J., and Guo, D.M.. Ultrasonic-vibration-assisted grinding of titanium: cutting force modeling with design of experiments, Proceedings of the ASME International Manufacturing Science & Engineering Conference, October 4-7, 2009, 2: 619-624, West Lafayette, IN, USA.
4. Qin, N., Pei, Z.J., and Guo, D.M.. Nanotopography in silicon wafer manufacturing: a literature review, Proceedings of ASME International Manufacturing Science & Engineering Conference, October 4-7, 2009, 1:721-728, West Lafayette, IN, USA.
5. Qin, N., Pei,, Z.J., Guo, D.M., and Cong, W.L.. Effects of tool design on edge chipping in ultrasonic-vibration-assisted grinding, Proceedings of the 2010 ASME International Manufacturing Science and Engineering Conference, October 12-15, 2010, Erie, Pennsylvania, USA.
6. Qin, N. and Pei, Z.J.. Four empirical models for pelleting of cellulosic biomass, Proceedings of the 2010 ASME International Manufacturing Science and Engineering Conference, October 12-15, 2010, Erie, Pennsylvania, USA.

7. Qin, N., Pei, Z.J., Guo, D.M., and Cong, W.L.. UVAG of brittle materials: DoE with a cutting force model, Proceedings of the 2010 Industrial Engineering Research Conference, June 5-9, 2010, Cancún, Mexico.
8. Qin, N., Pei, Z.J., Cong, W.L., Treadwell, C., and Guo, D.M., Ultrasonic-vibration-assisted grinding of brittle materials: a mechanistic model for cutting force, Proceedings of the ASME 2011 International Manufacturing Science and Engineering Conference, June 13-17, 2011, Corvallis, Oregon, USA.
9. Qin, N. and Pei, Z. J.. Fundamental research on silicon wafer fine grinding: 2010 progress report, 2011 NSF CMMI Grantees Conference, Jan 4-7, 2011, Atlanta, GA.
10. Zhang, M., Song, X.X., Deines, T., Zhang, P.F., Zhang, Q., Cong, W.L., Qin, N., and Pei, Z.J.. Ultrasonic-vibration-assisted pelleting of switchgrass: effects of binder material, Proceedings of the 2010 Industrial Engineering Research Conference, June 5-9, 2010, Cancún, Mexico.
11. P.F., Zhang, Deines, T., Cong, W.L., Qin, N., Pei, Z.J., and Nottingham, D.. Ultrasonic vibration-assisted pelleting of switchgrass: effects of moisture content on pellet density, spring-back, and durability, Proceedings of the 2010 Flexible Automation and Intelligent Manufacturing International Conference, July 12-14, 2010, Hayward, CA.
12. Cong, W.L., P.F., Zhang, Qin, N., Deines, T., Zhang, M., and Pei, Z.J.. Ultrasonic-vibration-assisted pelleting of switchgrass: effects of ultrasonic vibration, The 14th International Manufacturing Conference in China (IMCC2011), October 13-15, 2011, Tianjin, China.

Working paper

1. Qin N. and Pei, Z. J.. Experimental study in rotary ultrasonic machining- a review.

Posters

1. Qin, N., Zhang, P.F., Cong, W.L., Sun, W.P., Zhang, X.H., Li, Z.C., Lu, W.K., Liu, J.H., and Pei, Z.J.. CAREER: Fundamental research on silicon wafer fine grinding to foster a quantum leap in manufacturing of silicon wafers, Poster section of 2011 NSF CMMI Grantees Conference, Jan 4-7, 2011, Atlanta, GA.
2. Qin, N. and Pei, Z.J.. Effects of tool design on edge chipping in Ultrasonic-vibration-assisted grinding of advanced ceramics, Poster section of 2011 NSF CMMI Grantees Conference, Jan 4-7, 2011, Atlanta, GA.
3. Zhang, P.F., Cong, W.L., Qin, N., Sun, W.P., Zhang, X.H., Li, Z.C., Lu, W.K., Liu, J.H., and Pei, Z.J.. Career: Fundamental research on silicon wafer fine grinding to foster a quantum leap in manufacturing of silicon wafers, Poster section of 2009 NSF Civil, Mechanical and Manufacturing Innovation Grantees and Research Conference, June 22-25, 2009, Honolulu, Hawaii.
4. Cong, W.L., Zhang, P.F., Qin, N., Zhang, M., Song, X.X., Zhang, Q., Nottingham, D., Clark, R., Denies, T., Pei, Z.J., and Wang, D.H.. Ultrasonic-vibration-assisted pelleting of cellulosic biomass for biofuel manufacturing, Poster section of the ASME International Conference on Manufacturing Science and Engineering (MSEC), October 4-7, 2009, West Lafayette, IN.